Regulation of recombinant human dynein complex studied *in vitro*

Rupam Jha

University College London

and

The Francis Crick Institute

PhD Supervisor: Dr Thomas Surrey

A thesis submitted for the degree of

Doctor of Philosophy

University College London

September 2016

Declaration

I Rupam Jha, confirm that the work presented in this thesis is my own. Where information has been derived from other sources, I confirm that this has been indicated in the thesis.

To Mummy

Abstract

In cells, cytoplasmic dynein is important for cell division and retrograde transport of organelles and macromolecules. Although a microtubule minus end directed motor, dynein often localises to the plus ends of microtubules. The growing microtubule plus ends are thought to serve as important sites of cargo loading and initiation of dynein driven transport. During mitosis, dynein interacts with the plus ends of cortical and kinetochore microtubules where its activity appears essential for spindle positioning, chromosome alignment and checkpoint protein removal. In cells, to track plus ends, dynein interacts with its key regulators—dynactin and Lis1—which, together with the cargo adaptor BicD2, are also involved in dynein driven motion away from the plus ends. How do these dynein regulators control the plus end localisation versus minus end motion of dynein on dynamic microtubules? To address this, I study the regulation of the recombinant human dynein by dynactin, Lis1 and BicD2 on dynamic microtubules in the presence of the end binding protein EB1 using an *in vitro* reconstitution approach combined with TIRF microscopy. This allows simultaneous investigation of dynein motility and microtubule end tracking in the same assay and sheds light on the mechanism of dynein regulation for the two dynein processes.

Acknowledgement

I am grateful to my supervisor, Thomas Surrey for giving me the opportunity to work under his supervision. I would like to thank him for his guidance, and encouragement to develop independent thinking. I thank Guillame Charras and Julie Welburn for agreeing to review my thesis, and my thesis committee members, Martin Singleton and Michael Way for their suggestions on my PhD project.

I would also like to thank present and former members of Surrey Lab: Martina for her guidance and help during the first year of my PhD; Johanna for her useful suggestions in these four years; Michael, for his inputs on this thesis; Franck, for encouragement, music and coffee sessions. Einat, Todd, Iris, Jono, Tanja, Nic, Claire, Christian, Hella and Julian for their valuable help and support during these four years.

A special thanks to my family for their love and support.

Table of Contents

Table of figures

List of tables

Abbreviations

%: Per cent (one part of hundred); **+TIP**: Plus end tracking protein; proteins that accumulate specifically at growing microtubule ends; **aa**: Amino acid; **ATP:** Adenosine triphosphate; **ADP:** Adenosine diphosphate; **BicD2:** BicaudalD homologue 2, **BSA**: Bovine serum albumin; **cc**: coliled-coil; **c-terminal**: carboxy -terminal end of a protein or polypeptide; **CAP-Gly domain**: Cytoskeleton-associated Protein Glycine-rich Domain; **CLIP**: Cytoplasmic linker protein; **Da**: Dalton (unified atomic mass unit) **kDa**: kiloDalton; **MDa:** megaDalton; **DDB:** A complex of dynein, dynactin and BicaudalD2. **DHC**: Dynein Heavy Chain; **DIC:** Dynein Intermediate Chain; **DLIC:** Dynein Ligh Intermediate Chain; **LC:** Dynein Light Chain; **DNA:** Deoxyribonucleic acid; **EBs**: End Binding protein (EB1, EB2 and EB3 in huma); **e.g**.: exempli gratia ("for example"); **EM:** Electron microscopy; **EMCCD:** Electron-multiplying charge-coupled device; **ER**: Endoplasmic reticulum; **fps**: Frames per second; number of frames in a time laps movie per seconds; **GFP:** Green fluorescent protein; **GMPCPP**: Guanosine-5'-[(α, β)methyleno] triphosphate **GTP:** Guanosine triphosphate; **His_6/ 6xHIS**: Histidine tag (a linear sequence of 6 for protein purification or antibody mediated detection; **i.e.**: id est ("that is" or "which means") **Lis1:** Lissencephaly 1; **M**: Molarity (moles per litre); **MAP**: Microtubule associated protein; **mGFP**: monomeric green fluorescent protein; **mCherry**: A fluorescent protein (similar to GFP) with different spectral properties; **mRNA:** messenger Ribonucleic acid**; MT**: Microtubule; **NHS:** **NudE/L**: **N-terminal**: Amino-terminal end of a protein; **OD:** optical density; **p value**: Significance value in statistical tests (Dorey, 2011); **p150** (p150 ^{glued}): Subunit of the dynactin complex with a molecular weight of 150 kilodalton, synonym; **PCR:** Polymerase chain reaction; **pN**: pico Newton; **RNA:** Ribonucleic acid; **sem:** Standard error of mean; **sec (s)**: second; **S.D.**:Standard deviation; **SxIP:** Consensus sequence; a short linear motif within proteins that mediate protein protein interactions with EBs; **TIRF:** Total internal reflection fluorescence microscopy;

Standard prefixes for the metric SI units of measure: **M:** Mega (10^6); **k:** kilo (10^3); **m:** milli (10^{-3}) **µ:** micro (10^{-6}); **n:**nano (10^{-9}); **p:** pico (10^{-12}).

Chapter 1. Introduction

1.1 Microtubule cytoskeleton

The microtubules cytoskeleton forms the framework of eukaryotic cells and is involved in many cellular functions (Wade, 2009). The microtubule arrangement generates the scaffold for cilia and flagella that are crucial for cell motility. During cell division, the microtubule filaments organise into spindles arrays to guide the step-wise process of chromosome separation. Another important role of microtubules is to serve as tracks for intracellular transport. This latter role is central to this thesis.

The microtubule filaments are composed of alpha (α) and beta (β) tubulin subunits. The α-β tubulin dimers align with the α tubulin of one dimer interacting with the β subunit of the adjacent dimer, to generate a protofilament (Figure 1.1) (Amos and Klug, 1974). Approximately 13 such protofilaments arrange (Nogales et al., 1999) to form hollow cylinders known as microtubules (Figure 1.1). Assembly from tubulin heterodimers leads to the polarisation of the two ends of the microtubule filaments, the α-tubulin forming the minus end and the β-tubulin forming the plus end (Desai and Mitchison, 1997). These polarized microtubules are dynamic and can switch between growth and shrinkage phases in a nucleotide dependent fashion—a property known as dynamic instability (Figure 1.2) (Mitchison and Kirschner, 1984).

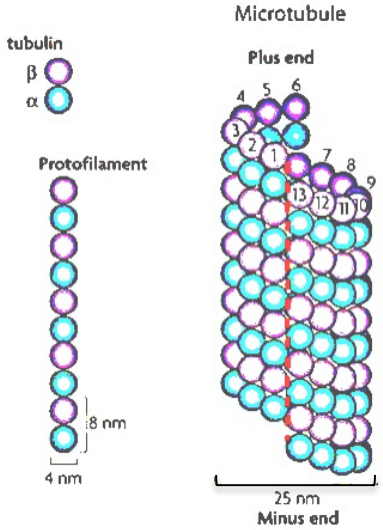

Figure 1.1 Microtubule structure

α -β tubulin dimer polymerises into polarised protofilaments. Approximately 13 protofilaments form the cylindrical microtubule. Adapted from (Akhmanova and Steinmetz, 2008)

In cells, microtubule filaments constantly grow and shrink in response to the environmental stimuli. This allows microtubules to sense the environment and produce force for processes such as cell division, cell shape change and cell migration (Desai and Mitchison, 1997; Volkov et al., 2013). Blocking the dynamic nature of microtubules through drugs such as nocodazole severely inhibits cell division, highlighting the crucial role of dynamic instability in cell division (Jordan et al., 1992; Vasquez et al., 1997).

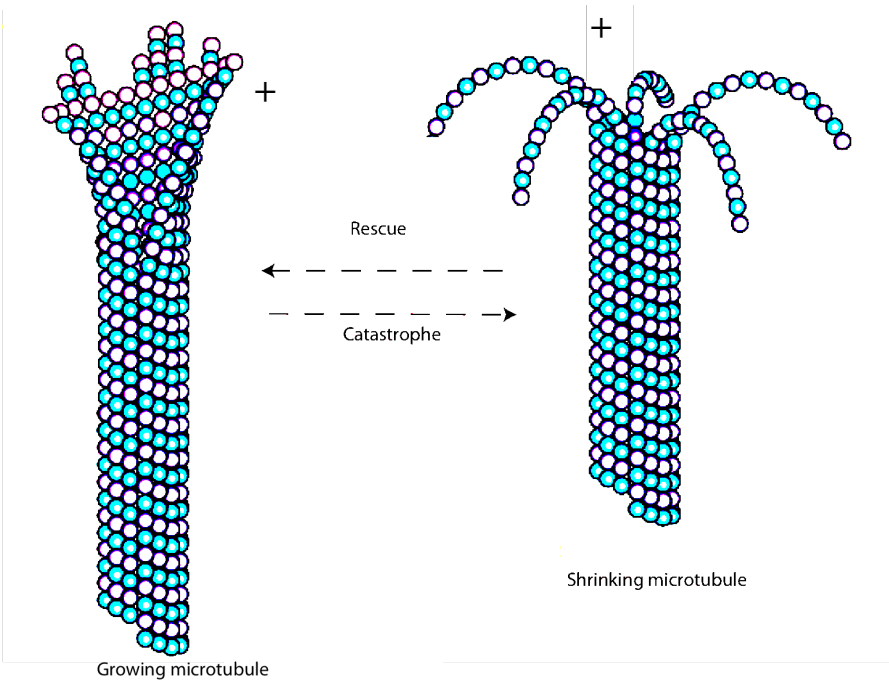

Figure 1.2 Dynamic instability of microtubule

Microtubules alternate between growing and shrinking phases. In the growth phase the microtubule end is protected by a stable GTP cap and shrinking phases in which the GTP cap is lost. The shift from a growing to a shrinking phase is referred to as 'catastrophe' and the reverse is referred to as 'rescue'. The plus end (indicated as '+' in the figure) is more dynamic than the minus end of a microtubule. Adapted from (Akhmanova and Steinmetz, 2008)

Microtubule plus ends are more dynamic than the minus ends. The growing plus end contains GTP bound β-tubulin (referred to as GTP cap) while the rest of the polymerised microtubule lattice remains in GDP-bound state (Amos, 2011; Stewart et al., 1990) (Figure 1.2). The hydrolysis of GTP tubulin i.e. loss of GTP cap at the plus ends leads to rapid depolymerisation of microtubules termed as 'catastrophe'; while the transition from depolymerisation to growth phase is termed as 'rescue' possibly due to

regaining of the GTP cap at the plus ends (Mitchison and Kirschner, 1984; O'Brien et al., 1987).

A group of proteins accumulate at growing microtubule plus ends and regulate the microtubule dynamics, microtubule organisation, and connection to other cellular structures such as ER, actin cytoskeleton and cell cortex (Akhmanova and Steinmetz, 2008). These proteins are known as plus end binding proteins or +TIPs. These +TIPs are classified into: (1) autonomous plus end tracking proteins, such as chTOG and end binding proteins or EBs that bind to the plus end of the microtubule directly; and (2) EB dependent plus end trackers that are recruited to the plus ends by EBs (Akhmanova and Steinmetz, 2008).

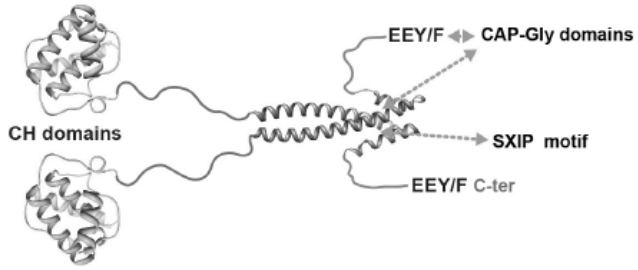

Figure 1.3. Schematic of EB protein

EBs are dimeric and each monomer has a CH domain (light green) at the N-terminal, and the EB homology (EBH) domain (dark green) that terminates in an acid EEY/F tail is present at the C-terminal. The CAP-Gly containing +TIPs bind to the EEY/F tail and the SxIP conating +TIPs bind to the EBH domain. Picture adapted from (Duellberg et al., 2013)

EBs (EB1, EB2 and EB3 in mammalian cells) interact specifically with the growing plus ends of microtubules and not the depolymerizing ends *in vitro* (Maurer et al., 2012) and *in vivo* (Tirnauer et al., 2002). The EB protein has an N-terminal Calponin Homology domain (CH-domain) responsible for a nucleotide-dependent interaction with the microtubule end; and a C terminal EB homology domain (EBH) terminating with an acidic EEY/F tail (Duellberg et al., 2013) (Figure 1.3). While the CAP-Gly domain containing +TIPs (e.g. CLIP170 and $p150^{glued}$ a subunit of dynactin) bind to the EEY/F tail of EB, SxIP motif containing +TIPs bind to the EBH domain (Figure 1.3) (Akhmanova and Steinmetz, 2008). The binding of the SxIP and CAP-Gly containing +TIPs appear to be competitive (Duellberg et al., 2014), possibly because of allosteric modulation of the tail region induced by the binding of SxIP proteins (Honnappa et al.,

2009; Honnappa et al., 2005). The +TIPs can further recruit several more proteins to the plus ends of the microtubule (Figure 1.4), for example, $p150^{glued}$ (the largest subunit of the dynactin complex) is involved in plus end localisation of the dynein complex (discussed later in this chapter).

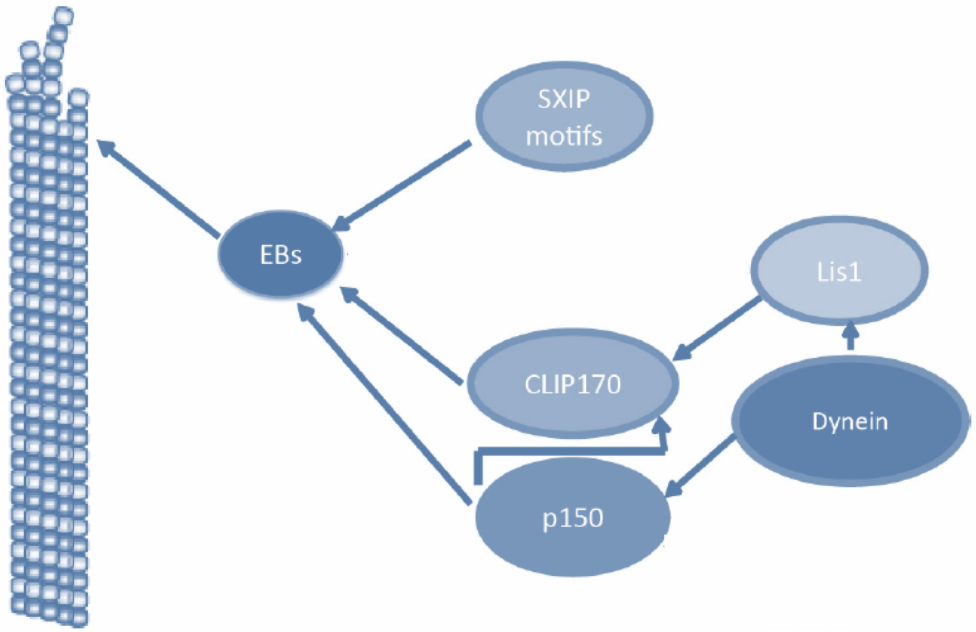

Figure 1.4 The +TIP network

A simplified representation of the +TIP network showing autonomus plus end tracking protein EBs that can directly interact with the growing plus ends of the microtubules and recruit other plus +TIPs such as, CAP-Gly containing CLIP170 and p150 and SxIP motif containing proteins to the microtubule plus ends. The EB dependent +TIPs can further recruit other proteins such as dynein motor and Lis1 to the plus ends.

Microtubule based molecular motors

Molecular motors are nanoscale enzymes that are fuelled by ATP and best known as transporter of cargos—organelles and macromolecules in cells (Vale, 2003). These enzymes hydrolyse ATP and undergo a series of conformational changes that results in their stepping/movement on the microtubule filaments. Based on the direction of stepping on polarized microtubule filaments, the microtubule-based motors are classified as plus end and minus end directed motors. The plus end directed motors mainly belong to the kinesin family, and the minus end directed motors are from the dynein family (Vale, 2003). Both families of motors have functionally similar domains: a motor domain that is the site of ATP hydrolysis and microtubule binding, and a tail

domain where the motor dimerises, interacts with accessory proteins, and binds to cargos (Vale, 2003) (Figure 1.4). However, the kinesin and dynein motors do not share sequence homology or structural similarities.

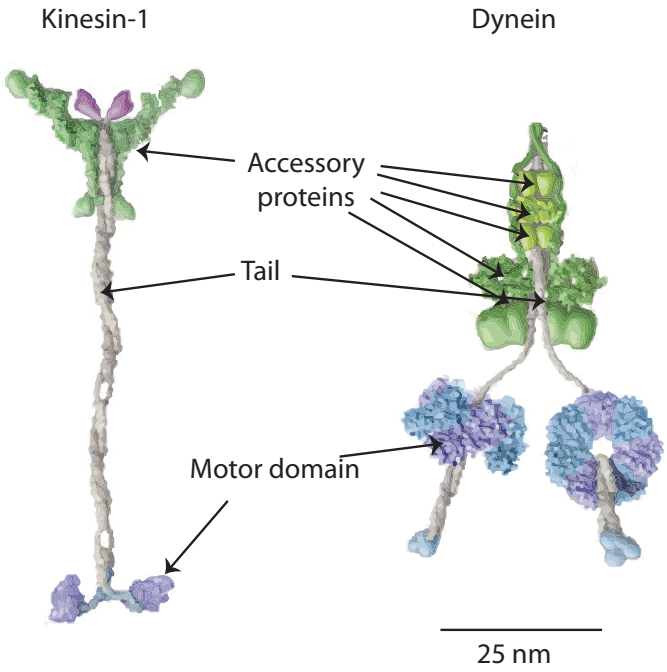

Figure 1.4 Molecular Motor proteins

Schematic representation of kinesin-1 (left) and cytoplasmic dynein (right). The motor domains that bind to microtubules and hydrolyse ATP are shown in blue and the accessory subunits that bind to the tail domain are shown in green. Adapted from (Vale, 2003)

Based on phylogenetic analysis, kinesin motors are classified into fourteen families: kinesin 1 to kinesin 14 (Lawrence et al., 2004). In eukaryotes the different families of kinesin motors have specialized to perform distinct cellular functions. Most the plus end transport of cargos is carried out by three classes of kinesin motors: conventional kinesin (also called kinesin 1), heteromeric kinesin (kinesin 2), and Unc104 (kinesin 3) (Vale, 2003). During cell division, Kinesin-5 family of motors are involved in spindle assembly (Amos, 2008), and Kinesin 13 motors regulate the microtubule dynamics at spindle poles, which is essential for spindle bipolarity (Ganem and Compton, 2004).

The microtubule minus end directed motor, the cytoplasmic dynein, is the focus of this thesis and its structure, function and regulation will be discussed in the remaining part of this thesis.

1.2 Dynein

Dynein was first isolated from cilia of *Tetrahymena* and identified as an ATPase (Gibbons and Rowe, 1965). This was the axonemal dynein, responsible for beating of cilia and flagella. Twenty years after the discovery of the axonemal dynein, cytoplasmic dynein was discovered (Paschal et al., 1987; Paschal and Vallee, 1987). In humans, the axonemal dynein genomic family has 13 members, while with only two genes the cytoplasmic dynein family is not as diverse. The cytoplasmic dynein 2 is restricted to the cytoplasm of cilia and flagella and carries out intraflagellar transport (Pazour et al., 1999; Porter et al., 1999); whereas several cellular functions have been ascribed to the single form of cytoplasmic dynein 1, referred to as 'dynein' hereafter.

While dynein from budding yeast performs a single task of nuclear positioning, its metazoan counterpart performs several functions (Figure 1.5). During cell division, metazoan dynein plays an important role in spindle assembly for proper chromosome segregation. Dynein is involved in organising the minus ends of spindle microtubules into a focused pole (Goshima et al., 2005; Merdes et al., 2000). At kinetochores, dynein is required for checkpoint protein removal (Gassmann et al., 2010) and chromosome alignment (Mao et al., 2010). The pulling force exerted by dynein onto the cortical microtubules is necessary for spindle alignment (Dujardin and Vallee, 2002). During interphase, dynein is involved in transport of cellular cargos, which is one of the best-studied functions of dynein (Allan, 2011; Vale et al., 2003).

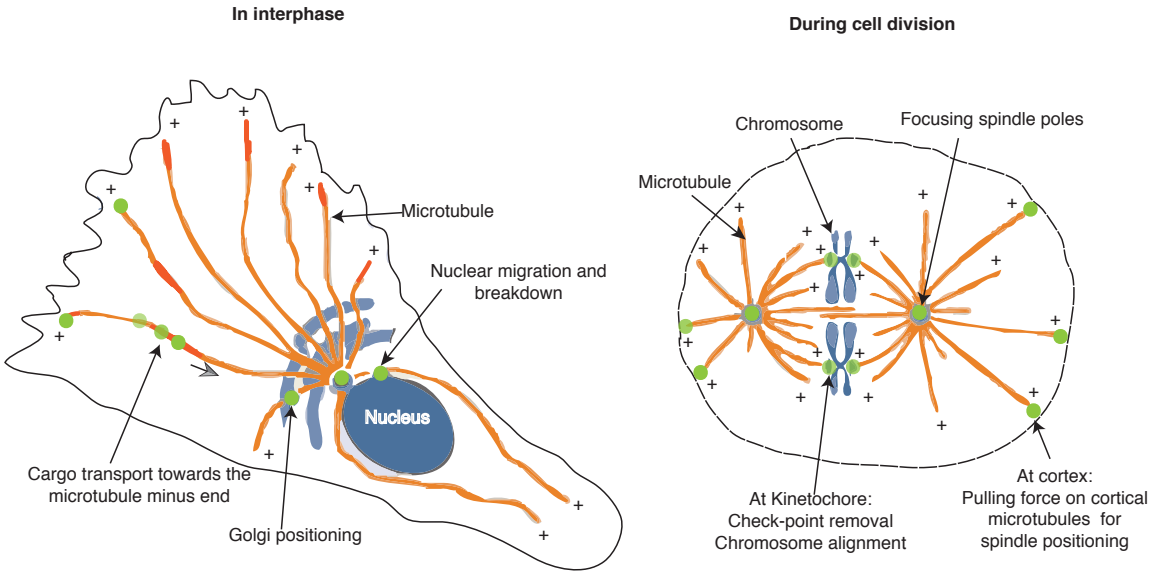

Figure 1.5 Diverse dynein functions in cells

During interphase (left) dynein (green spots) is involved in cargo transport from plus (+) ends of a microtubules (orange) to the minus ends (small arrow inside the cell indicates the direction of dynein motion). During cell division (right) dynein activity is required at the kinetochore, the spindle poles and the cell cortex (shown as green spots). The plus ends of microtubules are indicated with '+' (adapted from Roberts et al., 2013).

Dynein is responsible for transport of many organelles and macromolecules towards the microtubule minus ends (Allan, 2011). Some of the cellular cargos transported by dynein are: the Golgi complex (Corthesy-Theulaz et al., 1992), endoplasmic reticulum (Terasaki et al., 1986), endosomes (Aniento et al., 1993), mitochondria (Morris and Hollenbeck, 1995), and mRNPs (Schnorrer et al., 2000). Apart from these cellular cargoes, pathogens also hijack the dynein transport machinery (Henry et al., 2006) for their retrograde transport, for example: Ebola virus (van der Kant et al., 2013), Human Immune Deficiency virus type-1 30 (HIV1) (Lehmann et al., 2009) and *Salmonella* (Harrison et al., 2003).

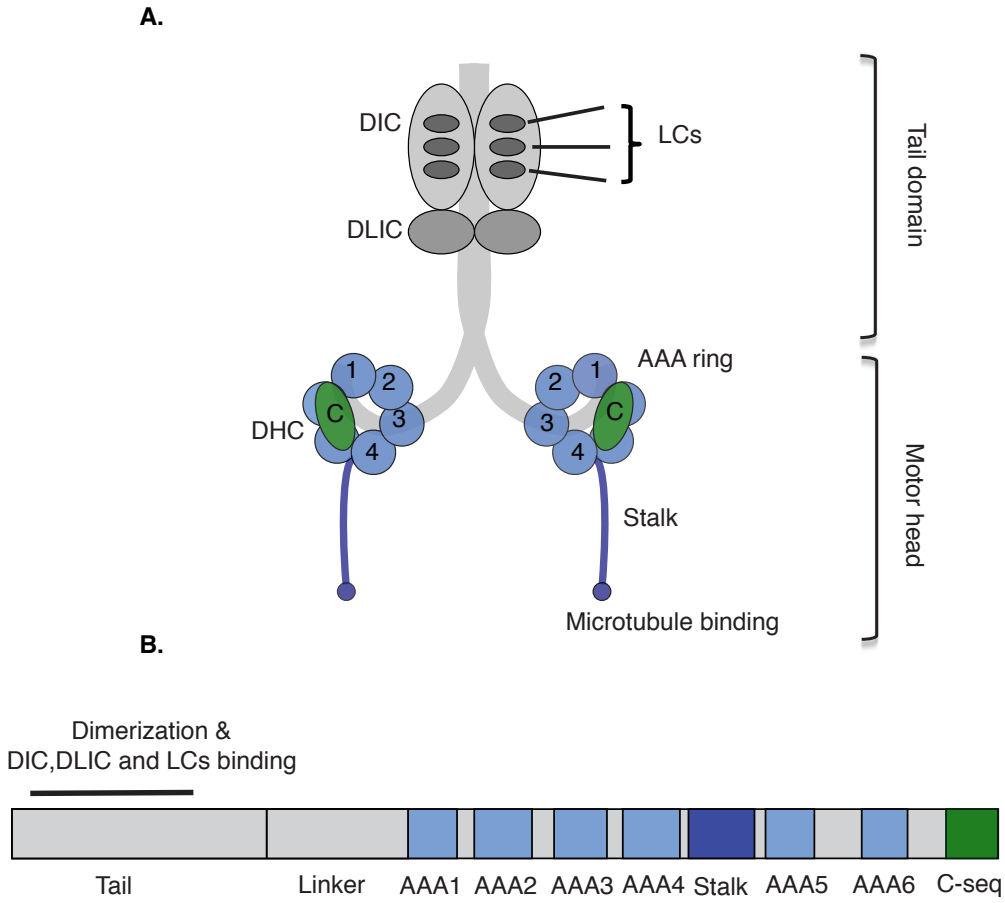

Figure 1.6 Composition of the dynein complex

(A) Schematic of the cytoplasmic dynein complex: Cytoplasmic dynein heavy chains (DHCs) with their motor and tail domains are shown, together with the non-catalytic subunits: the dynein intermediate chain (DIC), the dynein light intermediate chain (DLIC) and the light chains (LCs). **(B)** Domain organisation of the DHC sequence. The AAA1–AAA6 domains are in blue, the stalk with its microtubule-binding site in dark blue, the C-sequence in green, and the linker followed by tail in grey. The positions of the dimerisation region and of the binding region for the smaller subunits are indicated. Picture taken from (Jha and Surrey, 2015).

The dynein complex is composed of six subunits that homodimerise to constitute a 1.5 MDa sized motor (Figure 1.6 A) (Vallee et al., 1988). The complex is assembled around a dimer of the largest subunit of dynein, the dynein heavy chain (DHC). Each DHC subunit of dynein is 0.5 MDa in size and forms the catalytic subunit of dynein with a C-terminal motor domain that hydrolyses ATP and binds to the microtubule filaments, and an N-terminal tail domain that allows dimerisation and interaction with other non-catalytic dynein subunits. The remaining five subunits: the dynein intermediate chain (DIC), dynein light intermediate chain (DLIC) and three distinct light chains (LCs),

bind in pairs to the N-terminal tail of DHC (Pfister et al., 2006; Vale, 2003). While the DHC gene is present in single form, many isoforms of the non-catalytic subunits are found in cells (Pfister et al., 2006), indicating that dynein complexes with different subunit compositions may exist and could possibly have distinct functions.

Our knowledge of the dynein motor domain comes from the X-ray structures of *Dictyostelium* and budding yeast dynein (Carter et al., 2011; Kon et al., 2012). Unlike kinesin motors with single ATP binding sites, the dynein motor consists of six distinct domains of AAA+ (**A**TPase **a**ssociated with various cellular **a**ctivities), AAA1–AAA6 (Roberts et al., 2009) (Figure 1.6 B). The AAA1 domain forms the primary ATP hydrolysis site of dynein (Gibbons et al., 1987; Kon et al., 2004). AAA3 and AAA4 can also hydrolyze ATP, and the mutations in their ATP binding site hampers dynein motion (Cho et al., 2008; DeWitt et al., 2015; Kon et al., 2005; Kon et al., 2004). The AAA2, AAA5 and AAA6 do not hydrolyze ATP, however, they do play a role in communicating structural changes within the AAA+ ring (Schmidt et al., 2015).

The microtubule-binding domain emanates from a long stalk projecting out of the AAA4 of the motor ring (Kon et al., 2012; Vale, 2003) (Figure 1.6). Towards the N-terminal of the AAA+ ring of dynein motor lies its linker region (Figure 1.6 B) that serves as a mechanical element modulating conformational changes in dynein during its ATPase cycle (Hook, 2010; Roberts et al., 2012) (Figure 1.7). The linker remodelling is crucial for dynein's microtubule binding and unbinding that translates into dynein's stepping on microtubules, and its force production (Kon et al., 2004; Kon et al., 2012; Roberts et al., 2012; Roberts et al., 2009).

Although the dynein motor is generally conserved across species, there exists some fine structural differences: one of the most prominent differences in the dynein motor is the length of the C-sequence present at the C-terminal end of DHC sequence (Figure 1.6), which is 47 kDa in metazoan and *Dictyostelium* dynein and only 15 kDa in budding yeast dynein (Cho et al., 2008; Numata et al., 2011). This difference has been recently suggested to cause differences in motile properties of dynein (Nicholas et al., 2015) and will be discussed further in Chapter 2.

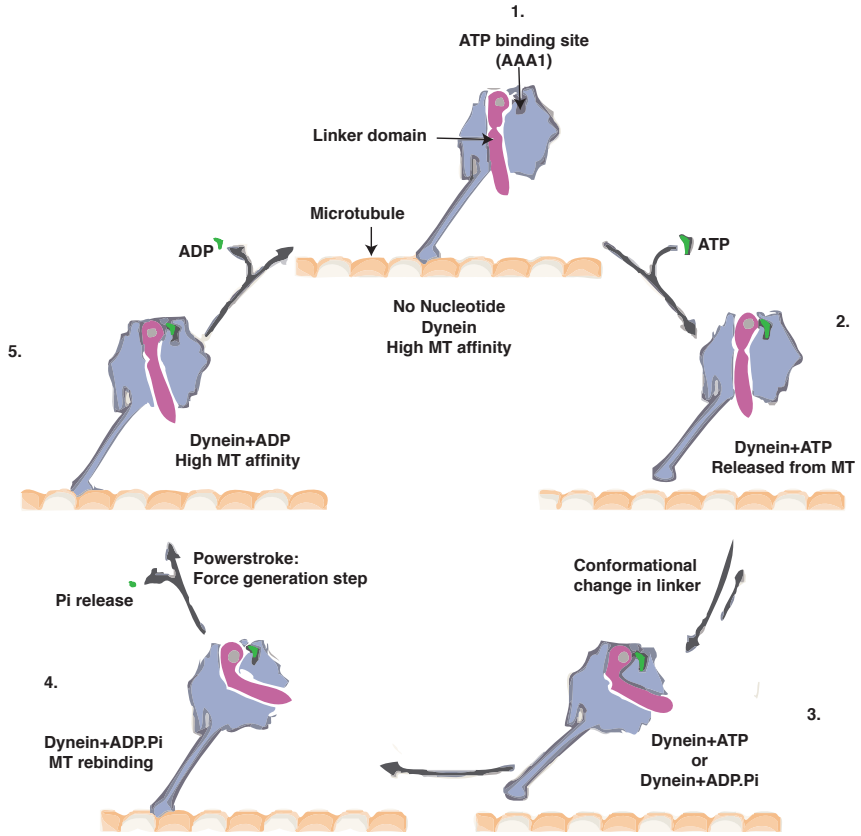

Figure 1.7 Enzymatic cycle of dynein

The dynein enzyme undergoes a series of changes in its microtubule binding and linker rearrangement in different nucleotide stage of its ATP hydrolysis cycle. The AAA1 domain forms the primary ATP binding site (indicated in the diagram) and the linker (shown in pink) changes its conformation that translates into stepping and force production. 1. In the absence of ATP dynein is tightly bound to the microtubule (MT). 2. Upon ATP binding MT affinity of dynein weakens resulting in dissociation of dynein from MT. 3. In the ATP bound state and as ATP hydrolyses to ADP+Pi the linker domain changes its conformation relative to the AAA ring. This linker remodeling shifts the dynein's microtubule binding domain forward to bind (stepping) MT at new site. 4. Upon ATP hydrolysis, when ADP.Pi (inorganic phosphate) is bound to dynein, it rebinds the MT at a new site by weak MT interaction. 5. Once Pi releases, dynein binds the MT strongly and the linker again changes its conformation. The conformational change in linker and high MT binding in ADP state is thought to represent dynein's force producing state known as its 'powerstroke'. ADP then releases from the nucleotide-binding pocket of dynein restarting the cycle. Adapted from (Roberts et al., 2013)

Motile properties of dynein

In vitro assays using dynein purified from diverse organisms have provided precise measurement of several properties of dynein. One of the first *in vitro* experiments to study dynein activity was microtubule gliding assay with purified surface-immobilized dynein that transported microtubules by their ensemble activity (Paschal and Vallee, 1987). Whereas, single dynein properties are studied through two approaches: bead assays—where dynein is adsorbed onto micrometer-sized plastic beads and bead motility is visualised by microscopy (Culver-Hanlon et al., 2006; King and Schroer, 2000; Mallik et al., 2005; McKenney et al., 2010; Toba et al., 2006; Wang et al., 1995); and the second method involves direct visualisation of labelled dynein by single molecule fluorescence microscopy (McKenney et al., 2014; Numata et al., 2011; Reck-Peterson et al., 2006; Schlager et al., 2014; Trokter et al., 2012). Using these assays, velocities of dynein from different species has been measured showing that *Dictyostelium* and metazoan dynein move (ranging from 0.3 to 1 μm/s) much faster than budding yeast dynein (~0.1 μm/s) (reviewed in (Jha and Surrey, 2015)).

Force measurement of dynein studied through laser trapping experiments also showed organism-specific differences: while force measured for single vertebrate dynein was 1–2 pN (Mallik et al., 2004; McKenney et al., 2010; Schroeder et al., 2010; Vershinin et al., 2008) force exerted by budding yeast dynein was up to ~7 pN (Gennerich et al., 2007). These variations in velocity and force production indicate that dynein shows species-specific dissimilarities, and some of these differences are suggested to arise from fine structural differences (Nicholas et al., 2015) in dynein from different species.

Processivity

For long-range retrograde cargo transport, dynein moves at a micron-scale before detaching from the microtubule—referred to as 'processivity' of a motor. *In vitro* evidence of processivity came from studying the motility of salt washed vesicles and plastic beads coated with purified brain dynein imaged by video enhanced DIC microscopy (Gill et al., 1991; Wang et al., 1995). Utilizing the genetically tractable lower eukaryotes, such as budding yeast (Reck-Peterson et al., 2006) and *Dictyostelium* (Numata et al., 2011) recombinant dyneins were generate. This allowed direct visualization of processive dynein motion by fluorescence microscopy. Single molecule

fluorescence imaging of recombinant dynein complex form budding yeast exhibited processive behavior (Kardon et al., 2009; Reck-Peterson et al., 2006). To dissect out the molecular mechanism of processivity, an artificially dimerised (using GST tag) and fluorescently labelled truncated DHC constructs lacking the N-terminal dynein tail were generated (Reck-Peterson et al., 2006). The budding yeast dynein dimers showed processively *in vitro* (Reck-Peterson et al., 2006); and, their processivity required intact dynein linker domains and dimerisation (Reck-Peterson et al., 2006). Similar recombinant dynein dimers from *Dictyostelium* moved processively when studied by single-molecule fluorescence imaging (Numata et al., 2011), and required dimerisation of dynein motor for processivity. Additionally, coordination between the two motor heads of dynein dimer was also required for processivity of Dictyostelium dynein; this co-ordination was attributed to the C-sequence of dynein motor (Numata et al., 2011), which is missing in budding yeast dynein.

In stark contrast to recombinant dynein from lower eukaryotes, fluorescently labelled full-length vertebrate dynein from cultured cells (Mazumdar et al., 1996; McKenney et al., 2014) or expressed in insect cells (Schlager et al., 2014; Trokter et al., 2012) lacked processivity when studied through fluorescence microscopy. The artificially dimerised vertebrate dynein fragments also showed nonprocessive behavior in single molecule fluorescence imaging experiments (Jha and Surrey, 2015; Nicholas et al., 2015; Trokter et al., 2012). These observations challenged the long-standing notion of processivity being an inherent property of dynein motor across species. It became apparent that unlike dynein from lower eukaryotes, vertebrate dynein is nonprocessive and the possible reason behind this was suggested to be inhibition of dynein motor (Carter et al., 2016; Torisawa et al., 2014; Urnavicius et al., 2015)(discussed further in Chapter 2).

How does the nonprocessive metazoan dynein drive long-range intracellular transport? Metazoan dynein interacts with many proteins that are known to regulate its several motile properties, including processivity (Kardon and Vale, 2009). One of the best studied regulators of dynein is the dynactin complex, crucial for almost all dynein-driven cellular activities (Schroer, 2004).

1.2.1 Dynein regulator: Dynactin

Dynactin was first studied as a co-purified /contaminant protein present in purified brain dynein that activated the dynein motility of salt-washed organelles[1], and was therefore named a dynein activator—dynactin (Gill et al., 1991; Paschal et al., 1993; Schroer and Sheetz, 1991b). Some of the cellular dynein functions where dynactin has been studied to be important are: recruitment of dynein to Golgi (Holleran et al., 2001; Holleran et al., 1996; Muresan et al., 2001), ER (Zong et al., 2012; Watson et al., 2004), endosomes (Johansson et al., 2007); nuclear envelope breakdown (Salina et al., 2002) spindle alignment at cortex (Kiyomitsu and Cheeseman, 2012; Kotak et al., 2012); and spindle pole focusing (Gaglio et al., 1997; Merdes et al., 2000; Merdes et al., 1996).

The large scale purification of dynactin from brain tissues (Bingham et al., 1998) enabled analysis of its structure and subunit composition (Schroer, 2004). The dynactin complex is composed of eleven different subunits with distinct stoichiometry assembled into a megadalton-sized multi-protein complex (Eckley et al., 1999; Imai et al., 2006; Schafer et al., 1994; Schroer, 2004). So far, the metazoan dynactin complex has mainly been purified from neuronal sources (Bingham et al., 1998; Schroer and Sheetz, 1991b; Urnavicius et al., 2015); large-scale purification from non-neuronal sources has not been reported, possibly due to low abundance of dynactin in non-neuronal cells. Furthermore the complicated subunit stoichiometry of the dynactin complex (Schroer, 2004) and insolubility of some of its subunits, for example, Arp1 (Cheong et al., 2014) and p150 (Moughamian et al., 2013), have prevented reconstitution of full-length recombinant dynactin complex.

Recent high resolution EM structure further elucidated the complex architecture of dynactin (Figure 1.8) (Chowdhury et al., 2015; Urnavicius et al., 2015). The dynactin complex is assembled around a polarized filament of **A**ctin-**r**elated **p**rotein-**1**—Arp1. The polymer of Arp1 proteins is capped by actin capping proteins at one end (barbed end); and has p25/27 and p62 subunits at another end (pointed end) (Figure 1.8). The p50 (dynamitin) subunits forms the shoulder and extends onto the Arp1 filament to scaffold each of the eight Arp1 monomers; this scaffolding is hypothesized to be important for determining the length of Arp1 filament (Figure 1.8). The p50 subunit

[1] Treatment with 600mM potassium iodide removed the native proteins presented on the organelle (Schroer et al., 1988)

also links the largest dynactin subunit–p150^{glued} (referred as p150 hereafter) to the rest of the dynactin structure (Figure 1.8).

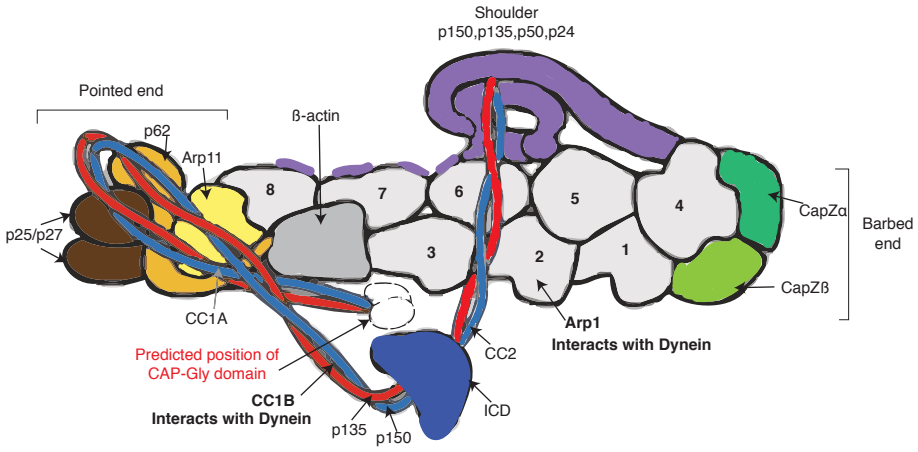

Figure 1.8 Schematic of the dynactin complex

The Arp1 filament (grey) has 8 Arp1 monomers labelled 1-8 capped with CapZ αβ towards the barbed end, and the p25/p27 (brown), and p62 (orange) subunits are present towards the pointed end. The filament also contains β-actin (dark grey) and Arp11 (yellow). The shoulder region (purple) contains p24 and p50 subunits. The purple dashed line below the Arp1 filament is thought to be an extended p50 region. The blue and red filaments protruding from the shoulder is the p150/p135 subunits, which consists of three coiled-coil (CC) domains, CC1A, CC1B and CC2, a globular domain known as **I**nter **c**oiled-coil **d**omain (ICD) is present between CC2 and CC1. The full-length p150 appears to be folded and docked onto the Arp1 filament. Dynactin is known to interact with dynein at two different sites; the CC1B domain and Arp1 filament (indicated in bold). But these interactions require additional cofactor that would undock the p150. The microtubule and EB1 binding CAP-Gly domain was not visible in the structure, but based on the orientation of p150 it is predicted to be buried between Arp1 filament and rest of the folded p150 (predicted CAP-Gly position shown with dashed line). Adapted from (Urnavicius et al. 2015).

Intriguingly, although dynactin copurifies with dynein from native sources (Bingham et al., 1998), mixing pure dynactin and dynein in solution does not show any detectable interaction (Mckenney et al., 2014; Schlager et al., 2014). Our understanding of the dynein-dynactin interaction mainly comes from immunoprecipitation (Vaughan and Vallee, 1995) and solution binding experiments (King et al., 2003) with the truncated fragments of the dynein and dynactin subunit. These experiments have shown that the CC1 domain of p150 interacts with the N-terminal of DIC subunit of dynein (Karki and Holzbaur, 1995; King et al., 2003; Siglin et al., 2013; Vaughan and Vallee, 1995). The

p150 subunit of dynactin also contains the microtubule binding and +TIPs binding—CAP Gly domain (Askham et al., 2002; Ligon et al., 2003).

Surprisingly, the recent dynein structure shows p150—the hub of interaction sites, in a folded conformation, where p150 sits in the groove of Arp1 filament (Carter et al., 2016; Urnavicius et al., 2015) (Figure 1.8). In this conformation, the dynein binding CC1 domain and the microtubule binding CAP-Gly domain appear to be inaccessible for interaction. This folded conformation of p150 is believed to represent an auto-inhibited state of dynactin, and in this conformation, its interaction with dynein is supposed to be weak (Carter et al., 2016; Urnavicius et al., 2015). The exact position of the microtubule and +TIP binding CAP-Gly domain in the current dynactin structure is unclear. However, based on the projection of the coiled-coil domains of p150 it is predicted to be buried in the Arp1 groove (Urnavicius et al., 2015) (Figure 1.8). The proposed mechanism for the release of auto-inhibition of dynactin and its complex formation with dynein (Chowdhury et al., 2015; Urnavicius et al., 2015) will be discussed later in this Chapter.

While the interaction site of dynactin lies at the dynein tail domain, Lis1–another ubiquitous dynein regulator can bind directly to the motor domain to control several dynein functions.

1.2.2 Dynein regulator: Lis1

Lissencephaly**1** or Lis1 is one of the most well conserved regulators of dynein across species. The first report of dynein regulation by Lis1 came from studies in filamentous fungi, where it was known to regulate dynein in nuclear migration (Efimov and Morris, 2000; Minke et al., 1999; Xiang et al., 1995), In mammalian cells, Lis1 is involved in several dynein functions ranging from pole focusing (Raaijmakers et al., 2013; Zylkiewicz et al., 2011), recruiting dynein to kinetochores (Faulkner et al., 2000) , chromosome alignment (Stehman et al., 2007; Vergnolle and Taylor, 2007), and organelle transport (Lam et al., 2010; Liang et al., 2004; Pandey and Smith, 2011; Smith et al., 2000; Splinter et al., 2012)

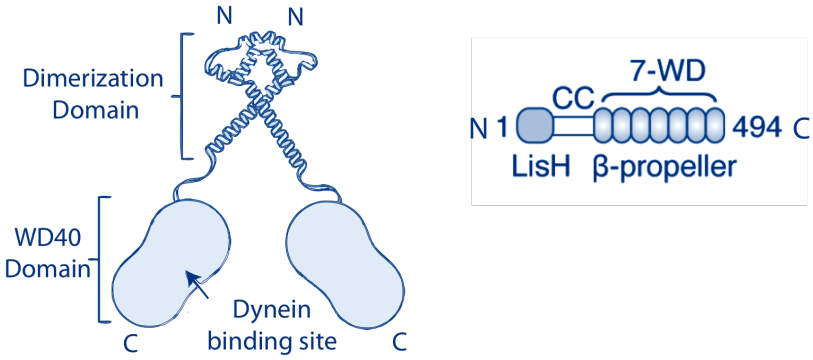

Figure 1.9 Schematic of Lis1

Lis1 is a dimeric protein that contains 7 WD-40 repeats towards the C-terminal which is a ß-propeller structure (shown in the right-hand side schematic). Each WD40 domain interacts with one dynein AAA+ ring. The LisH (**Lis**1 **h**omology) and the cc (**c**oiled-**c**oil) domain present at the N-terminal allow the dimerisation of Lis1 (Kim et al., 2004; Tarricone et al., 2004). Adapted from (Kardon et al., 2009)

Lis1 is 45kDa protein that dimerises via its N terminal coiled-coil region (Mateja et al., 2006) and interacts with dynein through its C-terminal WD repeats (Figure 1.9), which binds the DHC subunit at AAA+ ring (Huang et al., 2012; Kim et al., 2004; Tai et al., 2002; Tarricone et al., 2004). The exact location of Lis1's interaction site was previously reported to be AAA1 domain (Tarricone et al., 2004), however, the subsequent EM structure suggests that Lis1 binds at the interface of AAA3/4 (Huang et al., 2012; Toropova et al., 2014). Lis1 is the only known dynein regulator that binds to the dynein motor domain directly (Toropova et al., 2014).

Lis1 acts together with another protein—**nu**clear **d**istribution **E/L** (NudE/L) that binds to the dynein tail region to provide an additional layer of regulation(Efimov and Morris, 2000; Sasaki et al., 2000; Stehman et al., 2007). While some reports suggest that Lis1 and NudE/L may antagonistically regulate dynein (McKenney et al., 2010; Torisawa et al., 2011; Yamada et al., 2008), several reports have demonstrated that their regulation is synergistic, and increasing Lis1 concentration compensates for the absence of NudE/L activity both in cells and *in vitro* (Efimov, 2003; Huang et al., 2012; Li et al., 2005; Shu et al., 2004; Wang et al., 2011; Wang et al., 2013; Zylkiewicz et al., 2011). Lis1 has also been reported to interact with dynactin's p50 subunit (Tai et al., 2002), indicating that it may regulate the dynein-dynactin complex.

Besides the ubiquitous dynein regulators dynactin and Lis1, several adaptor proteins that recruit dynein to various cellular structures (e.g. cargo membranes, cell cortex, nuclear envelope) also regulate dynein transport (Kardon and Vale, 2009). For metazoan dynein one of the conserved regulator is BicD adaptor protein.

1.2.3 Dynein regulator: BicD2

Bicaudal-**D** (BicD) is a metazoan-specific cargo adaptor protein that links dynein to the membranes of organelles (Kardon and Vale, 2009). It is best known for its role in mRNA transport in *Drosophila* (Bullock and Ish-Horowicz, 2001). There are two homologues of BicD in mammals—BicD1 and BicD2 (Terenzio and Schiavo, 2010). BicD2 is better characterized for its role as cargo adaptor for dynein driven transport. It is largely a coiled-coil protein with three coiled-coil domains that bind to crucial components of bidirectional transport: the dynein-dynactin complex, kinesin-1, and Rab receptors present on vesicles (Figure 1.10) (Splinter et al., 2012; Splinter et al., 2010).

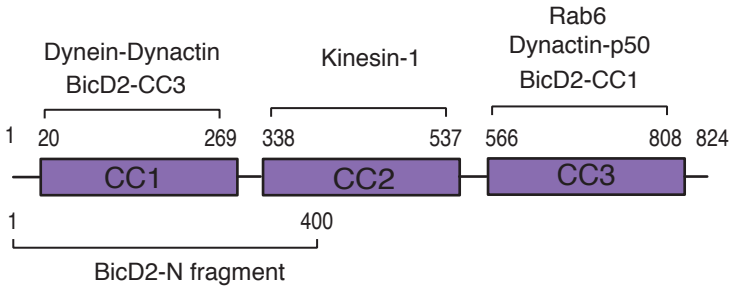

Figure 1.10 Schematic of BicD2 protein

BicD2 is largely coiled-coil (cc) in structure, and consist of three cc domains. The numbers represent the amino acid position. The binding partners are mentioned on top of the protein scheme. The CC1 binds to the dynein-dynactin complex, the CC2 binds to kinesin-1, and the CC3 interacts with Rab proteins present on the membrane of cargoes. CC3 has also been shown to bind to p50 subunit of dynactin. The CC1 and the CC3 bind to each other for BicD2 autoinhibition. BicD2-N fragment of N-terminal 1-400 amino acid used for previous *in vitro* reconstitution experiments and in this study is indicated below the molecular scheme.

The full-length BicD2 is known to show intramolecular inhibition, where its N-terminal CC1 binds to the C-terminal CC3 to assume a folded conformation (Figure 1.10) (Hoogenraad et al., 2001; Stuurman et al., 1999). Owing to this autoinhibition of full-length BicD2, an N-terminal fragment of BicD2 (Figure 1.10) is generally used for

biochemical and structural studies of dynein regulation (Chowdhury et al., 2015; McKenney et al., 2014; Schlager et al., 2014; Urnavicius et al., 2015). Recently, point mutations in BicD has also been linked to spinal muscular atrophy (Neveling et al., 2013; Oates et al., 2013), and some of these mutations were shown to enhance its interaction with dynein-dynactin (Oates et al., 2013). In the context of organelle transport, the possible effects of enhanced dynein-dynactin binding by mutant BicD2 remains to be studied.

1.3 Regulation of motile properties of dynein

1.3.1 Regulation by Dynactin

Several conflicting observations have been reported for the role of dynactin in regulation of dynein motion. *In vitro* bead assays using purified mammalian dynein and dynactin reported a modest twofold increase in dynein run length, and attributed this increase to the microtubule binding CAP-Gly domain of dynactin (Culver-Hanlon et al., 2006; King and Schroer, 2000). Similar increase in processivity was also observed by fluorescence imaging of yeast dynein-dynactin complex (Kardon et al., 2009), however, the CAP-Gly domain was not important for this processivity enhancement. Further, deletion of the CAP-Gly domain of p150 did not affect dynein driven organelle transport in insect cells (Kim et al., 2007) HeLa cells and (Dixit et al., 2008) neurons (Moughamian and Holzbaur, 2012). Dynactin has also been shown to induce bidirectional dynein motion in a study using fluorescent dynein-dynactin complex purified from GFP-p50 expressing transgenic mice (Ross et al., 2006), however, the dynein motion in this study appears rather diffusive than processive.

Recent reports suggest that vertebrate dynactin complex shows weak binding to the microtubule and dynein and does not activate processivity of the nonprocessive vertebrate dynein (Mckenney et al., 2014; Schlager et al., 2014). Furthermore, vertebrate dynactin does not affect the ensemble microtubule gliding velocity of purified dynein (Wang et al., 2013). Overall, the vertebrate dynactin complex is not a strong regulator of processive dynein motion when studied in the absence of other dynein regulators (Mckenney et al., 2014; Schlager et al., 2014).

1.3.2 Regulation by Dynactin and BicD2

Recent *in vitro* experiments revealed that processive motion of vertebrate dynein requires two components: the dynactin complex and a cargo adaptor BicD2-N (an N-terminal fragment of BicD2) (Figure 1.10). BicD2-N facilitates the dynein-dynactin interaction, to form a dynein-dynactin-BicD2 (DDB) complex with highly processive motility (up to 10 μm) (McKenney et al., 2014; Schlager et al., 2014). Besides BicD2-N, other cargo adaptors such as: kinetochore adaptor Spindly (Griffis et al., 2007), endosome adaptors Rab11-FIP3 (Horgan et al., 2010), and Hook3 (Zhang et al., 2014) also activates the processive motion of human dynein in the presence of dynactin (McKenney et al., 2014). Therefore, a general mechanism of activation of dynein motion was proposed where processivity is activated when dynein binds to the cargos via cargo adaptors and dynactin (McKenney et al., 2014) (Figure 1.11).

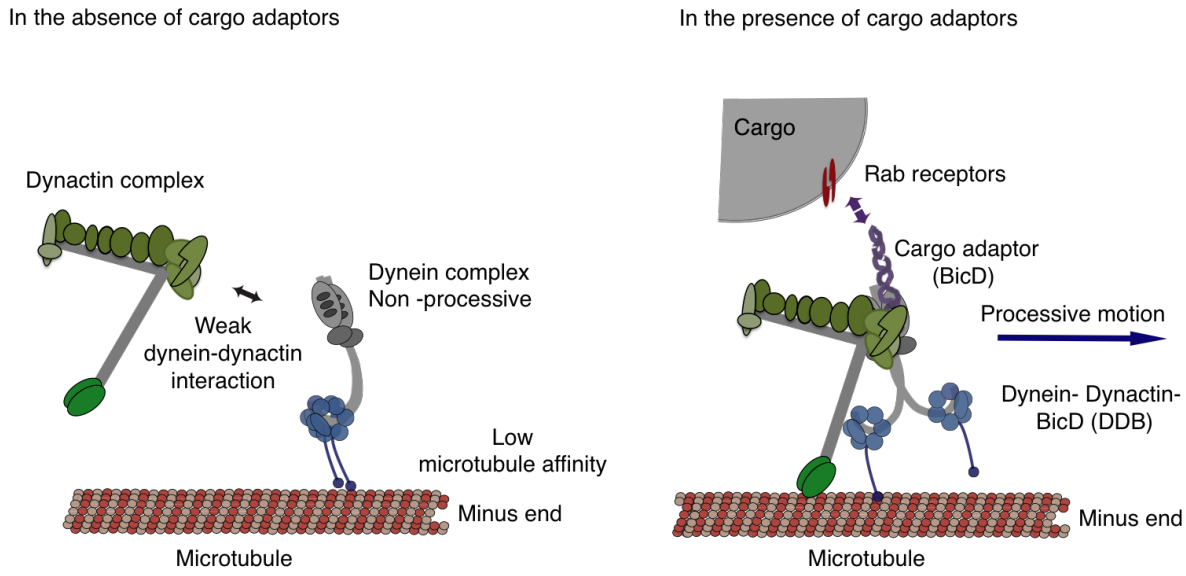

Figure 1.11 Schematic representations of processivity activation of dynein by dynactin and BicD2

When bound to cargo (grey), cargo adaptor proteins like BicD2 (shown in purple) transform nonprocessive mammalian dynein (left) to processive dynein (right). Picture taken from (Jha and Surrey, 2015).

Formation of the DDB complex is suggested to produce rearrangements in dynein and dynactin structures to activate dynein and unfold the p150 subunit dynactin to allow the interaction of the CAP-Gly domain with the microtubule (Carter et al, 2016;

Chowdhury et al., 2015; Urnavicius et al., 2015). The structural basis of stabilisation and processivity enhancement of dynein-dynactin by BicD2-N was elucidated recently through cryo EM and negative-stain EM (Chowdhury et al., 2015; McKenney et al., 2014; Schlager et al., 2014; Urnavicius et al., 2015).

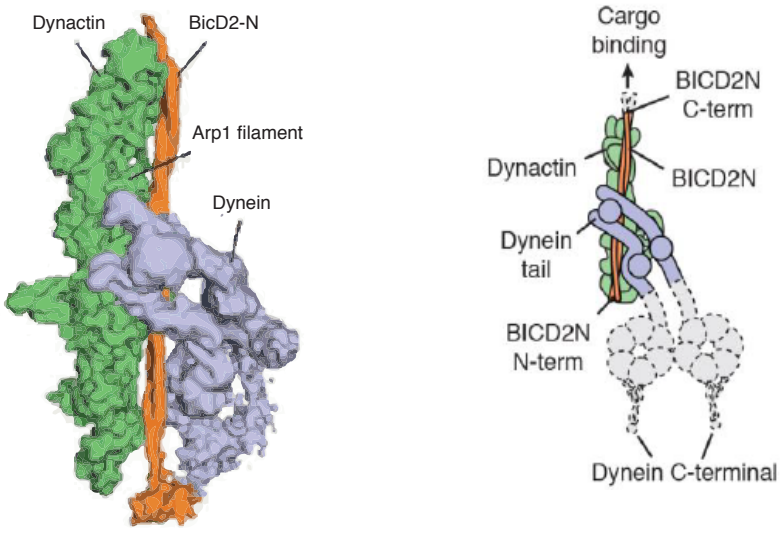

Figure 1.12 Structure of the DDB complex

The cryo-EM structure of dynein tail-dynactin-BicD2-N complex (Left). Schematic representations (right) showing formation of DDB complex where BicD2-N is sandwiched between dynein tail and dynactin's Arp1 filament. Picture taken from (Urnavicius et al., 2015).

Attachment of BicD2 to the dynein-dynactin complex was suggested to activate dynein and dynactin by the following mechanism:

1. Activation of dynein: BicD2-N binds along the length of the dynactin Arp1 filament and forms an interaction interface with the dynein tail (Figure 1.12) (Urnavicius et al., 2015). However, the two dynein tails bind asymmetrically to the Arp1 filament. The asymmetry introduced in the dynein tail is expected to cause separation of dynein motor heads, which is known to release dynein's auto inhibition (Torisawa et al., 2014) and activate dynein processivity.
2. Activation of dynactin: The binding of BicD2-N to the Arp1 is also suggested to undock the p150 subunit, which was folded in the groove of the Arp1 filament (Figure 1.9). The unfolding of p150 is thought to expose the CC1 and

the CAP-Gly domain, which allows the dynein-dynactin (Karki & Holzbaur 1995, King et al., 2003, Siglin et al., 2013, Vaughan & Vallee, 1995) and the dynactin-microtubule interactions.

Intriguingly, expression of BicD2-N fragment did not lead to processive dynein motion in cells, unless this fragment was directly coupled to cargos (Splinter et.al, 2012). The reason behind this lack of dynein processivity in BicD2-N expressing could be competition with endogenous cargo adaptors. Moreover, a neuronal isoform BicDR-1 coupled to Rab positive vesicles lead to an increase in the velocity of dynein-driven vesicle transport in cells (Schlager et al., 2014b). Additionally, in bead assays with purified proteins, attachment of BicD2 and dynactin also increased the velocity of dynein (Belyy et al., 2016). Whether this effect is specific to BicD2 or can be generalized to other cargo adaptors remains to be studied. Formation of DDB complex lead to enhancement of yet another motor property of mammalian dynein: its force production (Belyy et al., 2016). When DDB complex was attached to the beads, it exerted a force fourfold higher than dynein. This high force production further enabled dynein to compete in the tug-of-war with single kinesin-1 motor without the need of teaming up of many dynein motors, as previously report (Rai et al., 2013).

To summarize, vertebrate dynein alone seems to be a nonprocessive motor with weak affinity for microtubules and generates low force. Adding dynactin to this weak motor does not cause any noticeable change in its motile properties. Nevertheless, when dynactin is attached via cargo adaptor BicD2 to vertebrate dynein, it enhances several motile properties of dynein to generate an extremely processive, high force producing motor.

1.3.3 Regulation by Lis1

The mechanism of Lis1 regulation is best characterized in yeast where Lis1 is known to increase the processivity of yeast dynein by increasing its microtubule affinity (Huang et al., 2012). For vertebrate dynein, while Lis1 alone had no effect on processivity of dynein, Lis1 and NudE together increased the processivity of dynein in bead assays

(McKenney et al., 2010). Furthermore, Lis1 reduced the speed of dynein for both yeast and mammalian dynein (Yamada et al., 2008; McKenney et al., 2010; Huang et al., 2012). Lis1 also increased the microtubule affinity of both fungal and vertebrate dynein (Huang et al., 2012; McKenney et al., 2010; Toropova et al., 2014; Yamada et al., 2008). A clutch like role of Lis1 was proposed to be responsible for this enhanced microtubule attachment. Lis1 seems to restrict the movement of the dynein linker (Figure 8) (Toropova et al., 2014), which is crucial for dynein's microtubule binding and unbinding as ATP is hydrolysed (Figure 8) (Toropova et al., 2014; Huang et al., 2012). Thus, the increase in microtubule affinity of dynein by Lis1 is not due to blocking its ATP activity but due to restriction in conformational change of dynein motor (Figure 1.13).

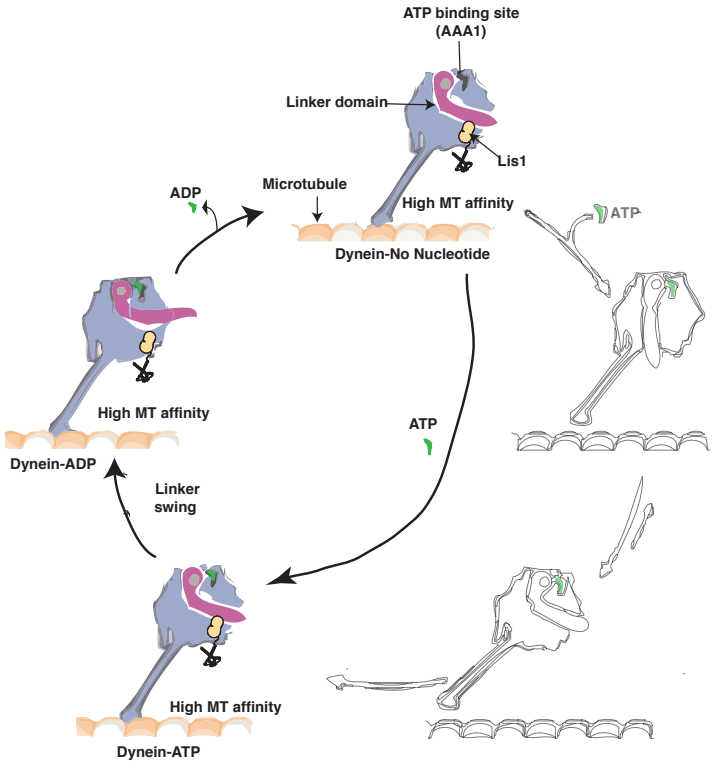

Figure 1.13 ATPase cycle of the dynein-Lis1 complex

Lis1 binds to the dynein AAA+ ring (at AAA3/4) and blocks the stages of linker movement that originally occurs during ATPase cycle, ultimately blocking the microtubule release of dynein. The linker can move up to a certain extent upon ATP hydrolysis (close to AAA2) (referred to as 'Linker swing' in the figure). However, Lis1 sterically blocks the linker's return to its normal position (closed to AAA5) on dynein's ring that is essential for microtubule binding and unbinding of dynein. (Black outline schematic represents steps in dynein ATPase cycle skipped by dynein-Lis1)

In the presence of Lis1, metazoan dynein generates high persistent force (McKenney et al., 2010), suggesting dynein adapts to sustain high load. An *in vivo* evidence of high load adaptation of dynein-Lis1 came from the observation in rat cortical neurons where blocking Lis1 activity by a functional blocking antibody specifically hampered the transport of large lysosomes (>1 μm), while the transport of small-sized lysosomes remained unaffected (Yi et al., 2011). In contrast, Lis1 knockdown in mouse DRG neurons using siRNA against Lis1, blocked transport of many cargoes, including lysosomes, independent of the cargo size (Moughamian et al., 2013). Whether this difference in cargo-size-related Lis1 regulation arises due to the technique used to inhibit Lis1 activity in the two studies remains to be tested.

Furthermore, while Lis1 is essential for cargo transport in mammalian cells and in fungi, its interaction with dynein appears weak, and in some cases, specifically bound to mammalian dynein in ADP state (McKenney et al., 2010). Recently, Lis1 was suggested to remain bound to dynein under high load on lipid droplets isolated from cultured mammalian cells, although Lis1 was not directly imaged in this study (Reddy et al., 2016). Further *in vitro* characterization of dynein-Lis1 interaction is required using fluorescently tagged proteins to conclusively comment on the nature of their interaction.

Taken together, these observations suggest that Lis1 acts as an inhibitor of dynein motion, since it reduces the velocity and clamps dynein onto the microtubules. Furthermore, Lis1 was shown to be essential for dynein-driven transport of BicD2 positive cargoes in cells, however, the impact of Lis1 regulation on DDB motion has not been studied *in vitro*.

1.4 Dynein at microtubule plus ends

Dynein from diverse organisms have been observed to localise at the plus ends of dynamic microtubules (Table1) (Fujita et al., 2015; Han et al., 2001; Kobayashi and Murayama, 2009; Lenz et al., 2006; Ma and Chisholm, 2002; Schuster et al., 2011; Sheeman et al., 2003; Vaughan et al., 1999). The dynamic microtubule plus ends are important sites of dynein activity during cell division and dynein-driven transport. At plus ends, +TIPs have been suggested to promote the initial interaction of cargos with microtubules (Moughamian et al., 2013; Pierre et al., 1992; Vaughan et al., 2002). During cell division, dynein interacts with the plus ends of the cortical and kinetochore microtubules where its activity appears to be essential for spindle positioning (McGrail and Hays, 1997; Moore et al., 2009), chromosome alignment (Varma et al., 2008) and checkpoint protein removal (Griffis et al., 2007). Dynein is hypothesized to tether microtubule plus ends and exert a pulling force onto cortical microtubules for spindle positioning, which was also demonstrated *in vitro* by studying pulling of microtubule plus ends by bead or barrier immobilized dynein (Hendricks et al., 2012; Laan et al., 2012).

Mechanism of plus end localisation of dynein

There are two known molecular pathways by which dynein accumulates at the microtubule plus ends (Table 1): plus end transport by kinesin motors, and dynactin-dependent plus end tracking. Broadly, the major difference between the two pathways is that the former pathway involves a vectorial anterograde transport of dynein by plus end directed motor, while the latter involves recruitment of dynein from the cytoplasmic pool by +TIPs. However, mixed versions of these pathways also exist in some systems and will be discussed further in this section.

Table 1: Molecular players of dynein's plus end localisation in different organisms summarized from some of the *in vivo* studies (and two *in vitro* studies). +TIP dependent plus end tracking highlighted with grey, and in some systems, such as *Ustilago* and neurons, both plus end tracking and plus end transport of dynein has been reported.

Organism	Essential components of plus end localisation	References	Expected functions at plus ends
S. cerevisiae	Kip2,Pac1 & Bik1	(Carvalho et al. 2004; Lee et al. 2003; Sheeman et al. 2003)	Spindle positioning
	In vitro Kip2, Pac1,Bik1 & Bim1	(Roberts et al. 2014)	
S. pombe	Ssm4 (p150 homolog) Dynein predominantly on shrinking plus ends	(Fujita et al., 2015)	Nucleat migration
A.nidulans	KinA(Kinesin-1 homolog) & dynactin	(Han et al., 2001; Lenz et al., 2006; Xiang, 2000; Zhang et al., 2003;)	Nuclear positioning during hyphal growth & transport initation
U.maydis	Kinesin-1,dynactin &Lis1	(Lenz el al., 2006; Schuster et al., 2011)	Cargo loading & transport initation
	dynactin &EB1*	(Schuster et al., 2011)	
Mammalian Neurons	Kinesin-1 & Lis1	(Yamada et al., 2008)	Cargo loading & transport initation
	Dynactin, CLIP170 & EB1	(Lloyd et al. 2012; Lomakin et al. 2009; Moughamian et al. 2013; Moughamian & Holzbaur 2012; Nirschl et al., 2016)	
Non-neuronal Mammalian cells	Dynactin, Lis1, CLIP170 & EB1	(Coquelle et al., 2002; Splinter et al., 2012)	Spindle alingnment., Chromosome separation, & tranport initiation
	In vitro p150 fragment & EB1	(Duellberg et al. 2014)	

* A sub-population of dynein is maintained at plus ends by dynactin-EB1 dependent end tracking and another dynein pool is brought to plus end through transport by kinesin-1 in *U.maydis* (Schuster et al., 2011)

1.4.1 Plus end transport of dynein

In lower eukaryotes plus end accumulation of dynein is brought about by kinesin driven transport (Table 1) (Carvalho et al., 2004; Zhang et al., 2003). Evidence of kinesin-dependent plus end transport of dynein was observed in budding yeast where the necessary components were: Kip2 (Kinesin 7), Pac1 (Lis1), and Bik1 (Clip170) (Carvalho et al., 2004; Lee et al., 2003; Sheeman et al., 2003)). Further mechanistic

details of this pathway were elucidated through *in vitro* reconstitution using purified proteins (Roberts et al., 2014). Kip2 transported a dimeric yeast dynein fragment, where processive yeast dynein showed a tug-of-war with Kip2. To bias the net transport in plus end direction, Bim1 and Bik1 acted as the processivity factors for Kip2, while Pac1-Bik1 interaction connected dynein and Kip2 (Figure 1.14). Kinesin-dependent plus end transport of dynein has also been reported in *Aspergillus* (Egan et al., 2012; Lenz et al., 2006; Zhang et al., 2003). However, dynactin was required for its plus end transport, and although Lis1 did accumulate at plus ends, it was redundant for plus end tracking (Egan et al. 2012). Additionally, in DRG neurons kinesin-1 was reported to transport dynein to the plus ends in the presence of Lis1 (Yamada et al., 2008), where Lis1 was shown to act as a repressor of dynein motion to enable its effective plus end transport.

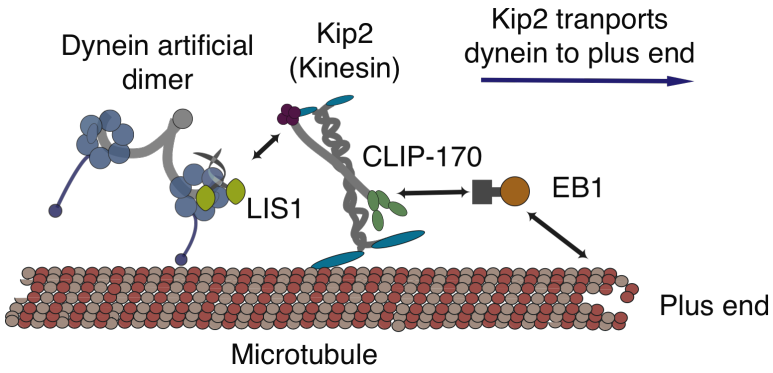

Figure 1.14 Plus end transport of yeast dynein

An artificial yeast dynein dimer is transported by the kinesin-7, Kip2 in the presence of the LIS1 homologue Pac1 and the CLIP-170 homologue Bik1. Additionally, the EB1 homologue Bim1 increases the processivity of plus end-directed Kip2-dependent dynein transport (Roberts et al., 2014). Picture taken from (Jha and Surrey, 2015).

1.4.2 Plus end tracking of dynein

A second pathway responsible for dynein's plus end accumulation requires dynactin and end binding proteins–EB1 and CLIP170. This pathway seems to be more prevalent in metazoans (Table 1). Several studies have established that the plus end tracking of dynein requires dynactin, CLIP170 and EB1 in neurons (Lloyd et al., 2012; Lomakin et

al., 2009; Moughamian and Holzbaur, 2012; Moughamian et al., 2013; Nirschl et al., 2016). However, both dynactin and Lis1 seems essential for dynein's plus end tracking in non-neuronal cultured cells (Coquelle et al., 2002; Splinter et al., 2012). Contradictory to this evidence, another study in non-neuronal cells suggested that dynein-dynactin localisation at kinetochore is independent of Lis1; instead, Lis1 requires dynein-dynactin for its plus end localisation (Tai et al., 2002). Whether the dependency of dynein and its regulator for their plus end localisation varies with the cell-type or in a cell-cycle-stage specific manner is not well understood.

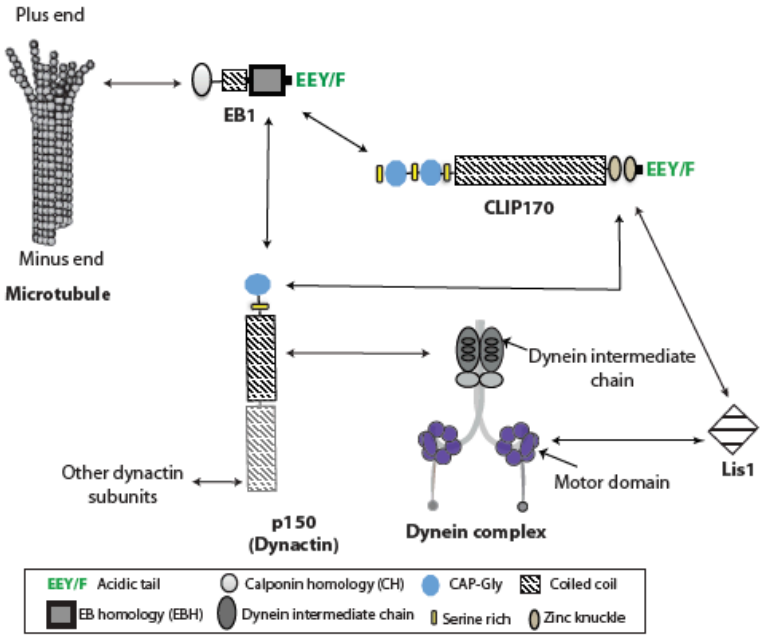

Figure 1.15 Plus end tracking of the recombinant human dynein complex

The human dynein complex interacts via dynein intermediate chain binds to the CC1 (coiled-coil1) of p150, the p150 CAP-Gly (SxIP-motif containing) domain interacts with EB1 (at EEY/F motif), the autonomous microtubule plus end binding protein that binds to the growing microtubule plus ends. In the presence of (other SxIP proteins) competitors for EB1 binding, p150 can also interact with EB1-recruited CLIP-170 (at EEY/F Zinc knuckle domain) where other SxIP proteins do not bind, thus providing an alternative interaction route for p150 and dynein (Duellberg et al. 2014). Picture taken from (Duellberg et al. 2014).

Furthermore, *in vitro* reconstitution study showed that the recombinant human dynein localises to the microtubule plus ends in the presence of EB1 and a fragment of p150 N-terminal 1-517($p150_{1-517}$) (Figure 1.15) (Duellberg et al., 2014). Additionally, in the presence of competing EB1 binding SxIP peptides, p150 interacted with CLIP170

recruited by EB1 at plus ends, thereby providing an alternate pathway for plus end localisation of dynein (Figure 1.15). However, a $p150_{1-517}$ fragment and the full-length p150 of the dynactin complex may show differences in their interactions with dynein and EB1 because to the folded conformation of the full-length p150. Whether the full-length p150 integrated to the dynactin complex can bind to EBs to track plus ends and recruit dynein to the plus ends remains to be studied. Moreover, Lis1 was not required for the plus end tracking of the recombinant human dynein. This could be because recombinant human dynein is naturally nonprocessive *in vitro* and does not require repression of motion by Lis1. On the other hand, in cells where dynein is processive, Lis1 was required for the dynactin-dependent plus end tracking of dynein (Coquelle et al., 2002; Splinter et al., 2012). Whether *in vitro* Lis1 is needed for plus end localisation of dynein in the presence of processivity factors remains to be tested.

To summarize, the plus end localisation of dynein involves two pathways: the vectorial transport by kinesin motors, which is well studied in lower eukaryotes and dynactin dependent plus end tracking studied in metazoans. *In vitro* reconstitution of plus end localisation of vertebrate dynein has identified EB1 and p150 fragment as necessary component (Duellberg et al., 2014), however, to fully grasp the mechanism of plus end tracking in physiological scenario, reconstitution with the full-length dynactin complex and Lis1 is required.

1.5 Initiation of dynein transport

In cells, dynactin and Lis1 have both been observed to play a role in initiation of dynein transport. The interaction of Lis1 and dynactin with CLIP170 seems to be crucial for loading dynein onto cargos at microtubule plus ends (Coquelle et al., 2002; Ligon et al., 2006; Pierre et al., 1992; Valetti et al., 1999; Vaughan et al., 1999). However, in mammalian cells, depletion of CLIP-170 had no effect on endosome movement (Watson and Stephens, 2006). Another study reported a site-specific regulation of initiation in neurons, where p150, specifically its CAP-Gly domain, was essential for initiation of Rab-positive and LAMP1-positive vesicle transport from the plus ends of distal neurites, while Lis1 was required for transport initiation along the entire length of

the axonal microtubule (Moughamian et al., 2013). Lis1 was also shown to initiate transport of endosomes and peroxisomes in *Aspergillus* (Lenz et al., 2006; Egan et al., 2012). Whether Lis1 is a constitutive initiator of dynein transport and p150 acts as an initiator only at plus ends remains to be studied.

Two recent reports have characterised the mechanism of dynactin dependent initiation of dynein transport *in vitro* (McKenney et al., 2016; Nirschl et al., 2016). Dynactin, especially its microtubule binding CAP-Gly domain, showed a preference for tyrosinated tubulin patches. The C terminal tail of alpha tubulin of freshly polymerized microtubule plus ends is tyrosinated (Janke, 2014), to which CAP-Gly proteins bind. Using recombinant yeast tubulin (lacks post-translational modification), McKenney et al., 2014, generated microtubule with fused stretches conataining detyrosinated and tyrosinated α tubulins. While purified metazoan dynein bound to either of the modified tubulin patches, the metazoan p150 of dynactin was specifically enriched on the tyrosinated patch. The DDB (dynein-dynactin-BicD2) motile events were higher on tyrosinated patches suggesting in the DDB complex, the CAP-Gly of dynactin binds to the tyrosinated plus ends ensuring the correct initiation of retrograde transport (McKenney et al., 2016). An *in vivo* evidence of this mechanism of CAP-Gly mediated initiation was observed in neurons where tyrosinated patches can be found at the tips of the neuritis (Nirschl et al., 2016); and p150's CAP-Gly domain is essential for initiation of vesicle transport in the neuritis (Lloyd et al., 2012; Moughamian and Holzbaur, 2012; Nirschl et al., 2016).

It is not known if similar tubulin modification is also required for Lis1-dependent initiation of dynein transport. Furthermore, while Lis1 was shown to be important for dynein driven transport of BicD2 positive vesicles in cells, whether, Lis1 acts as an initiator of transport of these vesicles was not studied.

1.6 Thesis goals

Regulation of metazoan dynein is complicated and involves several cofactors. The ubiquitous regulators of dynein dynactin and Lis1 seem to regulate overlapping dynein properties. *In vivo* both dynactin and Lis1 are essential for almost all dynein driven functions including plus end tracking of dynein (Coquelle et al., 2002; Splinter et al., 2012), and transport of BicD2 positive cargoes (Splinter et al., 2012). While *in vivo* studies have highlighted the essential nature of dynactin and Lis1 regulation, they fail to shed light on exactly what aspect of dynein transport requires dynactin and Lis1. *In vitro* reconstitution experiments using purified proteins have proved to be important in identifying dynactin and BicD2 as the minimal components of processive dynein motion, (McKenney et al., 2014; Schlager et al., 2014) and p150 and EB1 as components of dynein's plus end tracking (Duellberg et al., 2014). However, the experimental approaches used for these reconstitution experiments are different.

The reconstitution of end tracking of metazoan dynein was performed in the presence of p150 fragment and EB1 on dynamic microtubules, while the processivity factors—the full-length dynactin complex and adaptor protein—were absent in these experiments. On the other hand, the reconstitution of processive motion of metazoan dynein in the presence of the dynactin complex and adaptor BicD2 was reconstituted on static microtubules, which lacked the features of dynamic microtubule, and in the absence of EBs, hence no plus end tracking was observed. Therefore, these experiments did not provide an understanding of how dynein's plus end tracking versus processive motion is regulated by its key regulators and adaptor proteins. In this thesis, I study the simultaneous regulation of the processive behaviour and the plus end tracking of human dynein by dynactin, Lis1 and BicD2 in the presence of EBs on dynamic microtubules. My specific aims are:

1. **Modulation of processivity of recombinant human dynein**

   In this chapter, I report whether nonprocessive behaviour of recombinant human dynein arises due to various in experimental conditions such as, heterologous expression and design of the dynein constructs.

2. **Purification of dynactin complex and its functional verification in activating dynein motion.**

   Here I present a new purification method to purify non-neuronal human dynactin from cultured cells and neuronal dynactin from pig brains. Next, I test the activity of purified dynactin by reconstituting dynein-dynactin-BicD2 motion. The purified dynactin complex was used for the *in vitro* reconstitution studies presented in the following section.

3. **Regulation of plus end tracking versus minus end motion of human dynein studied on dynamic microtubules**

   Using purified proteins, I study the processive motion and plus end localisation of the recombinant human dynein complex simultaneously following *in vitro* reconstitution approach and TIRF imaging. I address the following:

   i. Reconstitution of processive motion of dynein on dynamic microtubules in presence on dynactin and BicD2
   ii. Reconstitution of plus end tracking of dynein-dynactin complex in presence of EB1
   iii. Effect of BicD2 on processive dynein motion versus microtubule end localisation of dynein
   iv. Effect of LIS1 on plus end tracking of dynein and initiation of its processive motion

Chapter 2. Modulation of processivity of recombinant human dynein

2.1 Introduction

For the long-range transport, dynein moves towards the microtubule minus end at a micron scale before detaching from the microtubules. This property is referred to as the average run-length or processivity. The first direct evidence of the processive behaviour of dynein was observed in a bead assay, where the movement of latex bead coated with purified chicken brain dynein was visualised by video-enhanced DIC microscopy (Wang et al., 1995). Thereafter, several studies reported the processivity of purified dynein from diverse sources ranging from fungi to vertebrate brains (Culver-Hanlon et al., 2006; King and Schroer, 2000; Mallik et al., 2005; Toba et al., 2006). Artificial dynein dimers from budding yeast (Reck-Peterson et al., 2006) and *Dictyostelium* (Numata et al., 2011) were also reported to exhibit processive behaviour. For budding yeast dynein, processivity is achieved due to its increased ratio of microtubule bound to unbound time (high duty ratio) of the individual motor domains. Unlike yeast dynein, *Dictyostelium* dynein dimer with a low duty ratio requires coordination between the two dynein motor heads for its processivity; this co-ordination is attributed to the C-sequence.

However, one of the surprising observations of dynein's processivity came from fluorescence imaging of recombinant human dynein, revealing a lack processivity (Trokter et al., 2012). Recombinant human dynein complex (McKenney et al., 2014; Schlager et al., 2014; Trokter et al., 2012) and artificially dimerised dynein motor fragments (Jha and Surrey, 2015; Nicholas et al., 2015; Torisawa et al., 2014; Trokter et al., 2012) showed weak microtubule binding with occasional diffusive or static binding episodes. This nonprocessive behaviour of human dynein observed in single molecule imaging is in apparent contrast with the processive behaviour of vertebrate dynein seen in bead assays and processivity of dynein from lower eukaryotes observed by direct fluorescence imaging.

At the commencement of the research detailed in this thesis, it was unknown whether the difference in processivity between dynein from lower eukaryotes and that from vertebrates reflected species-specific differences, or arose from assay-dependent variations. To this end, my first aim was to understand the reason behind the lack of processivity of recombinant human dynein motor.

One of the key differences in dynein studied from lower eukaryotes was the expression system used for the generation of the dynein constructs. While recombinant budding yeast dynein is expressed and purified from budding yeast (Reck-Peterson et al., 2006), recombinant human dynein constructs are generated through heterologous expression in insect cells (Schlager et al., 2014; Trokter et al., 2012). Therefore, I tested whether the lack of processivity of dynein arises due to its heterologous expression in insect cells. Furthermore, processivity of artificially dimerised yeast dynein required an intact linker domain (Reck-Peterson et al., 2006). Based on this, I tested if varying the length of the linker domain of artificially dimerised human dynein could alter its nonprocessive behaviour.

Around the same time, two other reports (Nicholas et al., 2015; Torisawa et al., 2014) also studied the molecular properties of dynein that could be responsible for the lack of processivity of the artificially dimerised metazoan dynein motor. The C-sequence present at the C-terminal end of DHC sequence (Nicholas et al., 2015), and auto inhibition of dynein (Torisawa et al., 2014) were subsequently suggested to be the reasons behind its nonprocessive behaviour. My experiments and these reports further corroborated the observation that metazoan dynein could inherently be nonprocessive.

In this chapter, to find out whether heterologous expression of dynein in insect cells caused the lack of processivity of dynein, I carried out a comparative study of budding yeast and human dynein motor fragments expressed and purified from insect cells. Next to verify if the truncation of dynein linker domain in artificially dimerised dynein motor leads to its nonprocessivity, I studied the dynein motor fragments of different linker lengths, by TIRF microscopy.

2.2 Results

2.2.1 Budding yeast dynein expressed in insect cells is a processive motor

To test whether heterologous expression of dynein in insect cells renders it nonprocessive, I expressed and purified artificially dimerised budding yeast dynein fragment from insect cells. Recombinant human dynein complex and artificially dimerised dynein fragments were also generated from insect cells by the same purification method. Since the processivity of budding yeast dynein is well established, it serves as a good control protein to check the effect of experimental conditions on processivity.

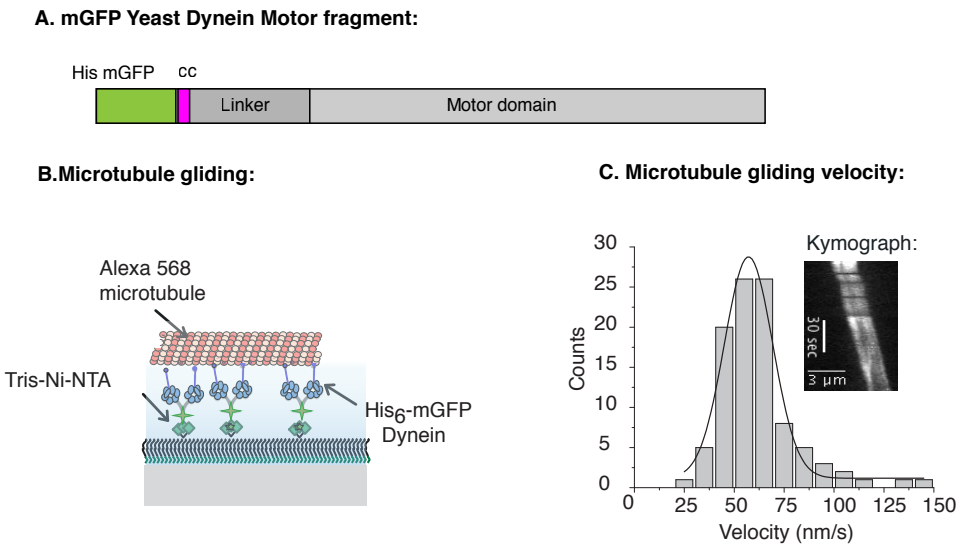

Figure 2.1 Ensemble activity of yeast dynein expressed in insect cells

(A) Construct design. An N-terminal His_6 tag followed by monomeric GFP (mGFP) (green), the neck coiled coil of kinesin-1 (CC, in pink) for dimerisation, and the budding yeast DHC sequence (grey) lacking the first 1218 amino acids (i.e. the tail). **(B)** Schematic representation of a microtubule gliding assay on Tris–Ni2+ -nitrilotriacetate(Ni-NTA)–PEG functionalized glass. 100 nM His_6 tagged GFP-cc-yeast Dyn_{331} motor was immobilized on to Ni-NTA surface, which produce ensemble activity to transport Alexa 568 labelled micrtotubules. **(C)** Histogram of microtubule gliding velocities (fitted with a Gaussian function; black line) and a representative total internal reflection fluorescence (TIRF) microscopy kymograph of gliding Alexa 568-labelled microtubule are shown. The mean gliding velocity ± s.e.m. was 57 ±0.8 nm/s). The experiment was performed at 25ºC. Image taken from (Jha and Surrey, 2015)

The yeast dynein construct (GFP-cc-yeast Dyn_{331}) was similar to the constructs used in the previous report (Reck-Peterson et al., 2006) and had DHC sequence without the tail domain (i.e. lacking the first 1218 amino acids), the N-terminal His_6 tag followed by monomeric GFP (mGFP), and the neck coiled-coil of kinesin-1 for dimerisation (Figure 2.1 A). After purification, the activity of yeast dynein was tested in a microtubule gliding assay. In this assay, the His-tagged dynein motors were immobilised on the Ni-Tris-NTA functionalised glass surface (Figure 2.1 B), allowing oriented attachment of motor that transported Alexa 568 microtubules present in solution, by their ensemble activity (Figure 2.1 C). The mean gliding velocity for GFP-cc-yeast Dyn_{331} was 57 nm/s (Figure 2.1 C), consistent with previously reported yeast dynein gliding velocities (Reck-Peterson et al., 2006).

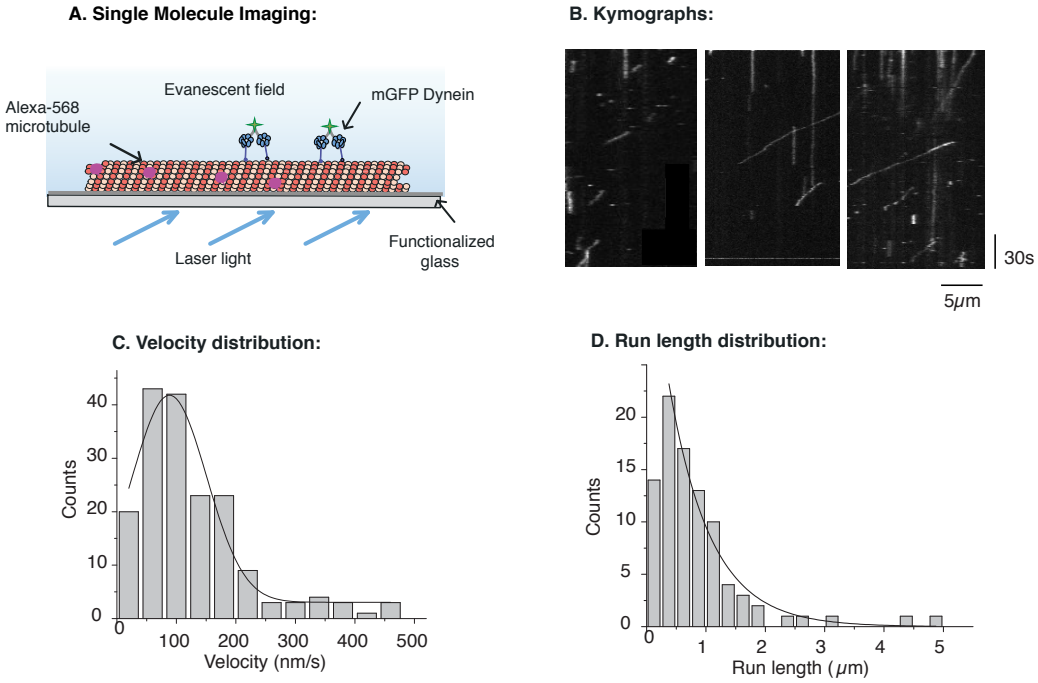

Figure 2.2 Single molecule imaging of yeast dynein expressed in insect cells

(A) Schematic representation of a single-molecule imaging assay with Alexa 568- and biotin-labelled GMPCPP microtubules immobilized via NeutrAvidin on biotin-PEG functionalized glass. **(B)** Kymograph showing processive runs of budding yeast dimers (100 pM GFP–cc-yeastDyn_{331} without the His_6 tag). **(C)** Histogram of velocities of single budding yeast dynein dimers moving along the Alexa 568-labelled microtubule (fitted with a Gaussian function; black line). The mean± s.e.m. velocity was 88± 6.6 nm/s. The run length distribution of single yeast dynein dimer (fitted with mono-exponential decay function; black line) is presented. The mean ±s.e.m. run length was 0.7 ±0.04 μm. The temperature was always 25◦C. Adapted from (Jha and Surrey, 2015)

Having tested the ensemble activity of GFP-cc-yeast Dyn_{331}, I set out to study its motile properties at the single molecule level to gain more insight into its processive behaviour. For this experiment, the N-terminal His_6 tag of GFP-cc-yeast Dyn_{331} was cleaved off. This protein was then imaged at 100 pM concentration on Alexa 568 labelled biotinylated GMPCPP microtubules that was immobilised via NeutrAvidin on the functionalised biotin glass surface (Figure 2.2 A). GFP-cc-yeast Dyn331, was indeed processive, as evident from the kymographs (Figure 2.2 B). Some long static binding episodes were also observed, perhaps due to the presence of dead motors, since dead motor removal by microtubule sedimentation was not performed in the purification procedure. Nonetheless, the mean velocity of moving GFP-cc-yeast Dyn_{331} was 88 nm/s (Figure 2.2 C), and the average run length was 0.7 μm (Figure 2.2D), consistent with previously reported measurements (Reck-Peterson et al., 2006).

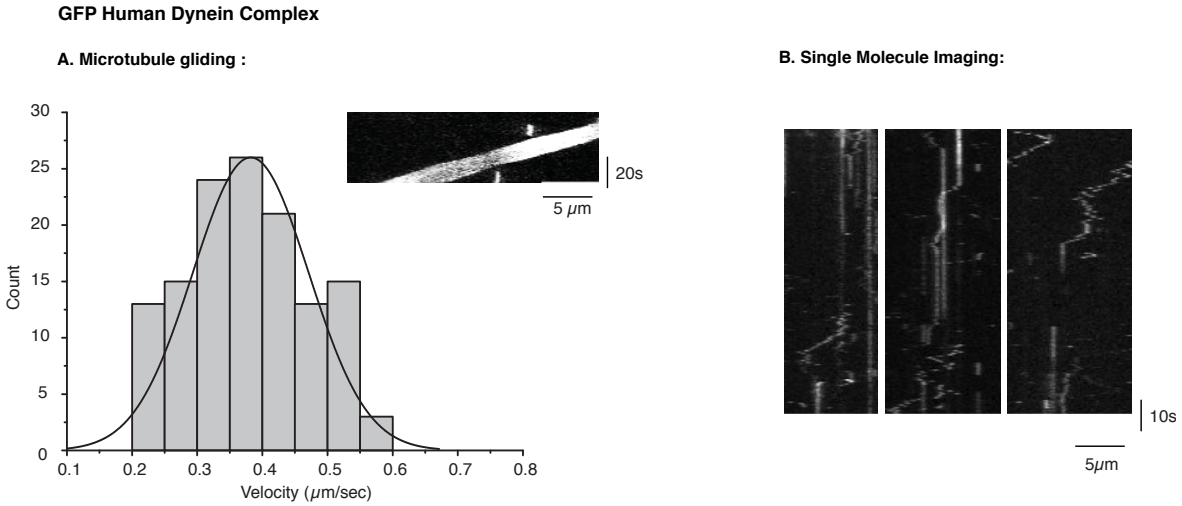

Figure 2.3 Single molecule imaging of recombinant human dynein complex expressed in insect cells

(A) Histogram of microtubule gliding velocities (assay as in Figure 2.1B) and corresponding representative kymographs as insets. The mean± s.e.m. was: 0.35±0.07 μm/s. **(B)** Representative TIRF microscopy kymographs of single molecule imaging of recombinant human dynein complex at 100 pM. (method as in Figure 2.2A).

Next, I studied the recombinant human dynein complex under the same imaging and buffer conditions as used for GFP-cc-yeast Dyn331. The recombinant human dynein

complex purified from insect cells could transport microtubules in gliding assay, consistent with the previously reports (Schlager et al., 2014; Trokter et al., 2012). When studied at single molecule level on immobilised GMPCPP microtubules, the recombinant human dynein complex showed diffusive and static binding behaviour without any detectable unidirectional motion, in agreement with the previous reports (Schlager et al., 2014; Trokter et al., 2012). The motile properties of artificially dimerised human dynein fragments, similar to GFP-cc-yeast Dyn331, were also studied under the same experimental conditions, discussed in the next section.

These observations indicate that yeast dynein retains its processive behaviour when expressed in insect cells, while human dynein produced in the same expression system is not processive.

2.2.2 Effect of varying linker lengths on motile properties of artificially dimerised human dynein

Since artificially dimerised human dynein motor (GFP-cc-Dyn380) is generated by truncation of DHC (Trokter et al., 2012), it is essential to define a minimal dynein motor with the right truncation, which retains most of the motile properties of dynein, such as, processivity. For yeast dynein, shortening of linker domain drastically affected its motile properties (Reck-Peterson et al., 2006). Based on this, I tested if varying the length of the linker domain of GFP-cc-Dyn380 could alter its nonprocessive behaviour. GFP-cc-Dyn380 studied previously (Trokter et al., 2012) had the DHC sequence from 1303 to 4646 amino acids. For this study, two additional constructs were generated by truncating DHC at amino acid 1330 and 1267 (Trokter et al., 2012) (Figure 2.4 A). I expressed and purified all these artificially dimerised dynein motor fragments from insect cells. Next, I studied the activity of these artificially dimerised dynein fragments in microtubule gliding assay. The gliding velocity observed for the three dynein fragments were in the range 0.3 to 0.38 μm/s (Figure 2.4 B) comparable to the previously reported velocities of mammalian dynein motor (McKenney et al., 2014; Schlager et al., 2014; Trokter et al., 2012). Furthermore, at the single molecule level, occasional static binding events were observed for all the three artificially dimierised dynein fragments (Figure 2.4 C). These results suggest that varying dynein linker length

by fifty-four amino acids did not lead to processive behaviour of artificially dimerised human dynein.

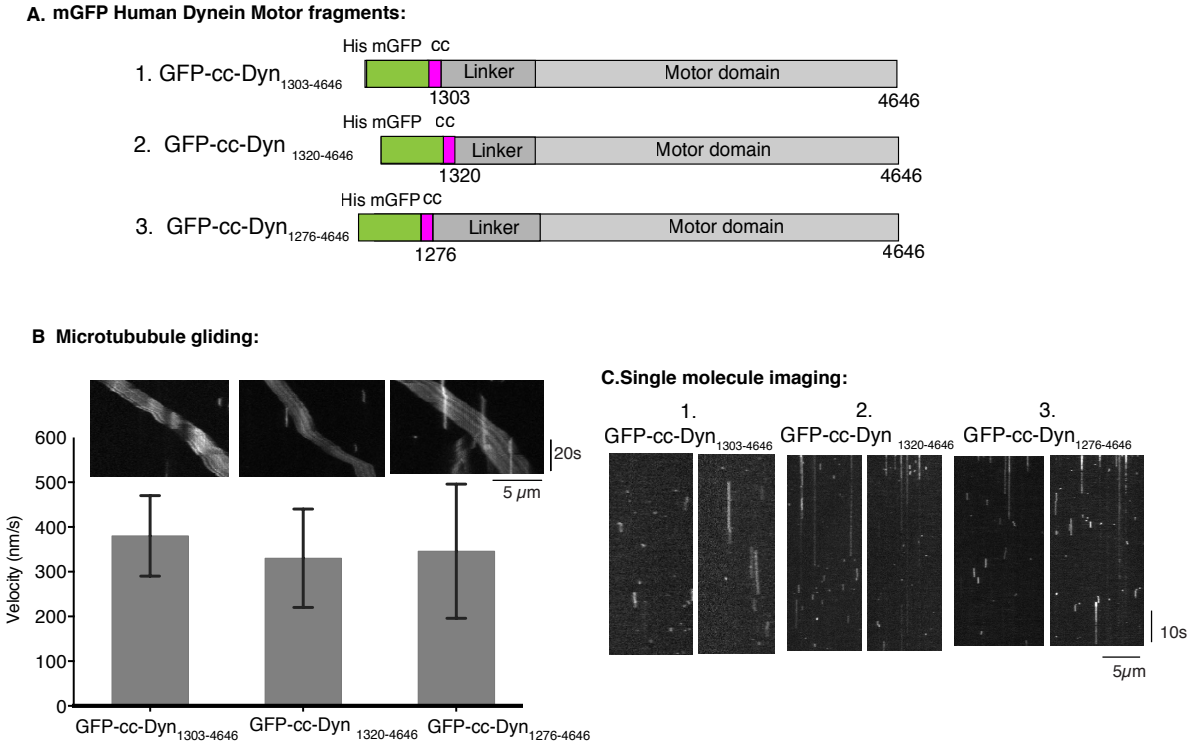

Figure 3.4 Effect of varying linker lengths on motile properties of artificially dimerised human dynein

(A) Construct designs. Three constructs with differently long N-terminal truncations were made, as indicated. The DHC amino acid sequence of the three constructs were: (1) 1303-4646 aa (2) 1320-4646 aa (3) 1276-4646 aa (B) Histogram of microtubule gliding velocities and corresponding representative kymographs as insets. The mean± sd. velocities were: 380±7.3 nm/s, 350±9.3 nm/s and 300±13.4 nm/s for constructs 1–3 respectively. (C) Representative TIRF microscopy kymographs of single dynein dimers at 50 pM concentration of each construct. None of the constructs showed detectable processive motility. These results demonstrate that the behavior of artificial human dimers does not depend on the exact position of the N-terminal deletions within the range of amino acids 1276–1320. The temperature was 25◦C.

2.3 Discussion

In this chapter, I validated that the heterologous expression and the design of the artificially dimerised motor constructs, specifically its linker length, did not contribute to the apparent lack of processivity of human dynein. Instead, the nonprocessive behaviour seems to be an intrinsic property the human dynein motor. In contrast, yeast dynein is a processive motor and retains its processive behaviour when expressed and purified from insect cells. Though the structure and sequence of the dynein motor are largely conserved between vertebrates and yeast, it is intriguing how its motile properties, particularly processivity is dissimilar.

Part of this difference could be explained by finer structural differences, such as the C-sequence, which is present at the C-terminal end of the dynein AAA+ ring, and has been suggested to be involved in the coordination of motor domains of *Dictyostelium* dynein, crucial for its processive stepping. For budding yeast dynein the c-sequence is three times shorter than *Dictyostelium* and mammalian dynein. Removal of the c-sequence from rat dynein did impart processivity to the motor (Nicholas et al., 2015). Though the mechanism by which the c-sequence could alter dynein's processive behaviour needs further elucidation. Another study revealed that artificially increasing inter-head separation of dynein's two motor heads by introducing random linker sequences resulted in the processive behaviour of artificially dimerised human dynein motor (Torisawa et al., 2014).

However, processivity achieved through deletion of c-sequence or by artificially increasing the motor head separation through artificial linkers does not represent the property of physiological dynein motor. Processivity of vertebrate dynein, therefore, seems to be a regulated property, activated upon attachment to cellular cargoes and by interaction with cargo adaptors and dynactin complex (McKenney et al., 2014; Schlager et al., 2014; Urnavicius et al., 2015)

Chapter 3. Purification of the dynactin complex and reconstitution of dynein motion in the presence of dynactin and BicD2

3.1 Introduction

Initially discovered as an activator of dynein motion (Schroer and Sheetz, 1991a), dynactin subsequently was shown to be a ubiquitous regulator of the dynein-driven cellular functions (Kardon and Vale, 2009; Schroer, 2004). For mammalian dynein, regulation by dynactin and cargo adaptor, BicD2 was recently shown to be essential for reconstitution of its processive motion (McKenney et al., 2014; Schlager et al., 2014; Urnavicius et al., 2015). Since the goal of my thesis is to study the regulation of multiple aspects of processive human dynein motion, purification of its essential regulator—dynactin—is necessary. Specifically, I set out to purify the human dynactin complex of matching species with human dynein and human dynein regulators in the *in vitro* reconstitution assays.

To my knowledge, large-scale purification of human dynactin has not established large-scale yet. This is possibly due to difficulty in obtaining sources from which large amounts of human dynactin could be isolated. Cultured human cells can be used as sources of human dynactin. However, due to low abundance of dynactin in these cell lines, large amount of starting material is required, making it challenging to apply pre-existing purification methods (Bingham et al., 1998; Urnavicius et al., 2015). These purification methods are designed to isolate dynactin from vertebrate brains (Bingham et al., 1998; Urnavicius et al., 2015), which have much higher levels of dynactin. The purification steps involve cycling brain lysate through multiple rounds of large-size ion exchange columns followed by several hours of sucrose gradient centrifugation. These purification steps would be difficult to scale-up[2] for enrichment of dynactin from large volumes of cell culture.

[2] Approximately 1 litre of cation exchange resin was used for dynactin enrichement from750ml brain lysate (Bingham et al., 1998). It will be difficult to build similar columns to load large volumes of cultured cell lysates.

Further, the purified brain dynactin has distinct subunit isoforms compared to other non-neuronal subunit isoforms (Dixit et al., 2008; Zhapparova et al., 2009). Therefore, assays with brain dynactin limit our understanding only to neuronal dynactin isoforms. In this regard, the purification of dynactin complex from non-neuronal cell lines also offers a possibility of observing if tissue specific differences exist in dynactin isoforms in the *in vitro* biochemical assays. Therefore, for my reconstitution experiments, I purified non-neuronal dynactin complex from HeLa S3 cell lines, and neuronal dynactin from pig brains.

In this chapter, I present a new two-step method to isolate dynactin from cultured human cells and pig brains. In the first step protein (BicD2) affinity matrix is used to enrich dynactin from high quantitates of cultured human cells. In the follow-up step anion exchange chromatography separates dynactin from non-specific proteins. The functional activity of purified dynactin can be studied by reconstituting dynein motion in the presence of essential processivity factors—dynactin and BicD2 (McKenney et al., 2014; Schlager et al., 2014). To this end, I reconstituted recombinant human dynein motion in the presence of purified dynactin complex and BicD2 fragment.

3.2 Results

3.2.1 Purification of dynactin complex

The first step in developing a purification method from HeLa S3 cells was to estimate the amount of starting material needed for isolation of milligram amounts of the dynactin complex. By quantitative western blot, using recombinant human p150 as a calibrating protein, I estimated that 300 l of HeLa S3 cell culture have 5 milligrams of the dynactin complex (Figure 3.1). The previous dynactin purification method (Bingham et al., 1998) documented a 25% recovery of initial dynactin pool present in brain tissues. Based on this recovery rate, I expected a yield of approximately 1 mg from 300 l of starting HeLa S3 cells. As previously mentioned (in section 3.1), enrichment of approximately 4 l of lysates, obtained from HeLa S3 culture will be difficult to attain using cation exchange chromatography. Therefore, a new approach was adopted to enrich or partially purify dynactin complex from such large volumes of

cells using protein affinity chromatography, followed by separation of dynactin from dynein and other contaminant proteins by anion exchange (Figure 3.1D).

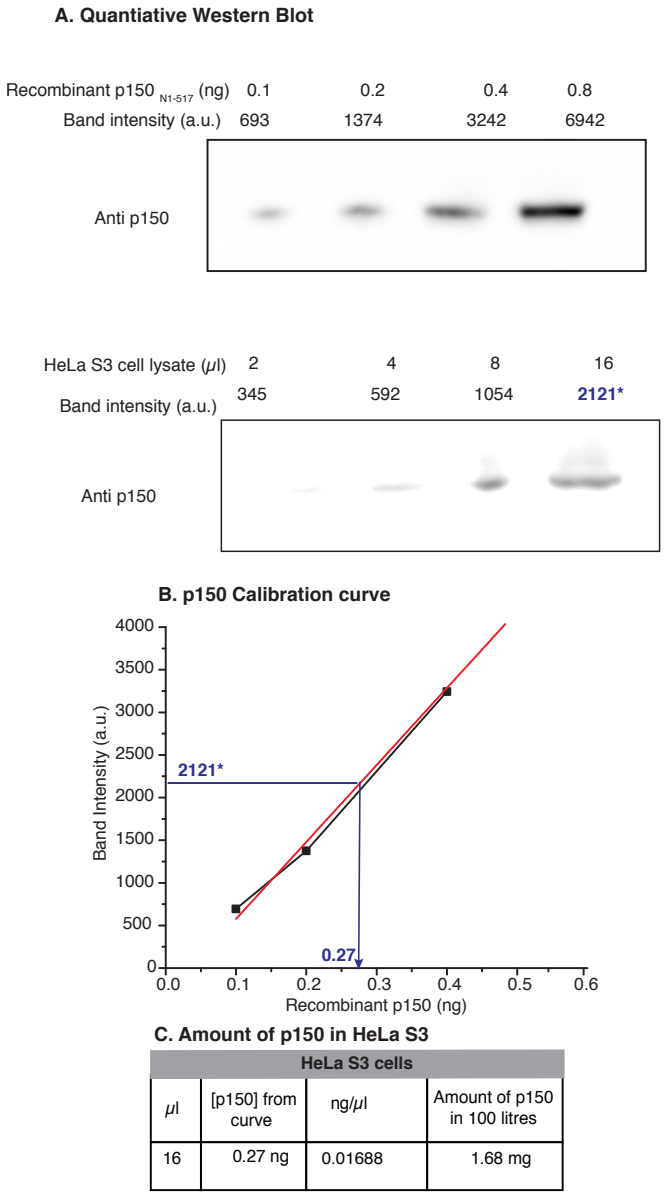

HeLa S3 cells			
µl	[p150] from curve	ng/µl	Amount of p150 in 100 litres
16	0.27 ng	0.01688	1.68 mg

Figure 3.1 Estimation of p150 amount in Hela S3 cells

(**A**) Quantiative western blotting: Dilutions of (0.1 ng to 0.8 ng) recombinant $p150_{1\text{-}517}$ and dilutions of known volume of HeLa S3 cell lysate were resolved in the same gel, followed by western blotting using the anti-p150 antibody. The band intensities were measured by band densitometry (intensities of band of the respective dilutions are mentioned on the top of the blots). (**B**) From the band intensities of dilutions of the recombinant p150 fragment, a calibration curve was generated. Based on the band density of 16 μl HeLa S3 cells the corresponding amount of p150 inferred (shown by the blue line). The red line shows the linear fit ($R^2 = 0.99$) **(C)** Calculation of amount of p150 (dynactin) in HeLa S3 cells based on the band intensity value labelled in blue.

3.1 D. Purification protocol overview

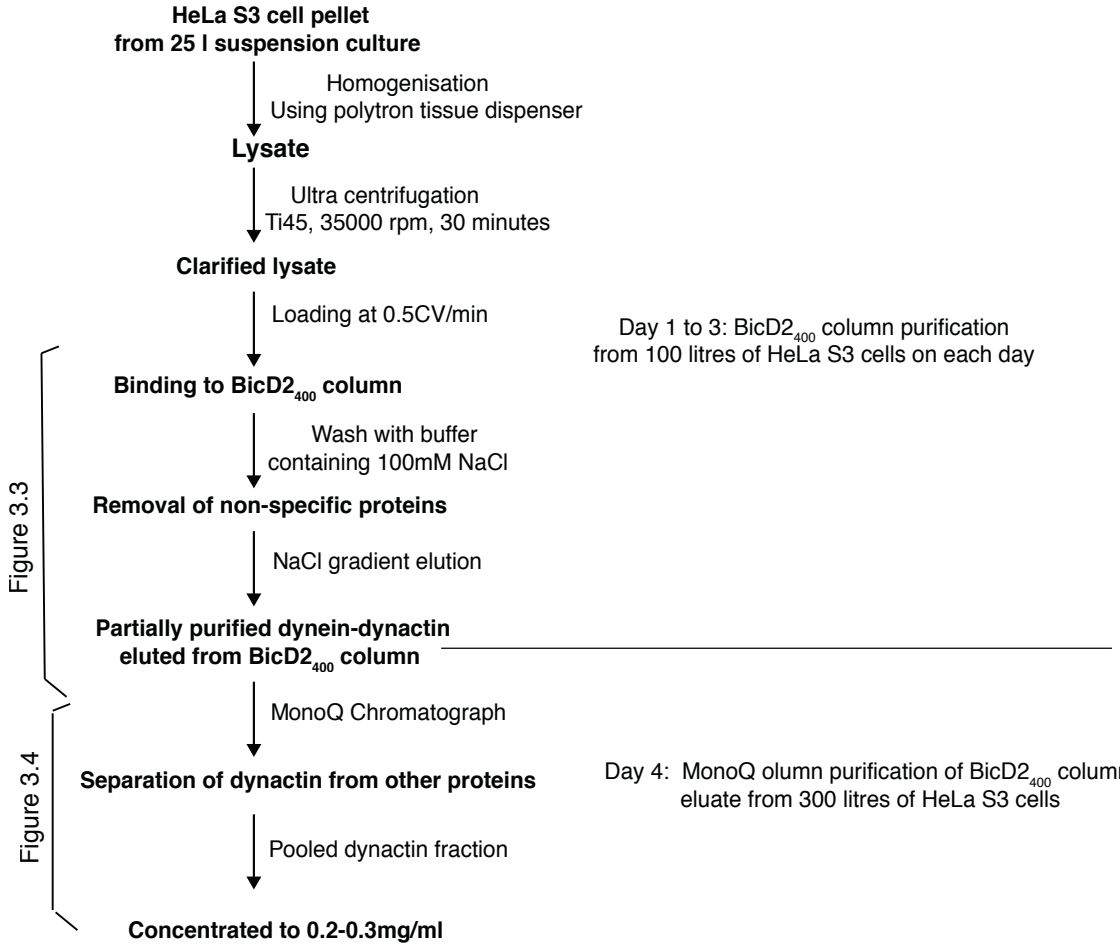

<u>BicD2$_{400}$ affinity column preparation</u>

The dynactin affinity purification method developed in this thesis, takes advantage of the interaction between dynein-dynactin complex with BicD2 (McKenney et al., 2014; Splinter et al., 2012). Based on this known interaction, I prepared a BicD2$_{400}$ affinity column by conjugating His$_6$ SNAP BicD2$_{400}$ (Figure 3.2 A and B) to an NHS (N-hydroxysuccinimide ester–activated Sepharose) column. The method followed for conjugating His$_6$ SNAP BicD2$_{400}$ to NHS matrix (described in the Methods chapter) was adapted from previously published technique (Widlund et al., 2012). Estimation of bound to unbound fraction of His$_6$ SNAP BicD2$_{400}$ indicated that at least 45 mg of protein conjugated to an NHS column of 5 ml column volume (Figure 3.2 C and D).

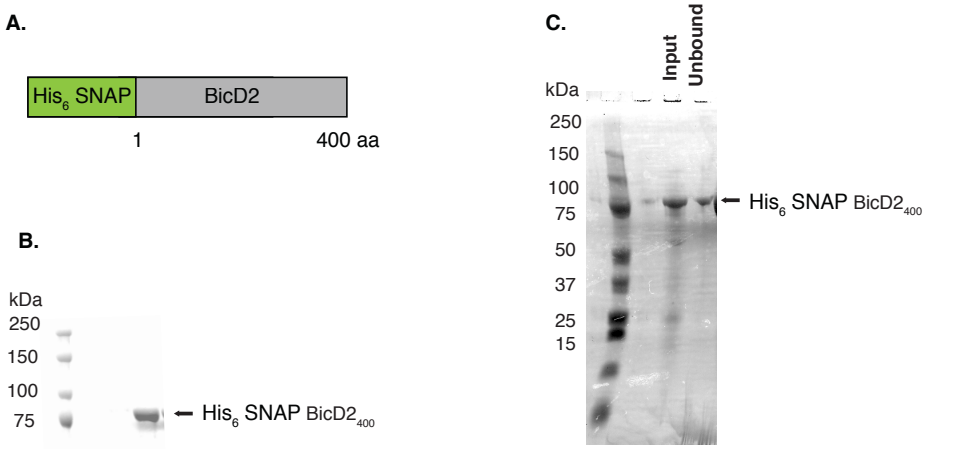

D.

Lane Intensity			% Conjugated to NHS column
Input	Unbound	Unbound:Input	
4614	2029	0.43 (43%)	57 % of total protein

Figure 3.2 Generation of BicD2$_{400}$ affinity column

(A) Molecular diagram of BicD2$_{400.}$ **(B)** Coomassie stained SDS PAGE of His$_{6}$-SNAP-BicD2$_{400}$ was expressed and purified from *E. coli* by one step IMAC purification. **(C)** Coomassie stained SDS PAGE of input material of His$_{6}$SNAP-BicD2$_{400}$ (Input) and unbound protein (Unbound) present in flow through after continuous circulation. **(D)** Input and Unbound lane intensity quantified from the Coomassie stained gel shown in C. Based on the intensity ratios, 43% of total protein did not conjugate to NHS column.

Purification of dynein-dynactin using BicD2$_{400}$ affinity column

HeLa S3 lysate from a cell pellet of 25 litres of culture was loaded onto one BicD2$_{400}$ column. Four such columns were used in parallel for purification from 100 l of Hela S3 cell culture. After loading, the column was washed extensively. This wash step removed weakly bound non-specific proteins. For final elution, I applied a linear salt gradient to resolve the separation of dynactin from other proteins. The elution profile revealed two major peaks. The Coomassie-stained gel from the fractions of the first peak showed that it was dynein enriched. The fractions of the second peak showed intense bands corresponding to the molecular weight of dynein and dynactin subunits (Figure 3.3). I collected and pooled the second peak (Figure 3.3A)—the dynein-dynactin enriched fractions (referred to as BicD2$_{400}$ column eluate hereafter) for the final round of purification.

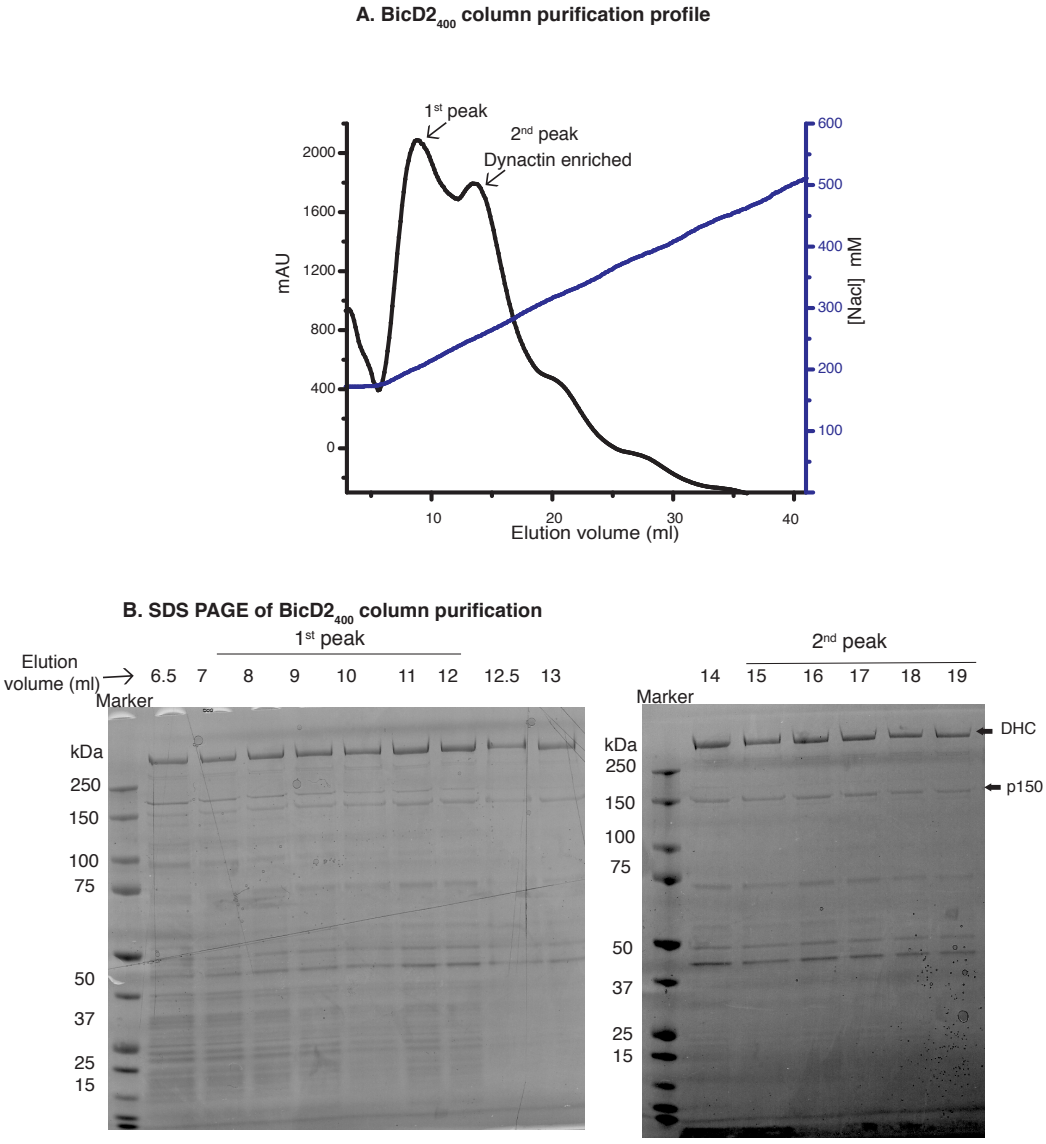

Figure 3.3 BicD2$_{400}$ affinity column purification from Hela S3 cells

(A) Elution profile (black curve) of BicD2$_{400}$ column purification by applying linear NaCl gradient (blue line). **(B)** SDS PAGE Coomassie stained gels of BicD2$_{400}$ column purification. Elution fractions from 6.5 ml to 19 ml elution volume were loaded on two separate gels. Molecular weights of the marker loaded are labelled on the left-hand side of the gels. The two peaks shown in purification profile are shown on top of the two gels. Positions of bands corresponding to dynein's DHC subunit and dynactin's p150 subunits are shown on the right-hand side of the second gel. Both the gels are from the same purification and were run in parallel.

Western blotting of BicD2$_{400}$ column eluate using antibodies against the p150 subunit of dynactin, and the DHC and DIC subunits of dynein confirmed the presence of dynein-

dynactin in purified fractions (Figure 3.4B). Five dynactin subunits and three dynein subunits were also identified by mass-spectrometry (Figure 3.4C). Analysis of band intensities corresponding to dynein-dynactin subunits in a Coomassie stained gel revealed that 69% of total proteins were subunits of dynein-dynactin complex (Figure 3.4A). The $BicD2_{400}$ affinity column generated for this purification was reused for multiple rounds of purification by washing the column extensively with high salt between each round.

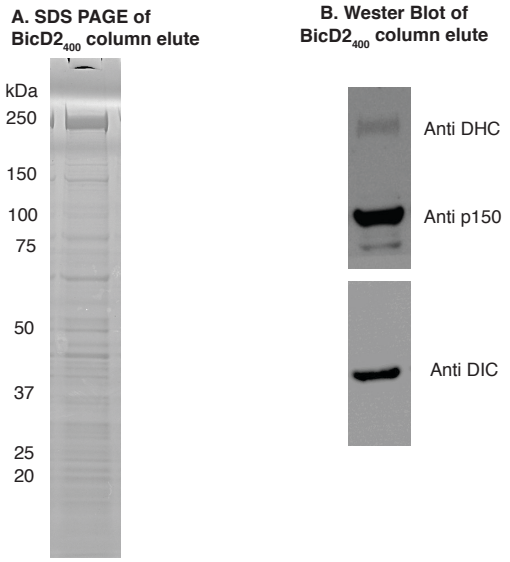

C. Mass-spectrometry analysis of $BicD2_{400}$ column elute

	Subunits	Accession Number	Unique peptide count	Sequence coverage (%)
Dynactin	p150	DCTN1_HUMAN	33	30
	p50	DCTN2_HUMAN	11	33
	Arp 11	ARP10_HUMAN	2	5
	ß actin	ACTB_HUMAN	4	11
	Arp 1	ACTR1A_HUMAN	5	11
Dynein	DHC1	DYHC1_HUMAN	173	40
	DIC2	DC1I2_HUMAN	13	21
	DLIC1	DC1L1_HUMAN	3	4

Figure 3.4 Identification of dynein-dynactin subunits in $BicD2_{400}$ column eluate

(A) SDS PAGE Coomassie stained gel of $BicD2_{400}$ column eluate. Bands from this gel were analysed by mass-spectrometry. **(B)** Western blotting of $BicD2_{400}$ column eluate, using antibodies against dynein's DHC and DIC and dynactin's p150 subunits. **(C)** Mass-spectrometry of $BicD2_{400}$ column eluate showing the presence of dynactin and dynein subunits. The percentage of sequence coverage and unique peptide picked up by LC/MS for each subunit is tabulated.

Separation of dynein-dynactin by anion exchange chromatography

The next step of purification involved the separation of dynactin from dynein and other non-specific proteins present in $BicD2_{400}$ column eluate. Due to their similar molecular mass, dynein and dynactin cannot be efficiently separated by size exclusion chromatography. However, the two complexes do exhibit a difference in their overall charge, making the separation by ion exchange chromatography possible. Anion exchange chromatography provided a good separation of dynactin from dynein in other purification protocols (Bingham et al., 1998; Urnavicius, 2015). Therefore, for my

second round of purification, I used Mono Q anion exchange column of 1ml column volume (Mono Q column) and eluted dynactin by applying a stepwise salt gradient, which was also used in other dynactin purifications (Bingham et al., 1998). $BicD2_{400}$ column eluate obtained from 300 l of Hela S3 cell culture was applied to Mono Q column. The first major peak at 320 mM NaCl was dynein containing peak (Figure 3.5), while dynactin eluted at a higher salt concentration (390 mM NaCl) (Figure 3.5). A total of 0.8 mg of dynactin complex was obtained from 300 l of HeLa S3 cell culture and was stored at 0.3 mg/ml concentration frozen in liquid nitrogen.

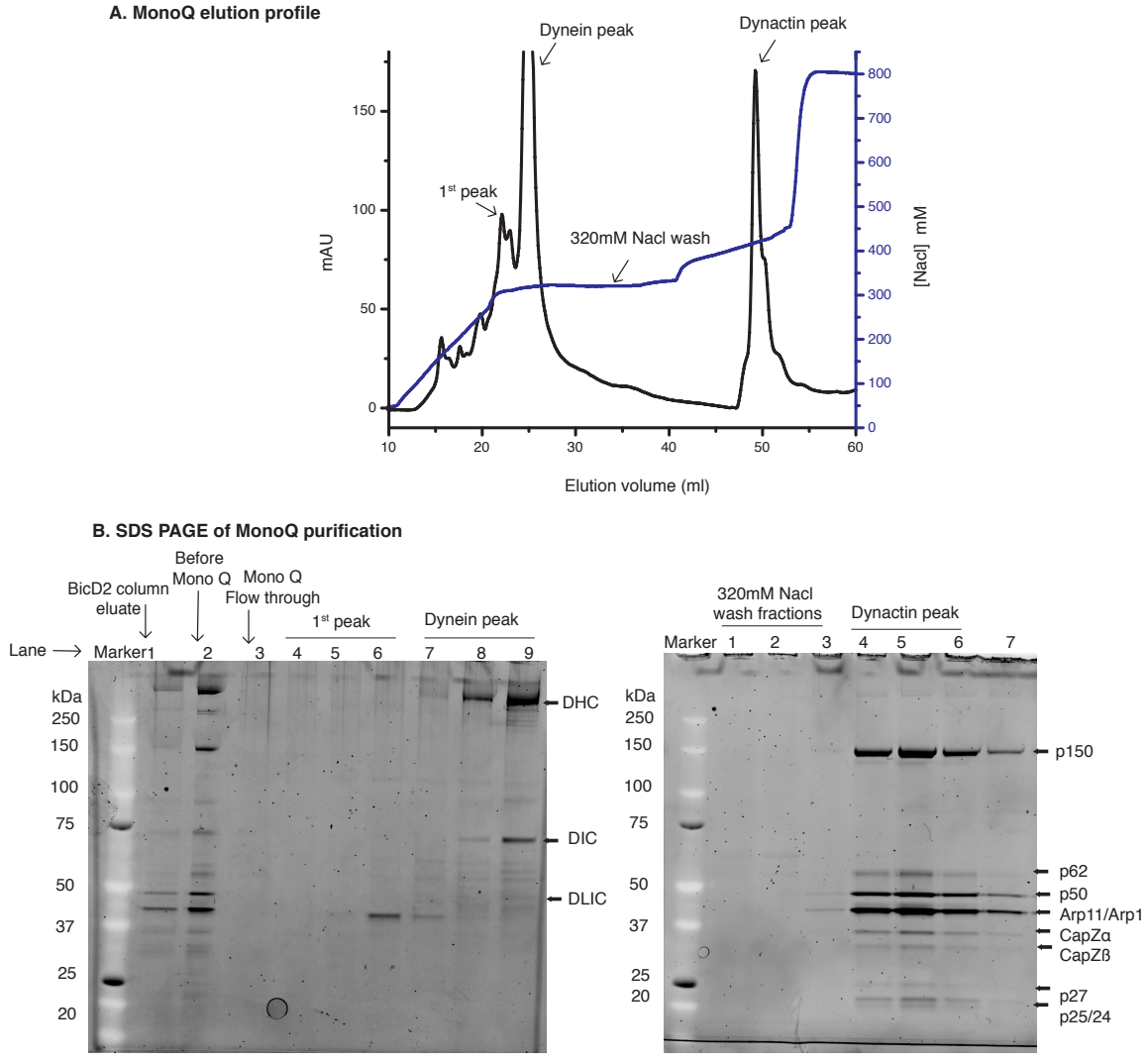

Figure 3.5 Dynactin purification by anion exchange chromatography

(A) Anion exchange chromatography using Mono Q 5/50HR column. Elution profile (black profile) shows a separation of dynein from dynactin by applying step-wise NaCl gradient (blue). **(B)** The peak fractions and the salt wash step labelled in the profile were loaded onto SDS PAGE gels and stained by SYPRO ruby. Bands corresponding to dynein subunits are marked on the right side of the first gel. Bands corresponding to dynactin subunits are marked on the right side of second gel.

The subunit composition of the purified dynactin was analysed by mass-spectrometry (Figure 3.6). All the eleven dynactin subunits were identified, indicating that human dynactin purified from Hela S3 cells is a complete dynactin complex (Figure 3.6B). Approximately 16% of the initially estimated dynactin amount was recovered from HeLa S3 cells using this two-step purification method. Band densitometry of the SYPRO ruby stained gel showed approximately 90% purity of human dynactin complex. Using the same method, the calculated molar ratio of subunit stoichiometry of dynactin subunit was, 2(p150): 1(p62): 4(p50): 11(Arp1+actin): 2(CapZα): 1(CapZβ): 1(p27): 2(p24+p25).

A.SDS PAGE of purified dynactin

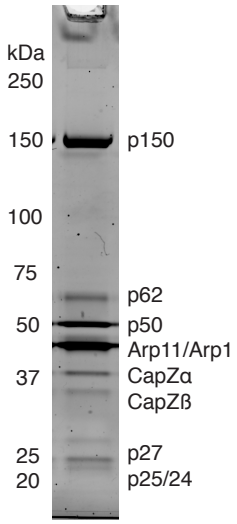

B. Mass-spectrometry analysis of purified dynactin subunits

Dynactin Subunits	Accession Number	Unique peptide count	Sequence coverage (%)
p150	A8MWX9_HUMAN	58	46
p50	DCTN2_HUMAN	21	52
p62	DCTN4_HUMAN	11	21
p24	DCTN3_HUMAN	11	45
p25	DCTN5_HUMAN	8	42
p27	DCTN6_HUMAN	2	9
Arp 1α	ACTZ_HUMAN	17	47
Arp 1ß	ACTY_HUMAN	7	43
Arp 11	ARP10_HUMAN	18	34
ß actin	ACTB_HUMAN	16	42
CapZß	B2R7T8_HUMAN	16	48
CapZα	CAZA1_HUMAN	12	35

Figure 3.6 Identification of dynactin subunits by mass-spectrometry

(A) SDS PAGE Coomassie stained gel of purified human dynactin complex. Bands corresponding to dynactin subunits are marked on the right side of second gel. **(B)** Mass-spectrometry of purified human dynactin complex showing the presence of all the dynactin subunits. The percentage of sequence coverage and unique peptide picked up by LC/MS for each subunit is tabulated. Except p27 subunit the sequence coverage of each the band was above 34% presenting a strong evidence of purification of complete dynactin complex.

Purification of neuronal dynactin complex from pig brains

Further, for the comparison of neuronal and non-neuronal dynactin in the *in vitro* reconstitution experiments, I also purified neuronal dynactin from pig brains using the BicD2 affinity purification method (Figure 3.7). The clarified lysate (100 ml) from two pig brains was then applied to one $BicD2_{400}$ column (Figure 3.7 A and B). The loading, wash and elution from $BicD2_{400}$ column were done following the same procedure as describe for dynactin purification from HeLa S3 cells. The $BicD2_{400}$ column eluate was loaded on the MonoQ column for separation of dynactin from other proteins. Stepwise salt gradient was applied to isolate dynactin (Figure 3.7.C). Approximately a total of 0.2 mg of dynactin was obtained from two pig brains and was stored at 0.2 mg/ml frozen in liquid nitrogen. Thus, the purification method described in this chapter can be used to purify neuronal and non-neuronal dynactin from brain tissues and cultured mammalian cells.

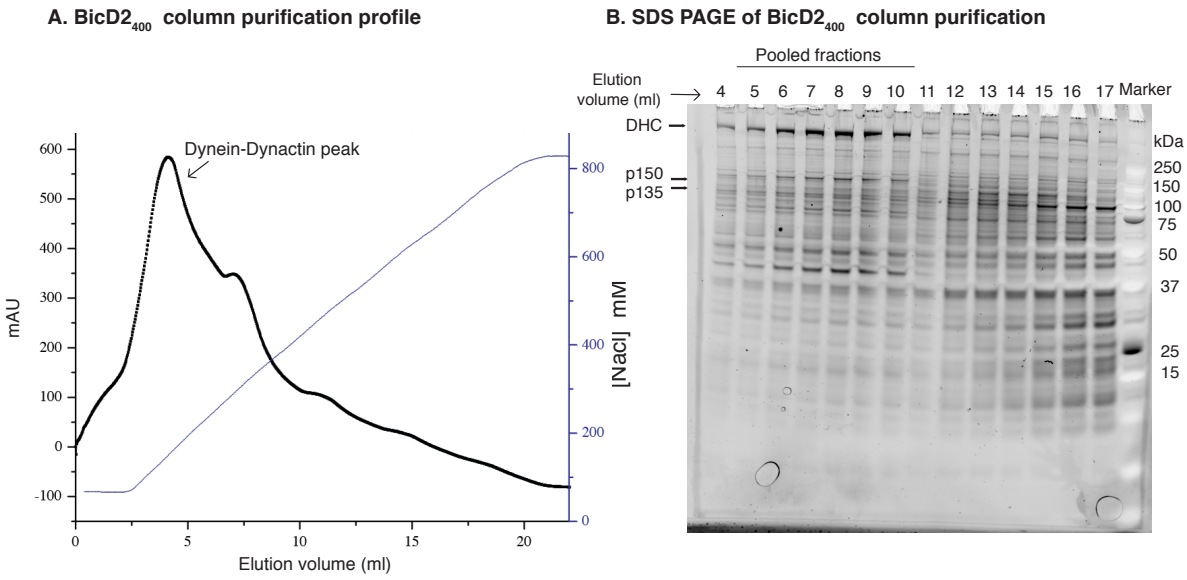

Figure 3.7 Purification of neuronal dynactin complex from pig brains

(A) Elution profile (black curve) of $BicD2_{400}$ column purification of pig brain dynactin by applying linear NaCl gradient (blue line). **(B)** SDS PAGE Coomassie stained gel of $BicD2_{400}$ column purification. Elution fractions from 4 ml to 17 ml elution volume were loaded on gel. Molecular weights of the marker loaded are labelled on the right side of the gels. The positions of bands corresponding to dynein's DHC subunit and dynactin's p150 and p135 subunits are shown on the left side of the gel. The fractions pooled and processed in the next round is indicated on top of the gel.

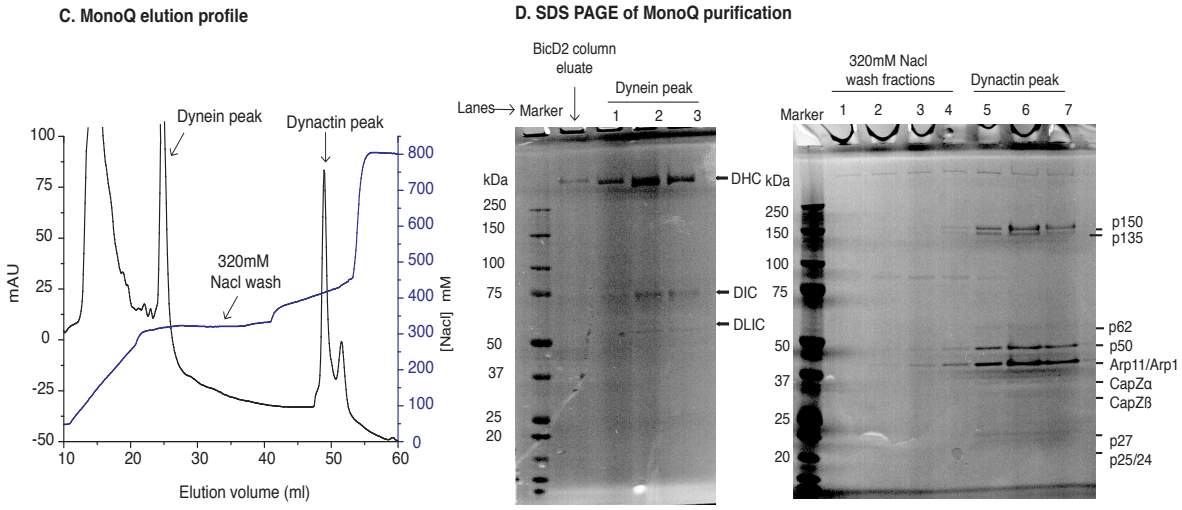

Figure 3.7 Purification of neuronal dynactin complex from pig brain

(C) Anion exchange chromatography using Mono Q 5/50HR column. Elution profile (black profile) shows a separation of dynein from dynactin by applying step-wise NaCl gradient (blue). **(D)** The peak fractions and the salt wash step labelled in the profile was loaded onto SDS PAGE gel and stained by Coomassie. Bands corresponding to dynein subunits are marked on the right side of the first gel. Bands corresponding to dynactin subunits are marked on the right side of second gel. Both the gels are from the same purification and were run in parallel.

3.2.2 Functional test of purified dynactin complex: reconstitution of dynein-dynactin-BicD2 motion.

The recent *in vitro* reconstitution of processive vertebrate dynein motion using dynactin and cargo adaptors offers a direct assay to test the activity of purified dynactin (McKenney et al., 2014; Schlager et al., 2014). The attachment of full-length dynactin complex to mammalian dynein via cargo adaptor $BicD2_{400}$ was essential for processive dynein motion. Therefore, to test the activity of purified dynactin complex, I studied the processive motion of GFP recombinant human dynein in the presence of purified human dynactin complex and recombinant $BicD2_{400}$ fragment on GMPCPP stabilised microtubules, by TIRF imaging (Figure 3.8 A).

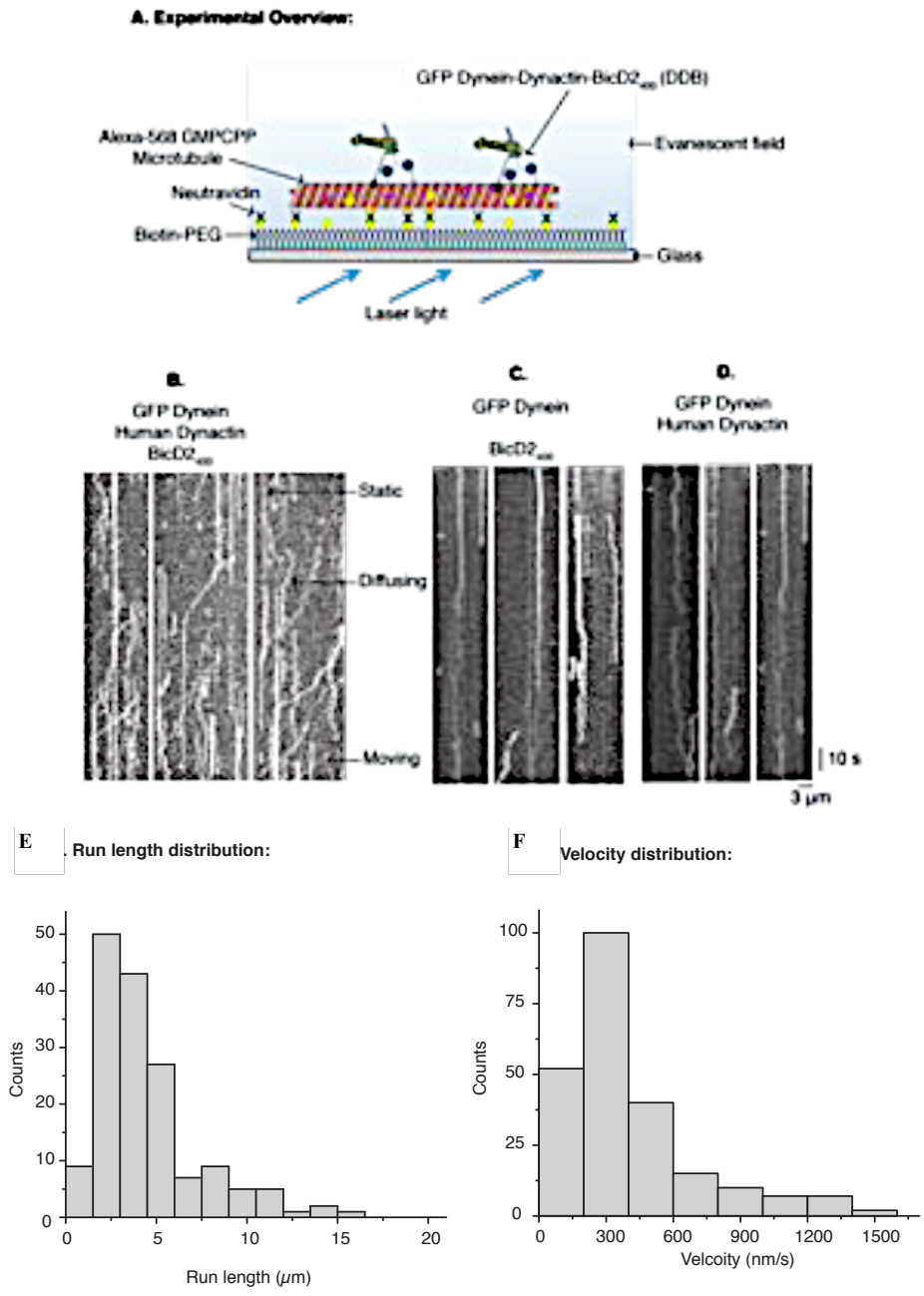

Figure 3.8 Reconstitution of DDB motion on stabilised microtubules

(A) Schematic overview of a TIRF imaging. 1 nM GFP tagged recombinant human dynein, 2 nM purified human dynactin complex, and recombinant 20 nM $BicD2_{400}$ (DDB) is studied on Alexa 568 labelled biotinylated GMPCPP stabilised microtubules immobilized via NeutrAvidin on biotin-PEG functionalized glass Imaged at 25ºC. **(B)** Kymographs showing DDB events. **(C)** Kymographs showing diffusive or static binding dynein events when dynactin is absent. **(D)** Kymographs showing diffusive or static binding events when in the absence of $BicD2_{400}$. **(E)** Run length distribution of processive DDB. The average run length ± s.e.m was 4.47± 0.23 μm (n =159 complexes). **(F)** Histogram of velocity distribution. The mean velocity ± s.e.m 406.36 ±19.30 nm/s (n=233 segments)

Consistent with previous findings (McKenney et al., 2014; Schlager et al., 2014), processive GFP dynein motion was observed only in the presence of purified dynactin complex and $BicD2_{400}$ (Figure 3.8.B). Removal of purified dynactin complex (Figure 3.8.C) or $BicD2_{400}$ (Figure 3.8.D) from this assay resulted in diffusive or static binding of GFP dynein, highlighting the crucial role of dynactin as a processivity factor. Three types of behaviour were observed for DDB in this assay, static binding, diffusion, and processive motion (for analysis see Methods). For processively moving DDB complexes, run lengths and velocities were measured and plotted as a histogram. The average velocity of moving DDB was 406.36 nm/s, and the mean run length was 4.5 μm agreeing with the ultra processive behaviour of DDB complex reported in earlier studies(McKenney et al., 2014; Schlager et al., 2014).

To conclude, full-length dynactin complex could be successfully purified from cultured mammalian cells and pig brains by BicD2 affinity purification method. The addition of the purified human dynactin, together with $BicD2_{400,}$ resulted in processivity of GFP-tagged human dynein, indicating that purified dynactin is functionally active.

3.3 Discussion

In this chapter, I presented a new method of purification of dynactin complex from HeLa S3 cells and pig brains. This is the first large-scale purification of non-neuronal human dynactin complex. Due to low abundance of dynactin in non-neuronal cells, a high amount of staring material was required. Using BicD2 protein affinity matrix, dynactin from large volumes of starting material, which would be difficult to process following previously described techniques (Bingham et al., 1998; Urnavicius, 2015). In this method, the recovery of dynactin (16%) was lower than the recovery reported for published methods (25%). However, compared to another protein-affinity based dynactin purification, such as microtubule affinity purification, with 2% recovery (Bingham et al., 1998), this method provides a much higher recovery. Furthermore, purification of dynactin from cultured cells by microtubule affinity would require large amounts of purified tubulin, which cannot be reused.

The BicD2 affinity purification method also offers a faster and less labour-intensive purification of brain dynactin compared to the previous protocols. Further, a single $BicD2_{400}$ affinity column is used for multiple rounds of purifications, since $BicD2_{400}$ is covalently conjugated to the NHS resin, providing a long-lasting reusable purification matrix unlike microtubule affinity purification method. For the affinity purification of dynactin, I tested only $BicD2_{400}$ fragment as affinity matrix for dynactin enrichment, however, in the future other dynactin interactors could be tested to try to further improve the yield of the affinity purification step.

Another advantage of developing a purification of dynactin from cultured cells is that it offers a system to genetically manipulate dynactin complex. In the future, using this method fluorescent dynactin complex can be generated from cell lines overexpressing a fluorescently tagged dynactin subunit. By tagging p62 subunit of dynactin in human cell line (McKenney et al., 2014) fluorescently labelled dynactin complex was co-purified with dynein and BicD2 complex in small quantities. The method presented in this chapter could be used to purify fluorescent dynactin from similar sources in large quantities.

Chapter 4. Regulation of processive motion and microtubule plus-end localisation of dynein

4.1 Introduction

Although dynein is a minus end directed motor, it also localises to the plus ends of microtubules (Kardon and Vale, 2009; Splinter et al., 2012; Zhang et al., 2003). The dynamic plus ends of microtubules are thought to serve as sites for cargo loading (Vaughan et al., 2002) and initiation of minus end directed dynein transport (Lloyd et al., 2012; Moughamian and Holzbaur, 2012). The key dynein regulators—dynactin and Lis1—appear to play a crucial role in both recruitment of dynein to plus ends and regulation of its minus end motion (Kardon and Vale, 2009; Splinter et al., 2012). However, the extent to which these two regulators control dynein's plus end recruitment versus its minus end motion remains unclear (Splinter et al., 2012). In this chapter, I investigate the role of human dynein regulators in controlling processive motion versus plus-end tracking of dynein on dynamic microtubules.

Metazoan dynein is recruited to microtubule plus ends through its interaction with the microtubule plus-end binding proteins (+TIPs)—dynactin and EBs (Duellberg et al., 2014; Moughamian and Holzbaur, 2012). For this pathway, the largest dynactin subunit p150, forms the hub of interaction sites, mediating interactions with EBs via its CAP-Gly domain (Moughamian and Holzbaur, 2012; Vaughan et al., 2002), and with the dynein intermediate chain via its CC1 domain (King and Schroer, 2000; Schroer, 2004; Vaughan and Vallee, 1995). Extensive *in vitro* characterisation of both neuronal and non-neuronal p150 fragments have provided information about its interaction with other +TIPs (Duellberg et al., 2014), its role as an anti-catastrophe factor and a microtubule nucleator (Lazarus et al., 2013). However, *in vitro* evidence of the plus-end tracking behaviour of the full-length dynactin complex or the dynein-dynactin complex is lacking. This is important to study, given the recent structural findings of the full-length dynactin complex, where the p150 subunit possibly assumes a folded/auto-inhibited conformation and has a weak binding to dynein and microtubules (Chowdhury et al., 2015; Urnavicius et al., 2015). It is unknown if in this conformation the dynactin

complex can recruit dynein to the microtubule plus ends, or whether additional cofactors are required to promote the dynein-dynactin-EB interaction at plus ends.

While *in vitro,* the p150-dependent plus end tracking of vertebrate dynein can persist in the absence of Lis1 (Duellberg et al., 2014), it is intriguing why both dynactin and Lis1 are involved in dynein's plus end targeting in non-neuronal cultured cells (Coquelle et al., 2002; Splinter et al., 2012). More generally, how dynactin and Lis1 may function together to target dynein to the plus ends remains unclear. Lis1 was shown to facilitate the dynein-dynactin interaction during mRNA transport in *Drosophila* extract (Dix et al., 2013) and for spindle formation in *Xenopus* egg extract (Wang et al., 2013), indicating a combinatorial role of dynactin and Lis1 in dynein regulation. For a processive yeast dynein, Lis1 biases its plus-end localisation by impeding the minus-end directed dynein motion (Roberts et al., 2014; Sheeman et al., 2003). For a non-processive metazoan dynein the inhibition of minus-motion was not required in the plus end tracking experiments. Lis1 could conceivably be important for metazoan dynein's plus-end tracking in cells where dynein processivity is activated by dynactin and BicD2 (Coquelle et al., 2002; Splinter et al., 2012). Direct evidence of such a combinatorial regulation of dynein's microtubule localisation is lacking.

Both in cells and *in vitro*, the dynactin(or p150)—dependent plus-end association of dynein does not require additional stabilisation of their interaction by adaptor protein BicD2 (Splinter et al., 2012; Duellberg et al., 2014). On the contrary, expression of the $BicD2_{400}$ fragment in mammalian cell lines abolished dynein localisation at the microtubule tips (Splinter et al., 2012). Similarly, in budding yeast, expression of a fragment of Num1 adaptor protein led to the removal of dynein-dynactin from the plus ends (Lammers and Markus, 2015). These observations point to a unique 'switch like' function of adaptor proteins, where they appear to remove dynein's plus-end localisation by activating the dynein–dynactin motion away from the plus ends. Although this potential switching mechanism of adaptor proteins has not been probed directly.

Another important function of dynein regulators at the microtubule plus ends is to initiate dynein transport. Deletion of the CAP-Gly domain of p150 caused a significant reduction of initiation of retrograde transport of LAMP1 and Rab5 positive vesicles in distal neuritis, while the transport along the axonal length was unaffected. (Lloyd et al.,

2012; Moughamian and Holzbaur, 2012). Instead, Lis1 seems to be crucial for initiation of dynein transport along the entire length of axonal microtubules (Moughamian et al., 2013). Lis1-dependent initiation of dynein transport was also observed for dynein in filamentous fungi (Egan et al., 2012; Lenz et al., 2006). It is unclear whether Lis1 and/or dynactin based initiation operates only for a subset of dynein cargos or is a general mechanism of initiation of dynein-driven transport.

What is the molecular mechanism by which dynein regulators control dynein's plus end localisation versus its processive minus end motion on dynamic microtubules? How is dynein motion initiated at the microtubule plus ends? To address these questions, I study the regulation of the recombinant human dynein complex by dynactin, EBs, Lis1 and BicD2 on dynamic microtubules following an *in vitro* reconstitution approach. This allows simultaneous investigation of human dynein motility and microtubule plus end tracking in the same assay. First, I reconstituted and characterised processive motion of recombinant human dynein on dynamic microtubules. Next, using the purified dynactin complex and EBs, I studied the plus end tracking behaviour of dynein in a dynamic microtubule assay. Finally, I investigated the combined effect of dynactin, BicD2 and Lis1 on the plus end localisation of dynein and in the initiation of its motion.

4.2 Results

4.2.1 Reconstitution of DDB motion on dynamic microtubules

In vitro studies of the motile properties of vertebrate dynein have only been performed on stabilised microtubules (McKenney et al., 2014; Schlager et al., 2014; Trokter et al., 2012). In cells, however, dynein transport occurs on the dynamic microtubule filaments, which can influence dynein's microtubule localisation and its motile behaviour. To characterise the motile properties of dynein on these constantly growing and shrinking tracks, I reconstituted the motion of recombinant human dynein, in the presence of dynactin and BicD2 (DDB) in a dynamic microtubule assay. The experimental

conditions used to study DDB motion on static microtubules were not compatible with the dynamic microtubule assay conditions. First, while DDB motion on static microtubules requires one type of nucleotide (ATP), studying DDB motion on dynamic microtubules required two types of nucleotides: GTP for microtubule dynamics and ATP for powering DDB motion. Second, the DDB motion on static microtubules has been studied at 25ºC, whereas the dynamic microtubule assay is generally performed at 30ºC (suitable for microtubule growth). The microtubule lattice of dynamic microtubules was also different from the stabilised GMPCPP microtubule tracks used for DDB motion in the previous studies Therefore the first step was to establish the right buffer and imaging conditions that allowed both microtubule growth and DDB motion.

In the presence of 17.5 μM tubulin (with 10% Alexa 568 labelled tubulin), microtubules were grown from the immobilised Alexa 568 labelled GMPCPP stabilised short microtubule stretches (GMPCPP seeds) (Figure 4.1A). These growing microtubules served as dynamic tracks for DDB motion. Two-colour TIRF imaging of GFP-tagged dynein and Alexa 568 labelled tubulin allowed simultaneous visualisation of the DDB motion and microtubule growth (Figure 4.1 B and C).

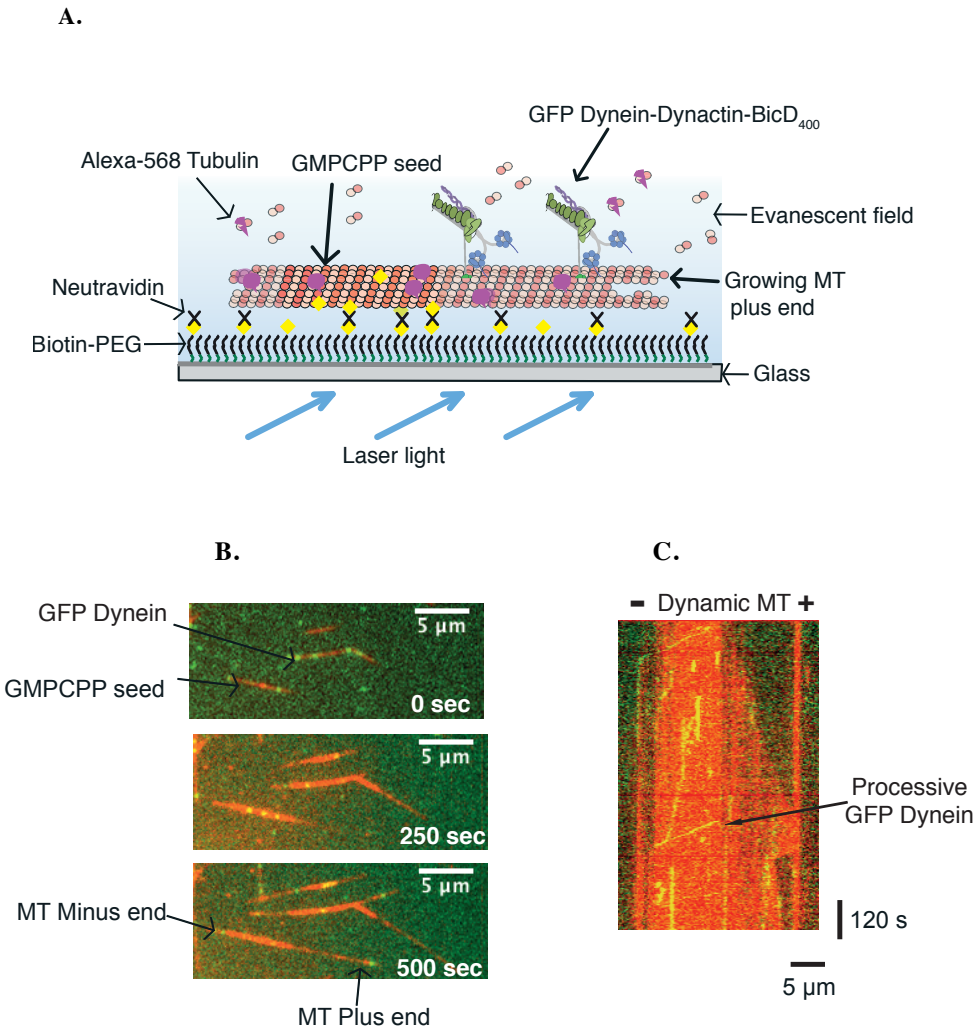

Figure 4.1 Reconstitution of Dynein motion on dynamic microtubule

(A) Schematic overview of TIRF imaging. GFP-dynein-dynactin-BicD2$_{400}$ complexes (DDB) were imaged on Alexa 568 microtubule growing from immobilized biotinylated Alexa 568 GMPCPP microtubule seed. GMPCPP seeds were immobilized by adding NeutrAvidin on biotin-PEG functionalised glass surface (modified from Bieling et al. 2010b). The experiment was performed at 30ºC. Images were acquired at 100 ms exposure in 488 nm channel and 561 nm channel, and 500 frames were acquired at a frame rate of 1 fps. **(B)** TIRF Imaging snapshot at 250 s time interval showing dynamic microtubule growth from GMPCPP seeds (red) and GFP dynein (green) binding to dynamic microtubules in the presence of untagged BicD2N$_{400}$ and purified dynactin complex. **(C)** Representative kymograph of dynamic microtubule (MT) (red) with the fast growing plus-end and the slow growing minus-end (shown as '+' and '–' respectively on top of kymograph) and GFP dynein (green) processive motion towards the minus-end of microtubule.

As reported by others (McKenney et al., 2014; Schlager et al., 2014) and in the previous chapter of this thesis, processive dynein motion was achieved only in the presence of purified dynactin complex and $BicD2_{400}$ fragment. I analysed GFP dynein events by semi-automated analysis of kymographs using KymographDirect, where unidirectional events and the diffusive and static trajectories present in single kymographs are Fourier filtered followed by automated analysis (Mangeol et al., 2016) (see Methods for analysis procedure). GFP dynein showed three major types of events on dynamic microtubules – static binding, diffusion, and processive motion (Figure 4.2A). The fast growing nature of the dynamic microtubule plus ends and slow growing minus ends in this assay helped in clear identification of the microtubule polarity and the directionality of DDB events. The unidirectional motions were directed towards the slow growing minus ends of the dynamic microtubules. The velocity of each moving segment was plotted as a histogram (Figure 4.2B). The mean velocity was 0.34 μm/s. The average run length of processive DDB was 4.1 μm (Figure 4.2C). These measurements agree with the previously published data of DDB motion on static microtubules (McKenney et al., 2014; Schlager et al., 2014) (Table 4.1).

Table 4.1 Motile properties of mammalian DDB reported in the *in vitro* studies

Method	Velocity (μm/s)	Run length (μm)	Reference
Fluorescence microscopy	0.40–0.50	5.0–9.0	(McKenney et al., 2014)
Fluorescence microscopy	0.38	8.5	(Schlager et al., 2014)
Bead assay	0.51	-	(Belyy et al., 2016)

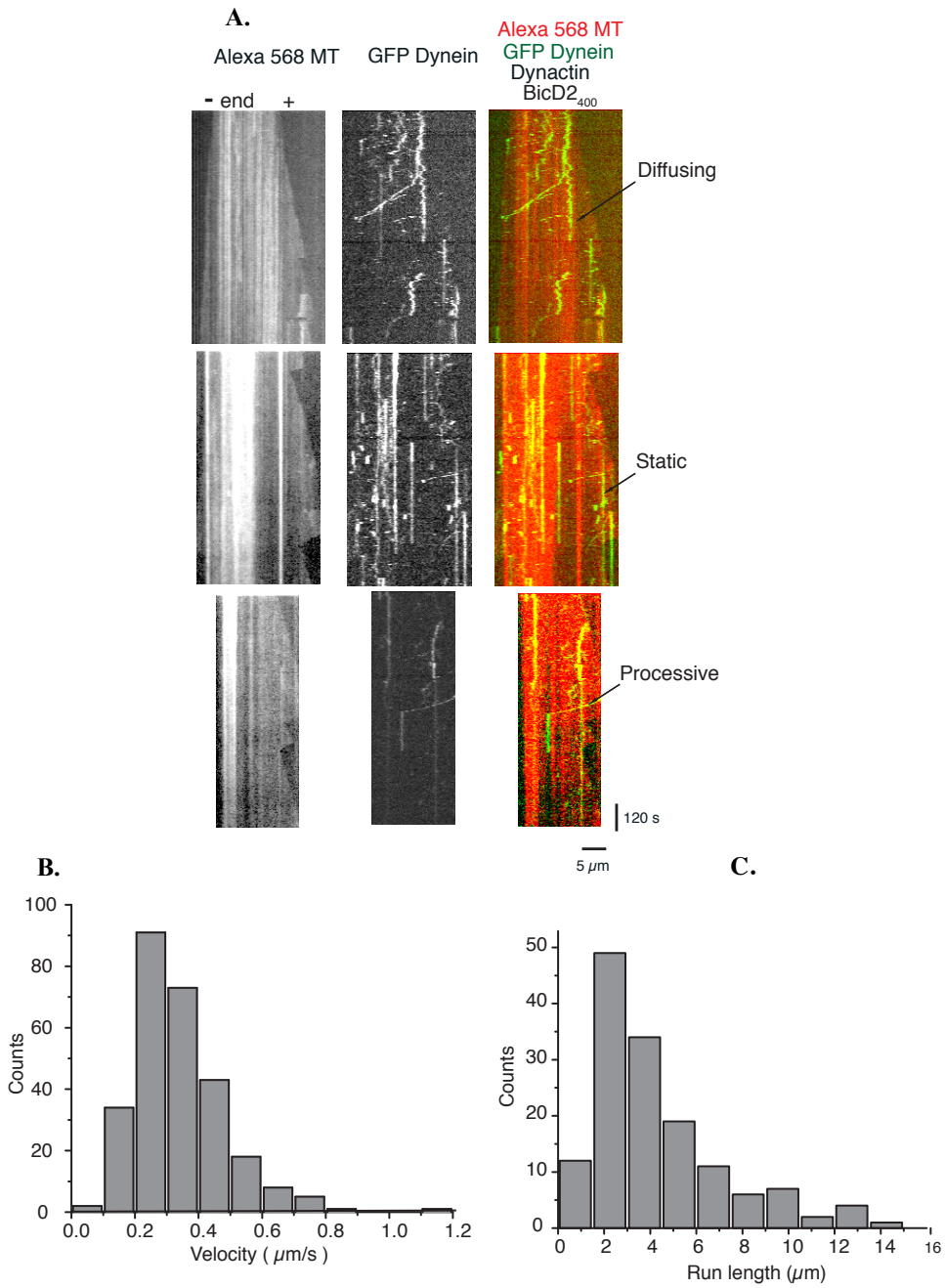

Figure 4.2 DDB motion on dynamic microtubule

(A) Kymographs: showing dynamic microtubules (first column and red in merge shown in third column) imaged in 561 nm channel and GFP dynein events (second column and green in merge shown in third column) in the presence of untagged purified human dynactin complex and $BicD2_{400}$. Motile behaviour of 10 nM GFP dynein (green) was studied in the presence of 20 nM of human dynactin and 200 nM $BicD2_{400}$ on dynamic microtubule (red) grown from Alexa 568 GMPCPP seeds (17.5 μM tubulin). The experiment was performed at 30ºC. Image was acquired at 100 ms exposure in 488 nm and 561 nm channel, and 500 frames were acquired at a frame rate of 1 fps. **(B)** Velocity distribution: Histogram of velocities of processively moving DDB. Mean± s.e.m = 0.34 ± 0.02 μm/s (n=366) **(C)** Run length distribution: Mean± s.e.m = 4.1 ± 0.13 μm (n=326)

To find out whether $BicD2_{400}$ attached to dynein during its processive run, I used fluorescently labelled $BicD2_{400}$ protein to visualise its colocalisation with the GFP dynein on dynamic microtubules (Figure 4.3A). To generate fluorescent $BicD2_{400}$, I expressed and purified an N-terminal SNAP-tagged $BicD2_{400}$, which was labelled with Alexa 647 to generate $SNAP^{Alexa647}BicD2_{400.}$ More than two-thirds of the moving GFP dynein contained $SNAP^{Alexa647}BicD2_{400}$ (Figure 4.3B). Quantification of the BicD2 colocalisation with moving dynein was not done in previous studies (McKenney et al., 2014; Schlager et al., 2014), though it was reported that not all moving DDB complexes contained both the labelled components, perhaps due to photo-bleaching (McKenney et al., 2014). I observed that very few diffusive and static binding episodes of GFP dynein had $SNAP^{Alexa\ 647}BicD2_{400}$ signals (Figure 4.3 B) indicating $BicD2_{400}$ primarily attached to the moving dynein-dynactin and is needed for the processive dynein motion.

In conclusion, these experiments provide the first *in vitro* reconstitution of the processive metazoan dynein motion on dynamic microtubules. The observed average velocity and run-length of moving DDB complex on dynamic microtubules agreed with those reported for DDB motion on stabilised microtubules (McKenney et al., 2014; Schlager et al., 2014), despite the variations in assay conditions of the two reconstitutions.

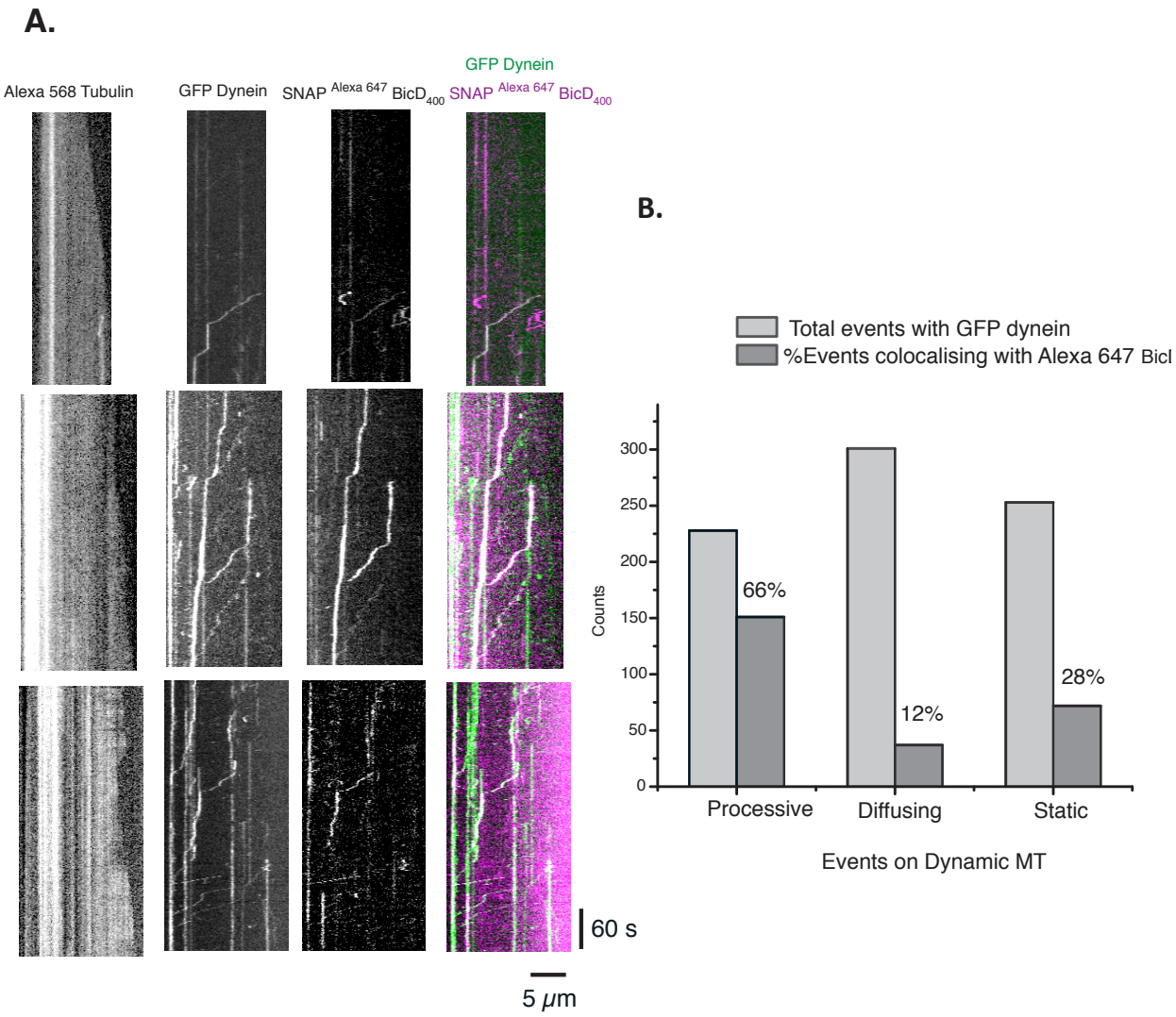

Figure 4.3 Three-colour imaging of DDB events on dynamic microtubules

(A) Kymographs: Motile behaviour of 10 nM GFP dynein (second column and green in merge) was studied in the presence of 20 nM human dynactin and 200 nM $SNAP^{Alexa\ 647}BicD2_{400}$ (second column and magenta in merge) on Alexa 568 dynamic MT (first column). The experiment was performed at 30ºC. Images were acquired at 100 ms exposure simultaneously in 488 nm and 640 nm channels and alternating in 561 nm channel, and 500 frames were acquired at a frame rate of 1 fps. **(B)** Types of DDB events: Number of processive moving, diffusing and static DDB events were quantified by counting GFP Dynein events (light grey columns) and percentage of events with both GFP Dynein and $SNAP^{Alexa\ 647}BicD2_{400}$ colocalisiation (dark grey columns).

4.2.2 Microtubule plus end localisation of dynein in the presence of dynactin complex

In cells, both dynein and the dynactin complex robustly track the microtubule plus ends (Moughamian et al., 2013; Splinter et al., 2012). However, *in vitro* evidence of plus end tracking of the dynein-dynactin complex is lacking. The previous *in vitro* reconstitution used a p150 fragment consisting of N-terminal 1-517 ($p150_{1-517}$) and EB1 as the minimal components necessary for plus end tracking of recombinant human dynein. It is unknown whether comparable to $p150_{1-517}$, the full-length dynactin complex (because of its proposed inhibited state) can interact with EB1 and human dynein at the microtubule plus ends, or whether additional cofactors are required. To understand this, I reconstituted the plus-end tracking of GFP labelled recombinant human dynein in the presence of the purified dynactin complex and EB1 in a dynamic microtubule assay (Figure 4.4 A and B).

In the presence of the human dynactin complex and EB1, the GFP dynein was observed to localise to the dynamic microtubule plus ends (Figure 4.4 C and D and Figure 4.5A). Upon removal of either EB1 or dynactin from this assay (Figure 4.5 B and C), the plus-end localisation of dynein was abolished, substantiating that EB1 and dynactin are essential for the dynein end-tracking pathway. Interestingly, I also observed dynein signal at the shrinking or depolymerising plus ends (Figure 4.4 C and D). Interaction of dynein with the shrinking plus ends has been previously reported for a yeast dynein motor fragment in the absence of +TIP regulators (Laan et al., 2012). However, the precise molecular mechanism of shrinking end localisation of dynein is not well understood. Whether the dynactin complex is present together with dynein at depolymerising microtubule plus ends is yet to be studied.

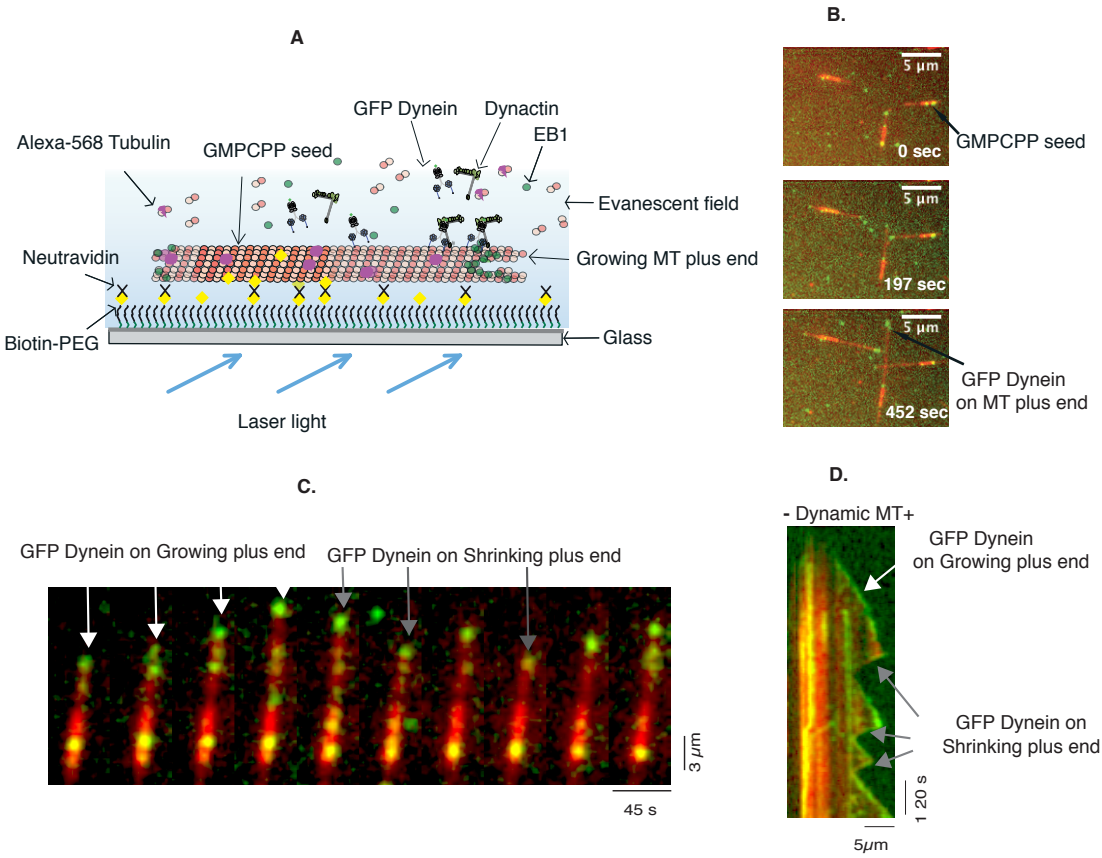

Figure 4.4 Reconstitution of plus end localisation of GFP dynein

(A) Experimental Overview of dynamic microtubule assay. Plus-end tracking behavior of GFP Dynein was studied in the presence of purified dynactin and EB1/3 on Alexa 568 labelled dynamic microtubules grown from immobilized Alexa 568 GMPCPP seed. The experiment was performed at 30ºC (modified from Bieling et al. 2010b). Image was acquired at 100 ms exposure in 488 nm and in 561 nm channel, and 500 frames were acquired at a frame rate of 1fps **(B)** TIRF imaging snapshot at three different time points during image acquisition showing dynamic microtubule growth from GMPCPP seeds (red) in the presence of 17.5 μM tubulin with 10% Alexa 568 tubulin and 10 nM GFP dynein (green) binding to plus ends of dynamic microtubules in the presence of untagged 20 nM human EB1 and 10 nM purified human dynactin complex. **(C)** Time series of TIRF microscopy images 20 nM GFP Dynein localising to growing (white arrows) and shrinking (grey arrows) microtubule plus ends in the presence of 20 nM human dynactin complex and 30 nM EB1. **(D)** Kymograph: Representative kymograph (of same microtubule shown in Time series A) showing GFP dynein (green) tracking plus ends in the presence of human dynactin and EB1. Image was acquired at 200 ms exposure in 488 nm and 561 nm channel, and 500 frames were acquired at a frame rate of 1fps. Temperature was 30ºC.

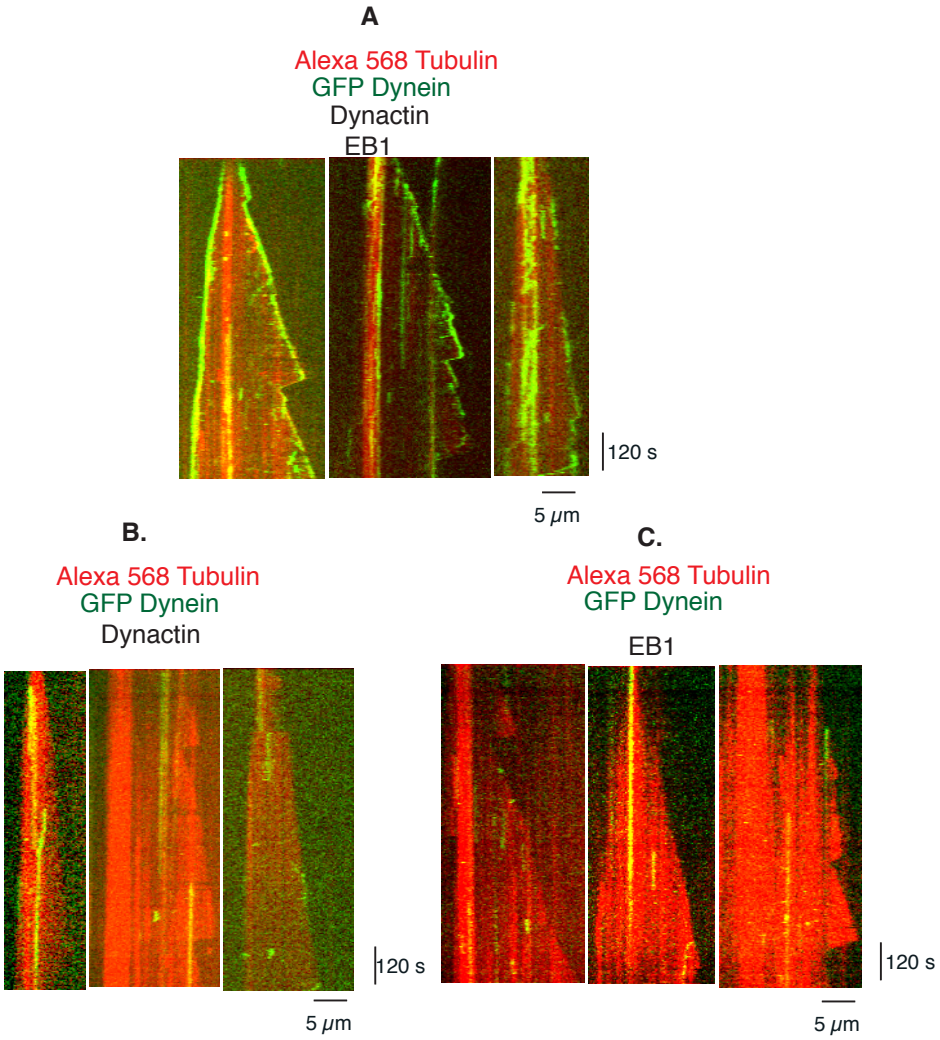

Figure 4.5 Two-colour imaging of plus-end tracking of GFP Dynein

(A) Kymographs of plus-end tracking behaviour of 10 nM GFP Dynein in presence of 20 nM human dynactin and 20 nM EB1. **(B)** Kymographs showing loss of end tracking behaviour of 10 nM GFP Dynein with 20 nM human dynactin in the absence of EB1. **(C)** Kymograph showing loss of end tracking of 10 nM GFP Dynein with 20 nM EB1 in the absence of purified dynactin. Image was acquired at 200 ms exposure in 488 nm and 561 nm channel, and 500 frames were acquired at a frame rate of 1 fps. The experiments were performed at 30ºC.

Next, I tested if there exists a difference in the end tracking behaviour of dynein, depending on the source of the native dynactin complex. This was important to test since the subunit isoforms of the neuronal and non-neuronal dynactin, particularly the p150 isoforms have different splice isoforms (Dixit et al., 2008), and show tissue-specific differences, e.g. in their microtubule binding (Lazarus et al., 2013). As

mentioned in Chapter 2, the neuronal dynactin complex was purified from pig brains, and the non-neuronal human dynactin complex was purified from HeLa S3 cells. I compared the GFP dynein intensities in the end tracking experiments done in the presence of 10 nM of pig brain dynactin and EB1 versus 10 nM purified human dynactin and EB1 (Figure 4.6 A). To quantify the fluorescence intensity of dynein at plus ends, averaged GFP dynein intensities were measured from kymographs: each kymograph was straightened and centred using the previously marked microtubule end positions. All kymographs from one data set were aligned and averaged. The fluorescence intensities were then averaged for all time points at each position along the resulting kymographs, to generate time-averaged spatial intensity profiles. The GFP dynein intensity measured at the plus ends showed no significant difference in the end tracking experiment with the neuronal and non-neuronal dynactin (Figure 4.6 B), indicating that dynactin from both the sources are equally efficient at least in recruiting dynein to the microtubule plus ends.

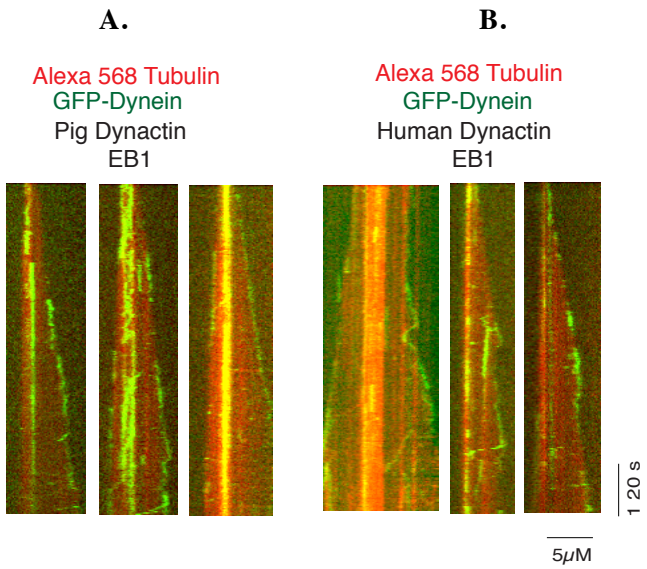

Figure 4.6 Comparison of GFP Dynein plus-end tracking in the presence neuronal and non-neuronal dynactin

(A) Kymograph showing end tracking behaviour of 10 nM GFP Dynein in the presence of 10 nM neuronal dynactin purified from pig brains, and 20 nM EB1. **(B)** Kymograph showing plus-end tracking behaviour of 10 nM GFP Dynein in the presence of 10 nM non-neuronal human dynactin purified from HeLa S3 cells, and 20 nM EB1.

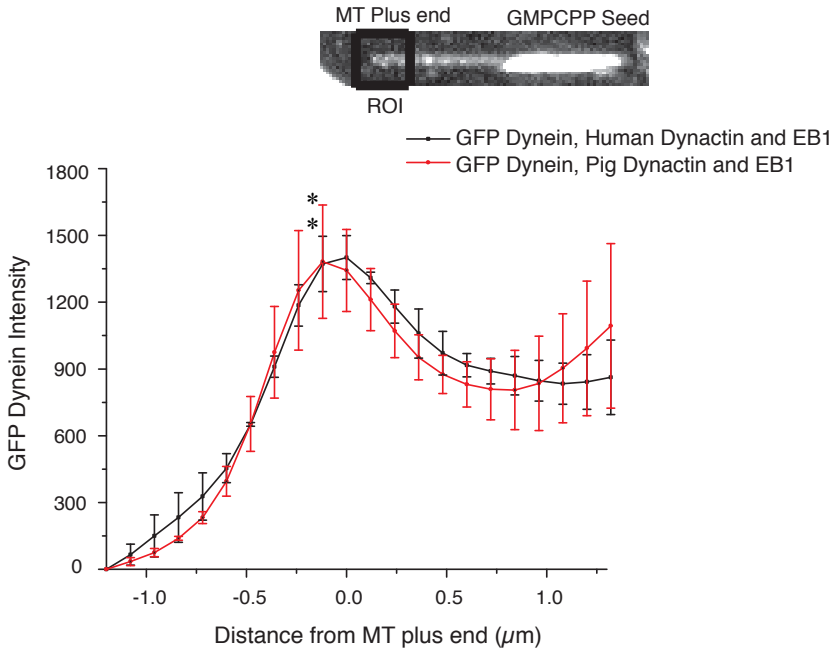

Figure 4.6. C Plot showing averaged GFP dynein intensity distribution at microtubule plus ends.

The averaged GFP Dynein intensities at the microtubule plus-end region were measured at microtubule plus ends for each condition and background-subtracted intensities were plotted against distance from microtubule plus ends. The profile shows mean GFP intensity from three different experiments. The error bars are the standard deviations. * P value (by the two-tailed t-test) equals 0.0522, this difference is not statistically significant.

Does the dynactin-dependent plus end localisation of dynein require its ATP-dependent motor activity? To address this, I carried out GFP dynein end-tracking experiment in the absence of ATP. ATP present in GFP dynein and purified dynactin protein storage buffer was removed by desalting these proteins to a buffer without ATP. GFP dynein tracked plus ends in the absence of ATP (Figure 4.7), suggesting the ATP-dependent motor activity of dynein is not required for the end tracking. It is conceivable that for plus end tracking, dynein hitchhikes its regulators to bind to the microtubules without requiring its ATP dependent activity. In the absence of ATP, overall microtubule recruitment of dynein was high. This is possibly due to the enzymatic cycle of dynein where high microtubule binding in the absence of consistent with the previous reports (Gibbons et al., 2005; Roberts et al., 2013; Trokter et al., 2012).

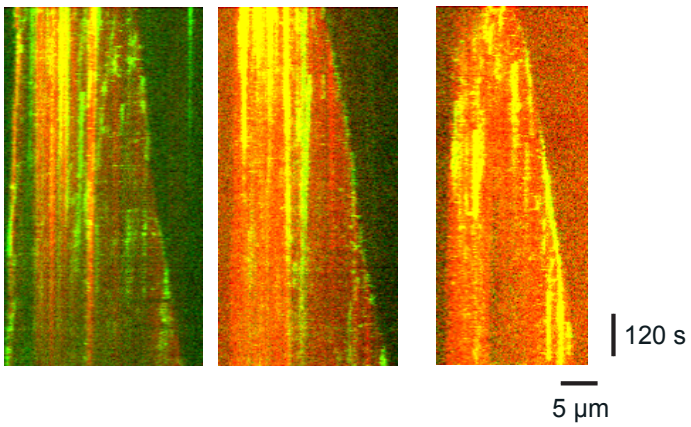

Figure 4.7 Plus-end tracking of GFP dynein in absence of ATP

Kymographs showing 10 nM GFP Dynein at microtubule plus-ends, in the presence of 10 nM human dynactin and 20 nM EB1, in the absence of ATP buffer. Image was acquired at 100 ms exposure simultaneously in 488 nm and 640 nm channels and alternating in 561 nm channel, and 500 frames were acquired at a frame rate of 1 fps. The experiment was performed at 30ºC

The important role of EBs for the plus end tracking of vertebrate dynein is well established, however direct *in vitro* visualisation of EB and dynein colocalisation on microtubule plus ends has not been performed so far. To generate labelled EB for this experiment, SNAP tagged EB3 was purified from *E. coli* and labelled with Alexa 647-SNAP dye to generate $SNAP^{Alexa\ 647}EB3$. Using a three-colour TIRF microscopy, GFP dynein and $SNAP^{Alexa\ 647}EB3$ were observed to colocalise at plus ends of Alexa 568 dynamic microtubules in the presence of the purified pig dynactin complex (Figure 4.8). This experiment provides the first *in vitro* evidence of direct colocalisation EB3 and dynein at microtubule ends, and confirms the EB3 dependent plus end tracking of dynein.

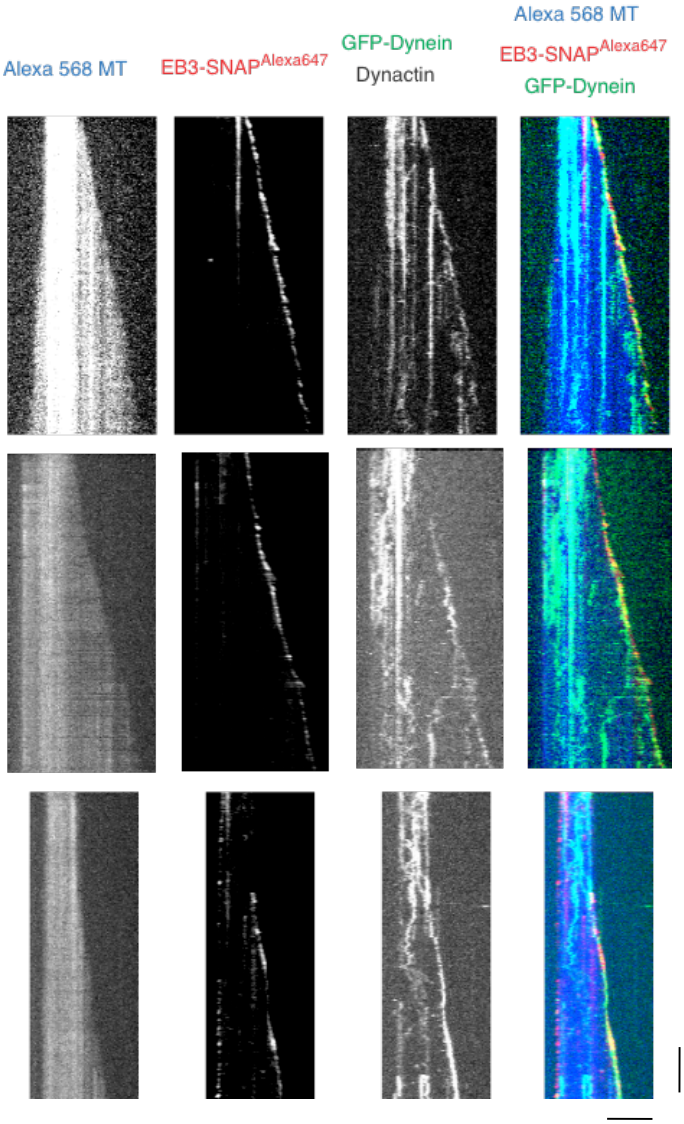

Figure 4.8 Three-colour imaging of plus end tracking of GFP Dynein

Kymographs showing GFP Dynein (third column of kymograph and green in merged kymograph) colocalisation with EB3-SNAP^{Alexa647} (second column of kymograph and red in merged kymograph), in the presence of pig dynactin, on Alexa 568 dynamic microtubule (first column and blue in merged kymograph). The protein concentrations were: 10 nM GFP dynein, 10 nM pig dynactin and 20 nM EB3. Image was acquired at 200 ms exposure simultaneously in 488 and 640 channels and alternating in 561 channel, and 500 frames were acquired at a frame rate of 1fps. The experiment was performed at 30ºC. The scale bar in x axis was 5 μm and in y axis was 120 s.

Next, I studied the impact of dynein-dynactin complex on microtubule growth velocity. I measured the growth velocities at 17.5 μM tubulin concentration, in the presence of 10 nM EB3 alone and in the presence of 10 nM each of dynein, dynactin and EB3. The

mean growth velocity increased 1.5 times upon addition of dynein-dynactin (Figure 4.9). This increase in growth velocity agrees with the previously reported microtubule polymerase role of dynactin's p150 fragment (Lazarus et al., 2013). Whether the increased microtubule growth velocity is because of the microtubule binding of p150 via the CAP-Gly domain or because of modulation of microtubule growth by other subunits of dynein and dynactin remains to be studied.

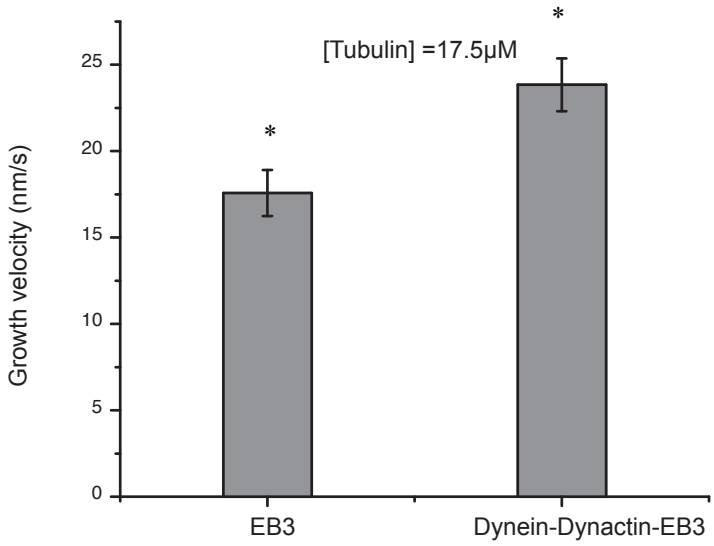

Figure 4.9 Microtubule growth velocity measurements

Microtubule growth velocities: Microtubule growth velocity in the presence of 10 nM EB3 and in the presence of 10 nM each of GFP Dynein, dynactin, EB3. The experiment was performed at 30ºC. *The two-tailed P value equals 0.0067 (the difference in growth velocities is statistically significant).

This is the first reconstitution of plus end tracking of metazoan dynein in the presence full-length dynactin complex and EB1. These findings show that human dynein can track growing and shrinking microtubule plus ends in the presence of purified neuronal as well as non-neuronal dynactin and EBs. The ATP-dependent motor activity is not required for the end tracking behaviour of human dynein. Further, dynein-dynactin caused an increase in microtubule growth velocity. A detailed analysis of regulation of microtubule dynamics by dynein and dynactin complex is required.

4.2.3 $BicD2_{400}$ removes dynein from microtubule plus ends

Recent *in vitro* reconstitution experiments (McKenney et al., 2014; Schlager et al., 2014) have highlighted the important role of $BicD2_{400}$ fragment in processive minus end directed dynein motion on stabilised microtubules. In cultured cells, however, expression of this $BicD2_{400}$ fragment led to removal of dynein from dynamic microtubule ends (Splinter et al., 2012). To test whether $BicD2_{400}$ directly acts as an inhibitor of plus end tracking behaviour of dynein, I introduced the purified $BicD2_{400}$ fragment to the dynein-dynactin end-tracking assay.

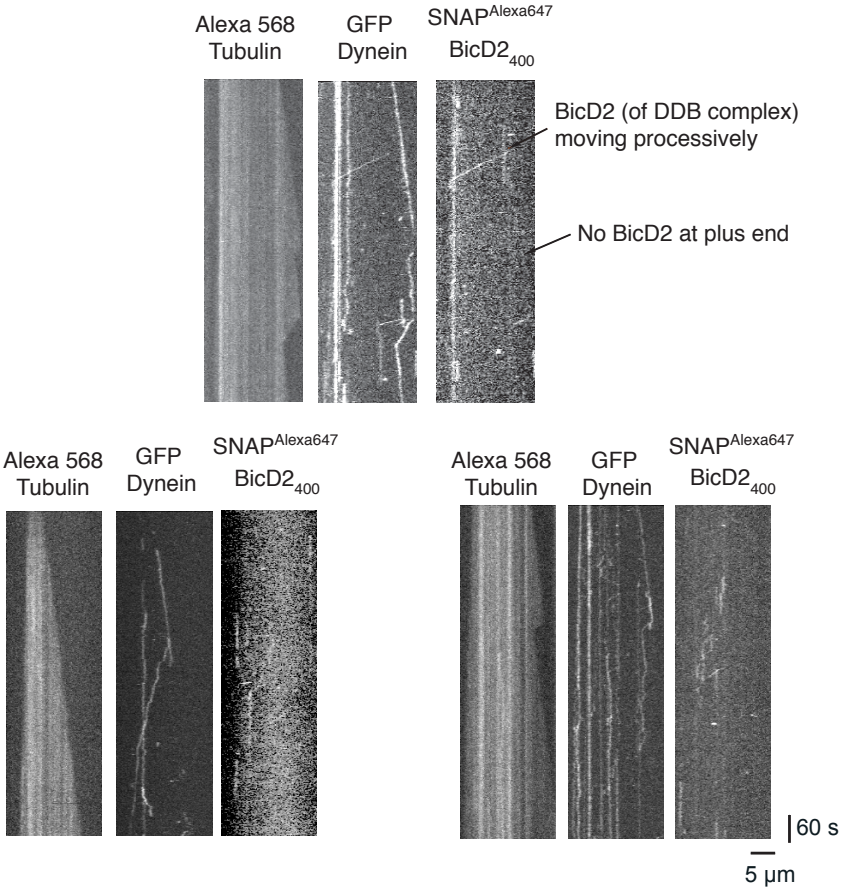

Figure 4.10 Kymograph showing DDB not present at plus ends

Kymographs showing 10 nM of GFP Dynein (second column of kymographs) tracking dynamic microtubule plus ends (first column of kymographs) in presence of 10 nM pig dynactin, 10 nM EB1, and 200 nM $SNAP^{Alexa\ 647}BicD2_{400}$ (third column of kymographs). Image was acquired at 100 ms exposure simultaneously in 488 nm and 640 nm channels and alternating in 561 nm channel, and 500 frames were acquired at a frame rate of 1 fps. $SNAP^{Alexa\ 647}BicD2_{400}$ did not colocalise with GFP dynein at microtubule plus ends but it was present with motile GFP dynein as a part of DDB complex. Temperature was 30°C.

First, I added 200 nM $BicD2_{400}$ to the GFP dynein end-tracking assay done in the presence of dynactin and EB1. At this concentration, I observed both plus end tracking and processive motion of GFP dynein. Simultaneous imaging of $SNAP^{Alexa\ 647}BicD2_{400}$ revealed that the BicD2 signal colocalised with the moving GFP dynein while no colocalisation was observed between $BicD2_{400}$ and GFP dynein at microtubule plus ends (Figure 4.10). This suggests that free $BicD2_{400}$ alone as well as the $BicD2_{400}$ bound dynein-dynactin (DDB complex) do not track plus ends of dynamic microtubules. Since the DDB complex does not appear to localise at plus ends, it is possible that attachment of $BicD2_{400}$ biases the plus end localisation behaviour of dynein. To this end, I tested whether increasing BicD2 concentration in the end tracking assay further reduced the plus end localisation of dynein.

I attempted to outcompete the plus end tracking behaviour of GFP dynein by adding twenty-five times higher amount (5 μM) of $BicD2_{400}$ compared to the $BicD2_{400}$ concentration in the previous assay (Figure 4.10). For this experiment, untagged $BicD2_{400}$ was used, since it could be purified in higher quantities compared to $SNAP^{Alexa647}BicD2_{400}$. At high $BicD2_{400}$ concentration, the plus end localisation of GFP dynein decreased starkly (Figure 4.11B) compared to its plus end accumulation seen in the absence of $BicD2_{400}$ (Figure 4.11A). The plot of averaged plus end intensity of GFP dynein showed diminished dynein intensity in presence of 5 μM $BicD2_{400}$ compared to GFP dynein intensity in the absence of $BicD2_{400}$ (Figure 4.11). This observation strongly indicates that $BicD2_{400}$ can deplete GFP dynein pool at microtubule plus ends and activate its processive minus end motion away from plus ends (Figure 4.11B).

To summarise, the dynein-dynactin-BicD2 complex did not localise to the plus ends of microtubules in the end tracking experiments presented in this section. Moreover, at high $BicD2_{400}$ concentration the plus end localisation of dynein was starkly diminished (Figure 4.11), thereby acting as an inhibitor of the dynactin-dependent plus end tracking of dynein.

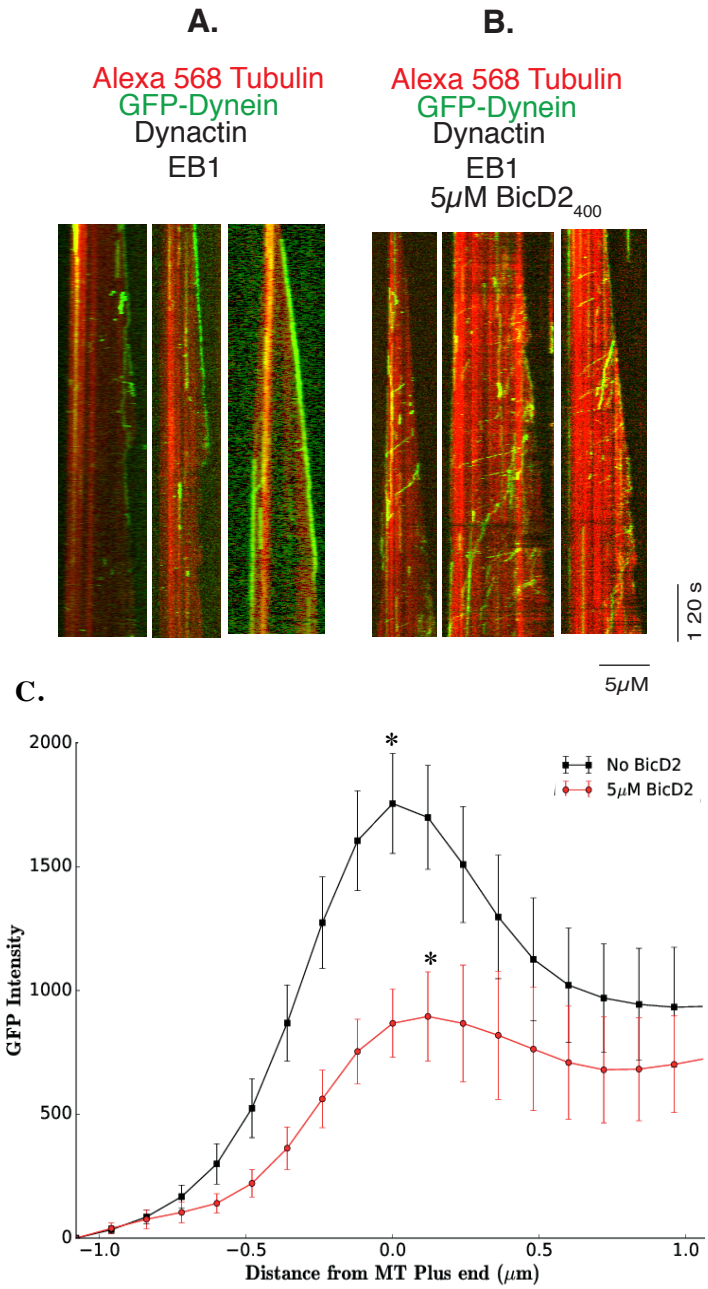

Figure 4.11 Effect of BicD2$_{400}$ on plus end tracking behaviour of GFP Dynein

(A) Kymograph: 10 nM GFP Dynein (green) seen at plus ends of Alexa 568 dynamic microtubules (red) in the presence of 20 nM purified pig dynactin and 20 nM EB1. Images were acquired at 200 ms exposure 488 nm and 561 nm channel, and 500 frames were acquired at a frame rate of 1 fps. The temperature was 30ºC. **(B)** When 5 μM of untagged BicD2$_{400}$ is added to the same GFP Dynein end tracking experimental conditions, the plus end tracking is diminished and processive runs were observed. **(C)** Averaged GFP Dynein intensity distributions at plus ends in the presence of 5 μM BicD2$_{400}$ (red curve) is reduced by more than half compared to GFP Dynein plus end intensity without BicD2$_{400}$ (black curve). Error bars shown are standard deviations of mean intensity profiles from three experiments for each condition. * P value < 0.0001 by Student two tailed t-test.

4.2.4 Lis1 regulates dynein transport and its microtubule localisation in dose dependent manner

The work presented so far in this chapter shows that the dynactin complex and EB1 are sufficient for plus-end localisation of dynein. However, in non-neuronal cells, this pathway required additional regulator—Lis1 (Coquelle et al., 2002; Splinter et al., 2012). It is possible that Lis1 is required to maintain dynein at plus ends by repressing its processive motion. To test this hypothesis, I studied whether Lis1 could rescue the reduced plus end accumulation of dynein induced by $BicD2_{400}$ (possibly by activating processive dynein motion away from plus ends) in the plus end tracking experiments. For these experiments, I expressed and purified full-length human Lis1 with a C-terminal mCherry tag (mCherry Lis1). I studied the combined effect of Lis1 and BicD2 on the plus end tracking of dynein in end tracking experiments where GFP dynein, dynactin, EB1, $BicD2_{400}$, and Lis1mCherry were studied on labelled dynamic microtubules. In the end tracking experiments, the concentrations of all the other proteins were fixed (10 nM GFP dynein, 20 nM human dynactin, 20 nM EB3 and 5 μM $BicD2_{400}$), while Lis1 was studied at two different concentrations: 1 μM and 5 μM.

Lis1 promotes and restores the microtubule plus end localisation of dynein

At 1 μM mCherry Lis1, GFP dynein was seen at the plus ends even in the presence of 5 μM $BicD2_{400.}$ (Figure 4.12 B) However, adding 5 μM mCherry Lis1 caused an increased accumulation of dynein at the plus ends, hence restoring the $BicD2_{400}$ induced reduction of plus-end tracking (Figure 4.12 C). I also observed an overall increased microtubule binding of GFP dynein in the presence of Lis1 (Figure 4.12 B and C). However, Lis1 did not seem to visibly repress the motion of DDB, as hypothesized earlier (Yamada et al., 2008; McKenney et al., 2010; Huang et al., 2012).

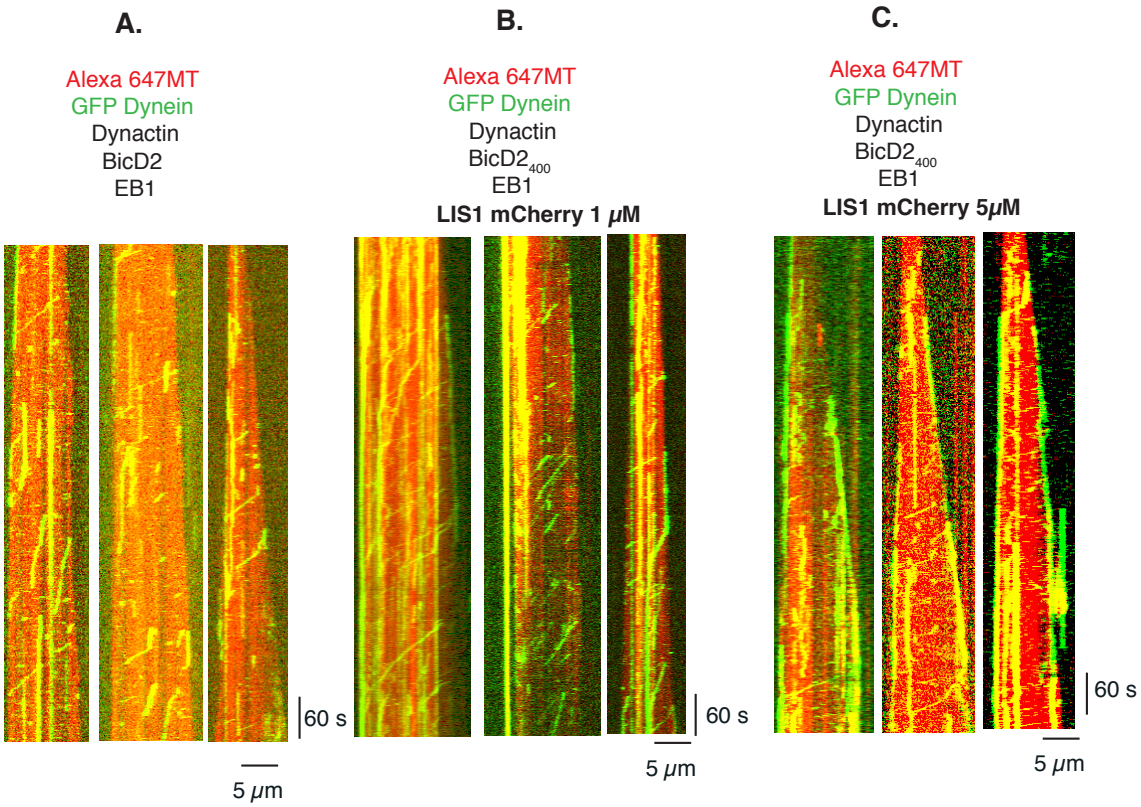

Figure 4.12 Lis1 promotes plus end localisation of GFP Dynein

(A) Kymograph: At 5 μM of untagged BicD2$_{400}$, 10 nM GFP Dynein (green in kymograph) not seen at plus ends of Alexa 568 dynamic microtubules (red in kymograph) in the presence of 20 nM purified pig dynactin and 20 nM EB1. **(B)** When 1 μM of Lis1 is added together with 5 μM BicD2$_{400}$ to the end tracking experiment, there was an increase in the plus end accumulation of GFP dynein **(C)** When 5 μM Lis1 was added together with 5 μM BicD2$_{400}$ to the GFP Dynein end tracking experimental condition plus end localisation of dynein was restored (shown in kymographs on right). Images were acquired at 200 ms exposure 488 nm and 561 nm channel, and 500 frames were acquired at a frame rate of 1 fps. The temperature was 30ºC.

4.12 D.

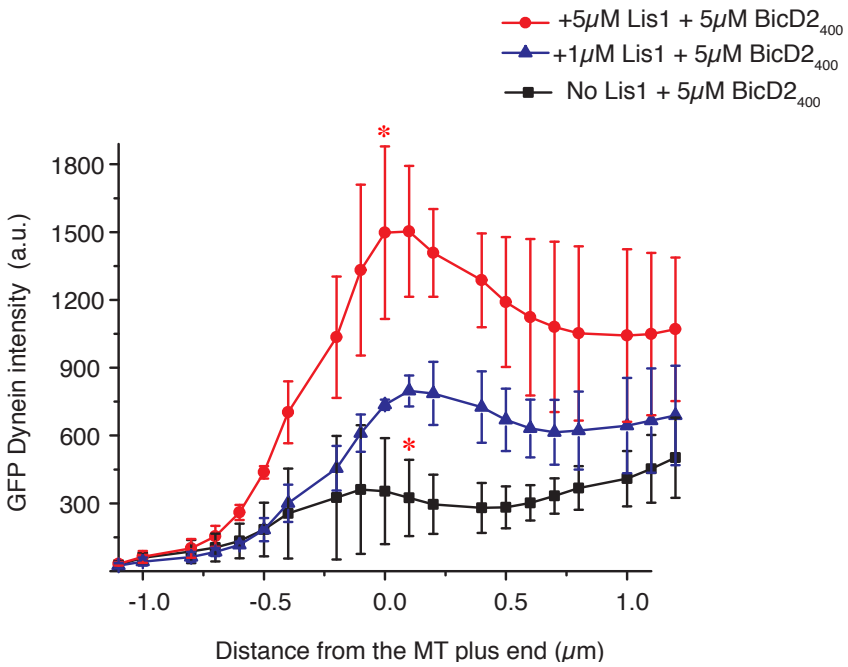

Figure 4.12.D The average GFP Dynein intensity at plus ends

The averaged GFP Dynein intensities profile at plus ends in the presence of 1 μM Lis1 (blue curve) showed an increase in plus end localisation of GFP dynein even in the presence of $BicD2_{400}$ compared to diminished GFP Dynein plus end intensity when 5 μM BicD2 alone was added (black). At 5 μM Lis1 (red curve) there was a further increase in the plus localisation of dynein. Error bars shown are standard deviations of mean intensity profiles from three experiments for each condition. * $P < 0.0001$ (Student two tailed t-test).

Lis1 initiates DDB motion

Adding Lis1 to the GFP-dynein plus-end tracking assay together with BicD2 did not impede the processive motion; rather, an increase in the frequency of DDB events was noticed (Figure 4.13C and D). This was not surprising, considering the established role of Lis1 as an initiation factor for dynein motion in fungi and neurons (Egan et al. 2012, Lenz et al. 2006, Moughamian et al. 2013). At 1μM Lis1 (Figure 4.13C), there was more than twofold increases in the number of motile events compared to the events from assays where DDB alone (Figure 4.13 A) or DDB with EB1 were studied (Figure 4.12 B). This observation suggests that Lis1 indeed acts as an initiator of DDB motion. Unexpectedly, at higher Lis1 (Figure 4.12C), there was a drop in the number of motile events (from 2 events/μm of MT length to 1.2 events/μm of MT length) (Figure 4.13D).

The reason behind this decrease in motile DDB events at high Lis1 concentration is not clear, but it does appear that at 5 μM Lis1 might outcompete $BicD2_{400}$ to repress dynein motility and maintain dynein at microtubule plus-ends (as seen in the GFP-dynein plus end tracking experiment in Figure 4.12). From the end tracking experiments with 1 μM and 5 μM Lis1, it appears that 1 μM Lis1 is the concentration regime where high motility is observed while 5 μM Lis1 is the regime of increased plus end tracking.

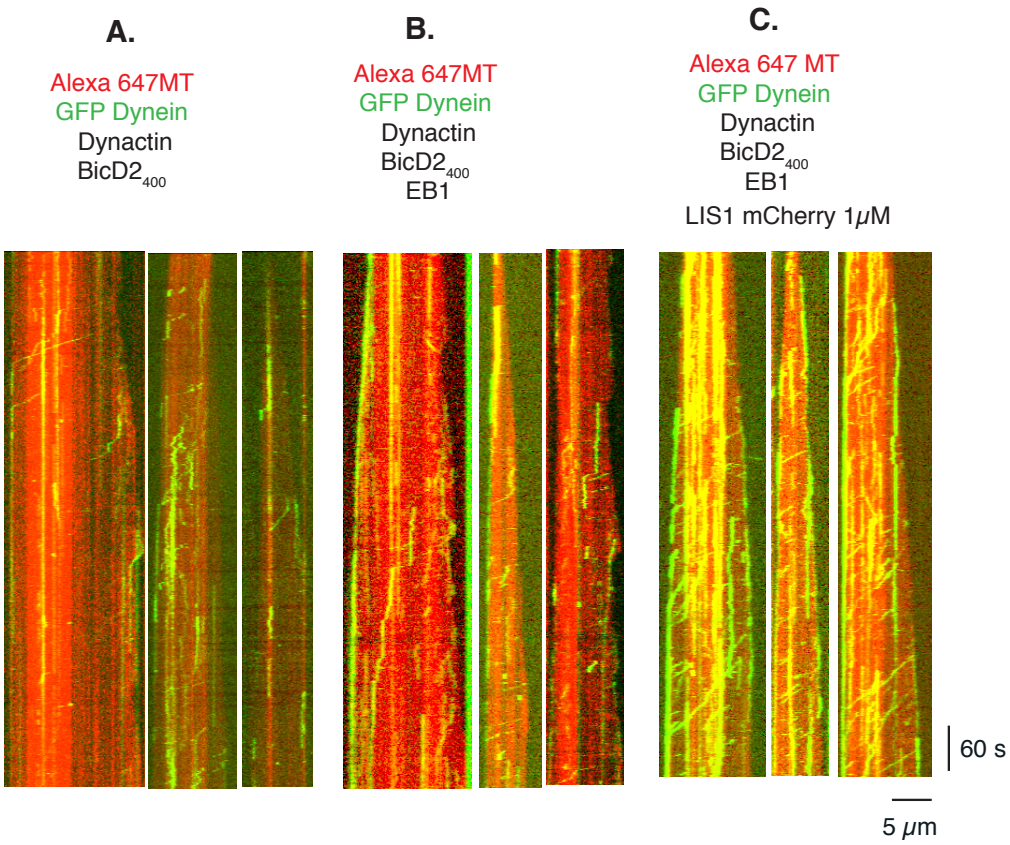

Figure 4.13 Lis1 increases the number of motile DDB events

(A) Kymograph showing DDB events. **(B)** DDB events in presence of EB1. **(C)** DDB events in presence of EB1 and 1 μM Lis1. Images were acquired at 200 ms exposure 488 nm (GFP dynein) and 640 nm (Alexa 647 microtubule) channels, and 500 frames were acquired at a frame rate of 1 fps. The temperature was 30ºC.

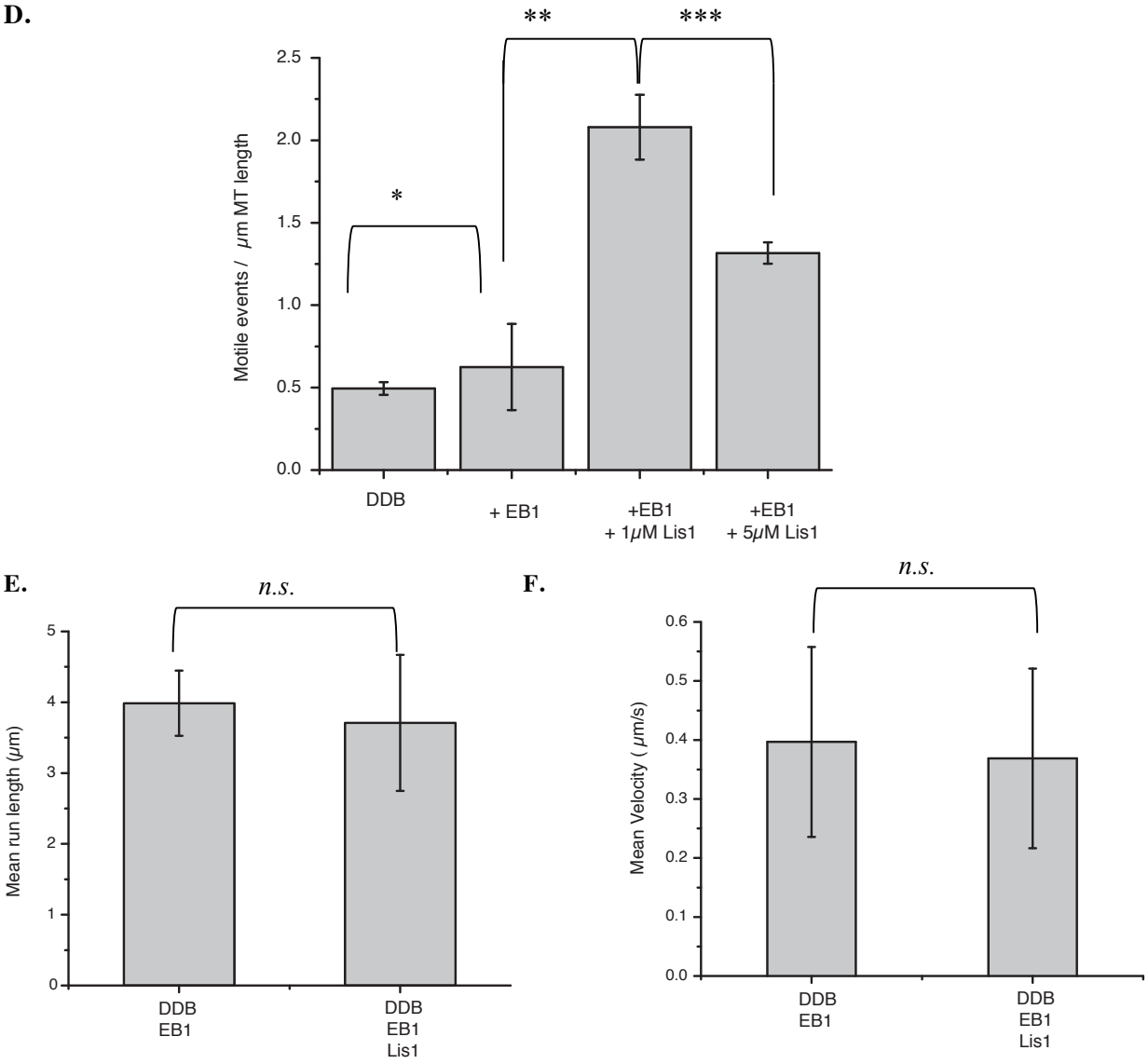

Figure 4.13 Lis1 increases the number of motile DDB events

(D) Frequency of motile events per micron of microtubule length, bar represents individual frequency of motile dynein in DDB complex alone, in presence of EB1, and 1 μM and 5 μM of Lis1 together with EB1. *P value equals 0.1486 (not statistically significant), ** P < 0.0001 (statistically significant) *** P < < 0.001 (statistically significant). Mean run length **(E)** and mean velocity **(F)** of processive DDB in presence of EB1 and in presence of 1 μM Lis1 together with EB1. Error bar is the standard deviation. Error bar shows standard deviation. P values (unpaired t-test) equals 0.84 and 0.97 for E and F respectively (not statistically significant indicated as *n.s.*)

Next, I studied if mCherry Lis1 is bound to processive DDB during its run. For this, I imaged GFP dynein and mCherry Lis1 sequentially. mCherry Lis1 was not seen on motile DDB (Figure 4.14). This agrees with the reported transient nature of Lis1-dynein

interaction (Egan et al., 2012; McKenney et al., 2011). Further, Lis1 is known to slow down dynein driven motion (Huang et al., 2012; McKenney et al., 2010;Torisawa et al., 2011; Yamada et al., 2008). However, I did not observe a reduction in the DDB velocity or run length when Lis1 was added (Figure 4.13 E and F), further supporting the evidence that processively moving DDB was not bound to Lis1. Surprisingly, I did observe mCherry Lis1 localise at dynamic microtubule plus ends (Figure. 4.14). Since Lis1 can directly bind to both dynein and dynactin (Dix et al., 2013; Tai et al., 2002; Wang et al., 2013), it is possible that dynein-dynactin recruit Lis1 to the plus ends. Supporting this hypothesis, dynein and dynactin have indeed been shown to recruit Lis1 at the plus ends of kinetochore microtubules in cultured mammalian cells (Tai et al., 2002). To sum up, the data suggest that Lis1 did not bind to moving DDB perhaps due to competition with BicD2 (see discussion in section 4.3.4); instead Lis1 localised (and possibly interacts) with the dynein-dynactin complex at the plus ends.

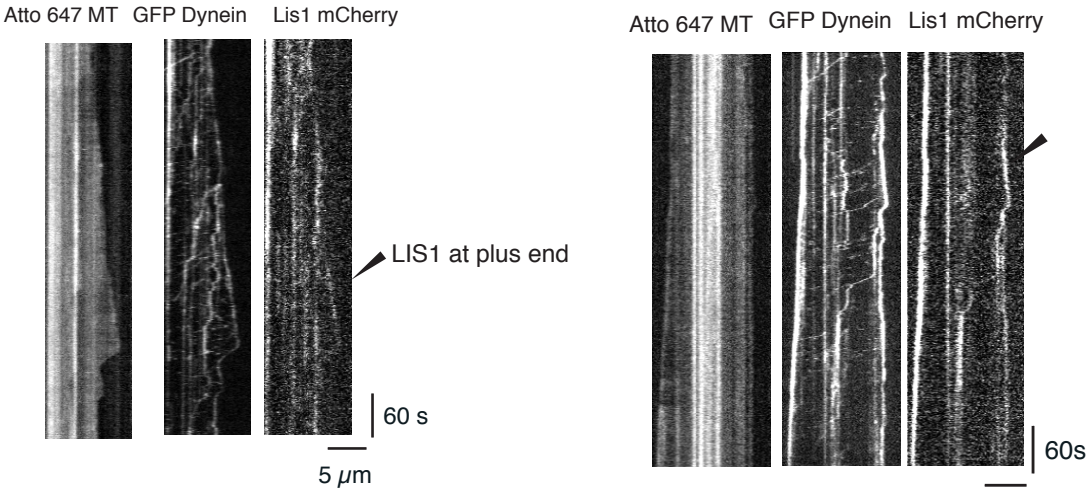

Figure 4.14 Three colour imaging of GFP dynein and mCherry Lis1 on dynamic microtubules in the presence of dynactin BicD2 and EB1.

Kymograph: Showing 5 μM mCherry Lis1 colocalisation with 10 nM GFP dynein, in presence of 10 nM pig dynactin complex and 20 nM EB1 on Atto 647 labelled dynamic microtubules mCherry. Lis1 did not colocalise with processive DDB runs.

Lis1 enhances the recruitment of GFP dynein to the microtubules

It is unclear how Lis1 may initiate dynein transport. One possibility is that Lis1 enhances the overall recruitment of dynein to the microtubules, where DDB could be assembled; hence the transport initiation could take place all over the microtubules. To test this, I studied the plus end tracking of GFP dynein in the presence of dynactin, EB1 and 5 μM mCherry Lis1. Here, GFP dynein localised not only to the plus ends, but all over the microtubules either statically bound or diffusing along the microtubules (Figure 4.15 B). Therefore, consistent with the previous reports (Huang et al. 2012, McKenney et al. 2010, Toropova et al. 2014, Yamada et al. 2008), Lis1 appears to be a general microtubule recruiter of dynein rather than a specific plus end recruiter and its property of enhancing dynein's microtubule attachment seems to be the mechanism by which Lis1 initiates dynein transport. This idea is also consistent with studies in neurons where Lis1 initiated transport along the entire microtubule length and not just the plus ends (Moughamian et al., 2013).

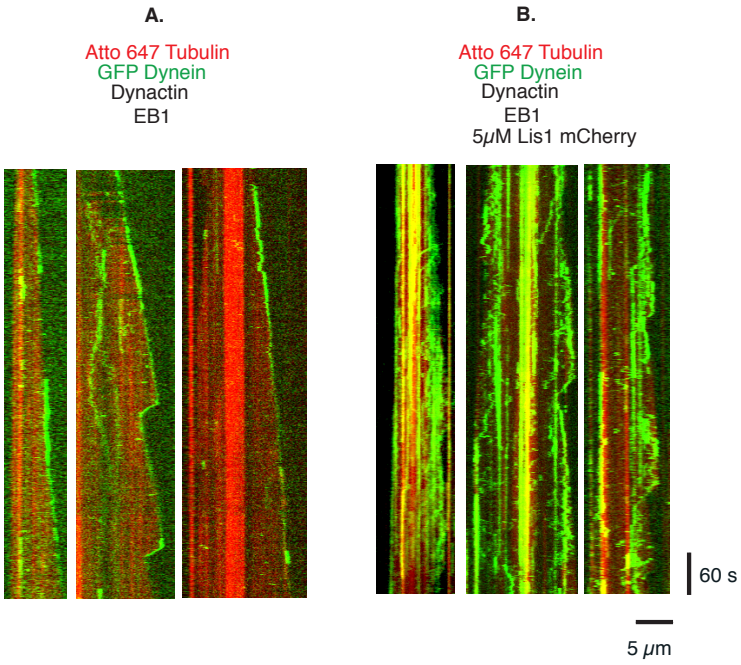

Figure 4.15 Lis1 recruits GFP Dynein to dynamic microtubules

(A) Kymograph: 10 nM GFP Dynein (green) seen at plus ends of Alexa 568 dynamic microtubules (red) in the presence of 20 nM purified pig dynactin and 20 nM EB1. Image was acquired at 200 ms exposure 488 nm and 640 nm channel, and 500 frames were acquired at a frame rate of 1fps. The temperature was 30ºC **(B)** When 5 μM of mCherry Lis1 was added to the same GFP Dynein end tracking experimental GFP dynein decorated the dynamic microtubule filaments, including plus ends.

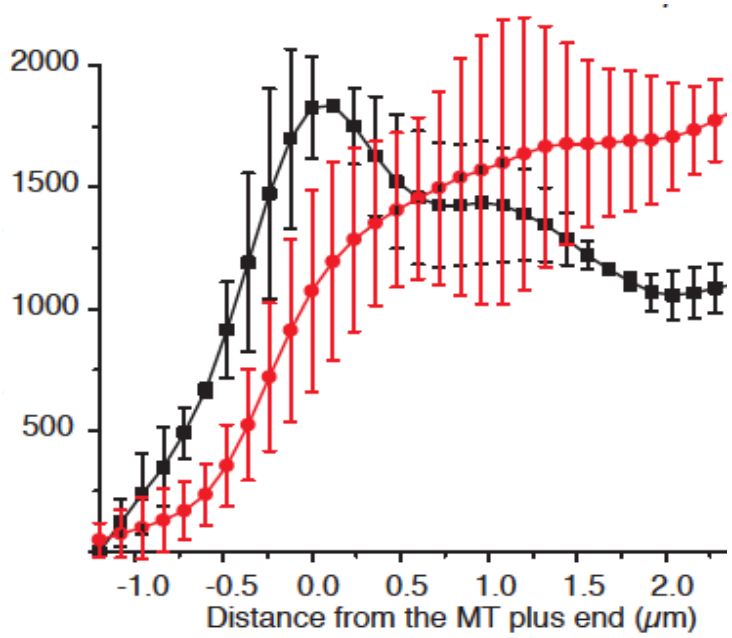

Figure 4.15 Lis1 recruits GFP Dynein to dynamic microtubules

(C) Averaged GFP Dynein intensities distribution at plus ends in the presence of 5 μM Lis1 (red curve) shows an overall increase in GFP dynein intensity compared to GFP Dynein plus end intensity without Lis1 (black curve).

In conclusion, two important roles of Lis1 were uncovered in this study: first as a promoter of plus end accumulation of dynein in the presence of processivity factors; and second as an initiator of DDB motion. Both these roles appear to be dose dependent. In the presence of the same amount of $BicD2_{400}$ and Lis1, plus end accumulation of dynein was favoured, while the BicD2 induced processive dynein motion appeared suppressed. When Lis1 was present in lower concentration than $BicD2_{400}$ there was an increased initiation of DDB motion, perhaps because of increased dynein recruitment to the microtubules where DDB complex is possibly assembled. Further, Lis1 seems to recruit dynein all over the microtubule, including the plus ends when BicD2 was omitted from the plus-end tracking assay. Therefore, it appears that in this study Lis1 and BicD2 compete to shift dynein's microtubule localisation and its processive motion.

4.3 Discussion

In this chapter, I presented an *in vitro* characterization of the plus-end localisation and processive motion of the recombinant human dynein complex on dynamic microtubules. I studied how the key dynein regulators dynactin and Lis1, adaptor protein BicD2, and end binding protein EB1, guide dynein's recruitment to the microtubule and regulate its processive motion. First, dynein in the presence of dynactin and $BicD2_{400}$ (DDB) showed processive motion on dynamic microtubules. Second, dynactin and EB1 was necessary for plus end tracking of GFP dynein. The DDB complex did not appear to track the plus ends of the microtubules, and high amounts of BicD2 reduced the end tracking of dynein in the *in vitro* end-tracking assay. Addition of Lis1 to the plus end tracking assay together with BicD2 showed a concentration dependent regulation of dynein, where an increased Lis1 concentration represented a plus end tracking regime and five times lower Lis1 represented high motility regime.

4.3.1 Regulation of microtubule localisation of human dynein

GFP human dynein localised to the microtubule plus ends in the presence of the purified dynactin complex and EB1. How does the supposedly folded and auto-inhibited dynactin subunit p150 (Chowdhury et al., 2015; Urnavicius, 2015) mediate its interactions with dynein and EB1? It is possible that the p150 CAP-Gly is exposed in the folded dynactin conformation, allowing its interaction with EB1, and transient but frequent dynein-dynactin interaction leads to their plus-end localisation. Since the CAP-Gly domain was not visualised in the recent dynactin structures (Chowdhury et al., 2015; Urnavicius, 2015), its orientation in the dynactin complex is unclear. However, based on the GFP dynein plus-end tracking experiment presented in this chapter, it may be speculated that the CAP-Gly domain and at least one of the dynein binding sites (CC1 or Arp1) of dynactin are not permanently masked.

I observed GFP human dynein tracking both growing and shrinking microtubule plus ends. In dividing cells, the interaction of shrinking microtubule ends with dynein at the kinetochore has been implicated in mediating chromosome separation during anaphase (Savoian et al., 2000; Sharp et al., 2000). Further, the pulling force exerted by dynein

with end-on attachment to the shrinking cortical microtubules is thought to be necessary for spindle positioning (Carminati and Stearns, 1997; Dujardin and Vallee, 2002; Grill et al., 2001; Koonce et al., 1999; Vallee et al., 2006; Yamamoto et al., 2001). The molecular mechanism behind the tracking of the shrinking plus ends remains poorly understood. It is possible that once recruited to the growing plus ends by dynactin and EB1, dynein independently remains bound to the depolymerising plus ends. Whether the dynactin complex colocalises with dynein at the shrinking plus ends is unclear. However, in cells dynactin's p150 did not track the shrinking plus ends (Dixit et al., 2008)

The dynactin-dependent end tracking of dynein did not require its motor activity, as dynein could track plus ends in the absence of ATP. For plus-end tracking, vertebrate dynein in fact hitchhikes its +TIP interacting regulators, dynactin complex in this case(Duellberg et al., 2014; Moughamian et al., 2013). Further, I showed that by binding to microtubule plus ends, dynein-dynactin induced an increase in microtubule growth velocity in agreement with the role of dynactin (p150) as a microtubule polymerase (Lazarus et al., 2013). Further characterization of other aspects of microtubule dynamics in the presence of dynein and dynactin will strengthen our knowledge of their role at plus ends.

4.3.2 Plus end tracking versus minus-end transport: Role of BicD2

The role of $BicD2_{400}$ as an activator of processive dynein-dynactin motion has been studied extensively (Chowdhury et al., 2015; McKenney et al., 2014; Schlager et al., 2014; Urnavicius, 2015). In this thesis, I studied another role of $BicD2_{400}$ as an antagonist of dynein's plus-end tracking behaviour. The results suggested that the DDB tripartite complex does not localise at microtubule plus ends, and at 5 μM $BicD2_{400}$, there is a clear abrogation of dynein's plus-end tracking behaviour. What is the molecular mechanism of this $BicD2_{400}$ induced removal of dynein from the microtubule plus ends? In principle, there could be a $BicD2_{400}$ induced allosteric modulation in the dynein-dynactin complex, which might prevent their interaction with EB1. Alternatively, the activation of dynein-dynactin motion in the presence of BicD2 could deplete the accumulated dynein pool at plus ends. This BicD2 induced depletion of

dynein from plus ends is reminiscent of the Num1 (yeast adaptor protein) fragment mediated removal of dynein from the microtubule plus ends seen in budding yeast (Lammers and Markus, 2015). Thus, similar to the biasing property of Num1 in budding yeast, BicD2 also seems to bias human dynein's behaviour from a non-processive plus-end tracking motor to a processive minus-end directed motor. Whether this biasing property can be generalised to other cargo adaptors of metazoan dynein remains to be tested.

4.3.3 Lis1 promotes and restores plus end tracking of dynein

Lis1 has been found to regulate several dynein properties across species (Cianfrocco et al., 2015; Kardon and Vale, 2009). Here, I investigated the role of Lis1 in controlling human dynein's plus-end tracking behaviour and its minus-end directed motion. Lis1 acts as a general microtubule recruiter of dynein-dynactin; however, in combination with BicD2, differential dynein-dynactin regulation was observed. 5 μM Lis1 could restore plus-end tracking of human dynein even in the presence of 5 μM BicD2. This observation supports the necessity of Lis1 in the plus end localisation of dynein in non-neuronal mammalian cells. In cells, several cargo adaptors drive dynein motion away from the plus ends, and Lis1 could conceivably inhibit dynein motion to sustain its plus-end localisation.

4.3.4 Lis1: An initiator of dynein motion

At a Lis1 concentration showing high motility in the dynein end tracking assay, a high number of motile DDB events were observed. This agrees with the previously studied role of Lis1 as an initiator of dynein transport in filamentous fungi (Lenz et al., 2006; Egan et al., 2012) and neurons (Moughamian et al., 2013). How does Lis1 promote the initiation of dynein transport? By increasing the dynein-dynactin recruitment to the microtubules, Lis1 probably favours the assembly of DDB complex on the microtubules. However, the binding of Lis1 to DDB, appeared transient, suggesting that Lis1 dissociates from the activated processively moving DDB complex. Therefore, BicD2

and Lis1 seem to compete for binding to the dynein-dynactin complex. However, Lis1 and BicD2 do not appear to share any binding site on dynein-dynactin; thus, the release of Lis1 upon BicD2 binding is likely allosterically governed.

At a Lis1 concentration showing high plus end tracking, I saw a decrease in the number of DDB runs, compared to when fivefold lower Lis1 was present. This surprising effect of reduced initiation at higher Lis1 concentration could be because Lis1 outcompetes BicD2 to favour the assembly of a non-processive dynein-dynactin-Lis1 complex thus preventing the formation of a processive DDB complex. This study provided direct evidence of Lis1 as an initiation factor and regulator of microtubule end localisation of dynein. Lis1 regulations seems to be multi-layered and dose-dependent. However, the picture is incomplete without the additional binding partner of Lis1, NudE/L, which further regulates the plus-end localisation and the transport properties of dynein (Huang et al., 2012; McKenney et al., 2010; Wang and Zheng, 2011). Furthermore, Lis1's interaction with CLIP170 (Coquelle et al., 2002; Tai et al., 2002), may provide yet another layer to dynein regulation.

4.3.5 Sequential regulation of multiple steps of dynein transport

The overall effect of dynein regulation studied here highlights an emergent role of Lis1 and BicD2 in controlling the plus-end tracking behaviour and the processive minus end directed motion of the dynein-dynactin complex. The direct implication of these multiple modes of dynein regulation could be in sequentially guiding each step of dynein driven cargo transport. From the data shown in this chapter, it is clear that dynein is recruited to microtubule plus ends by dynactin and EB1. Lis1 acts as recruiter of dynein to the microtubules, which together with BicD2, initiates dynein motion and at high concentration outcompetes BicD2 to increase the microtubule localisation of dynein to microtubule ends.

Chapter 5. Materials and Methods

5.1 Molecular Biology

For cloning DNA inserts were amplified from cDNA clones or preexisting expression plasmids using Kappa HiFi polymerase (KapaBiosystems; KK 2101) according to the manufactures recommendation. All the cloning was done using In-fusion (Clontech), which offers ligation free method. For this method, primers had to be generated so that the PCR amplicon contained 15 basepairs (bp) homologous to each end of the vector. The 5' end of the primer was vector specific and 3' end of the primer was gene-specific. All Primers were synthesized and purchased from Sigma Aldrich (desalt grade) and annealing temperatures were calculated using APE freeware (http://biologylabs.utah.edu/jorgensen/wayned/ape/).

Table 5.1 List of Primers

Primers for	Sequence (5' to 3')
Subcloning mGFP in the pdyn1 construct	Forward: CTCTATTTCCAGGGTATGAGCGTGAGCAAGG
	Reverse: CTCTATTTCCAGGGTATGAGCGTGAGCAAGG
pdyn1 Vector amplification	Forward: GGTTCTTCCGAACCTGGCG
	Reverse: ACCCTGGAAATAGAGATTCTCTGTAGTTGG
His_6SNAP	Forward: TATTTTCAGGGCGCCCGACAAAGATTGCGAA
	Reverse: GCCGACATGCCGCCACCGCCACC
His_6BicD_2400	Forward: TATTTTCAGGGCGCCGGAGGTGGCGGTGGCG
	Reverse: TTCGGATCCGGTACCTTACAGGCGCCGCAGGG
$His_6SNAPBicD_2400$	Forward: TGGCGGCATGTCGGCGCCGTCG
	Reverse: TTCGGATCCGGTACCTTACAGGCGCCGCAGGG

For gel extraction, PCR proucts were resolved on agarose gel, extracted, and purified using Gel Extraction Kit (Qiagen 28704). Vectors were linearised for 1 hour using standard restriction enzymes (all for New England Biolab, NEB, see table 2) and vectors were subsequently treated with Antarctic Phosphatase (NEB, M0289S) for another hour at 37˚C. After heat inactivation at 75 ˚C for 20 minutes, the vector and PCR amplicon were purified using the QIAquick Gel Extraction Kit. DNA concentrations were measured by spectrophotometer (Nanodrop). Inserts and linearized vectors were mixed in a 3:1 molar ratio and incubated with In-fusion enzyme mix for 15 minutes at 50ºC.

Then 50 µl of XL1 Blue *E. coli* cells (Stratagene) were transformed with 5 µl of infusion ligated mix using standard heat shock procedures (Froger and Hall, 2007) and Ampicilin (100 µg/µl,) or Kanamycin (50 µg/µl,) as a selection marker for agar plates. Plasmid DNA was isolated using QIAprep Spin Miniprep Kit (27104) from 6 ml liquid overnight cultures (at 37˚C, 160 rpm). Positive clones were selected by checking for inserts by restriction digestion followed by agarose gel electrophoresis and ethidium bromide staining. Sequences were confirmed by sequencing at GATC-Biotech (http://www.gatc-biotech.com).

Subcloning His_6mGFP in the pdyn3 construct

The dynein construct coexpressing all the six dynein subunit in one Multibac insect cell expression construct, called pDyn3 (Schlager et al., 2014) was gifted by Dr. Andrew Carter's lab (MRC LMB, Cambridge). The original pdyn3 construct was formed by Cre recombination of two plasmids (Schlager et al., 2014): pdyn1, where DHC (accession number NM_001376.4), with N-terminal His tag and SNAP tag was cloned into pACEBac1 (Vijayachandran et al., 2013); and pdyn2 with remaining 5 subunit of dynein DIC2 (AF134477), DLIC2 (NM_006141.2), Tctex1 (NM_006519.2), LC8 (NM_003746.2) and Robl (NM_014183.3) cloned into pIDC plasmid (Vijayachandran et al, 2013).

To generate the mGFP dynein complex from the original plasmid I replaced the N-terminal SNAP tag of pdyn1with the mGFP tag. The mGFP tag was PCR amplified from preexisting plasmid (mGFP-cc-yeastDyn331). The vector pdyn1 except the SNAP tag was also amplified by PCR. The amplified pdyn1 vector and mGFP tag was purified by gel extraction and ligated by Infusion enzyme (Clontech), as described above in this section. The mGFP pdyn1 was then fused to pdyn2 by using an *in vitro* Cre reaction (New England Biolabs) following the manufacturer's protocol to generate mGFP pDyn3. Briefly, the 0.3 μg pdyn1 and 0.2 μg pdyn2, 5 μl of Cre recombinase rection buffer, 1 μl of Cre recombinase enzyme, were mixed and ultrapure water was added to make the final reaction volume to 50 μl. This reaction was incubated at 37ºC for 30 minutes and then at 70ºC for 10 minutes, followed by transformation in XL1 Blue *E. coli* competent cells (Stratagene). The positive colonies were identified by PCR against all six dynein subunits and were further verified by sequencing.

5.2 Gel electrophoresis

Sodium dodecyl sulphate polyacrylamide gel electrophoresis (SDS-PAGE, (Laemmli, 1970)) for protein visualisation was done using NuPAGE 4-12% gradient gels (Invitrogen). Protein samples were denatured by adding Laemmli buffer and boiled at 70ºC for 10 minutes. A molecular weight marker, Precision plus Protein Standards (BioRad, 161- 0377) were used to identify the protein based on molecular weight. Gels were stained using coomassie brilliant blue (Meyer and Lamberts, 1965), and destained using buffer containing50% methanol, 10% glacial acetic acid.

The protein gels that were sent for mass-spectrometry were stained by commercial stain Instant*Blue* (SigmaAldrich) for 15 minutes and rinsed by distilled water for 5 minutes. The bands to be analysed were excised from the gel and sent to the proteomic laboratory for further processing. Gels from final step of dynactin purification from HeLa S3 cells were stained overnight with SYPRO ruby (Invitrogen), washed with ultrapure water and imaged using Image Quant LAS 400 detector (GE Healthcare).

For identification and processing of DNA agarose gel electrophoresis was performed using standard methods. Tris-Acetate-EDTA was used as running buffer and resolved gels were stained with ethidium bromide to visualize DNA. The stained DNA gel was visualized using Image Quant LAS 400 detector (GE Healthcare).

5.3 Western Blotting

Table 5.2 List of antibodies for Western blotting

Primary Antibody	**Raised in**	**Epitope**	**Company**	**Dilution**
Anti His	Mouse	6X His tag	Qiagen	1:2000
Anti DIC	Rabbit	Dynein Intermediate Chain	Invitrogen	1:1000
Anti DHC	Rabbit	Dynein Heavy Chain	Eurogentec	1:1000
Anti p150	Mouse	Dynactin p150subunit	BD bioscience	1:2000
Secondary Antibody				
Goat anti Rabbit HRP			Santacruz	1:10,000
Goat anti Mouse HRP			Santacruz	1:5000

Western blotting was performed to identify expressed and purified dynein and dynactin, and to monitor His tag cleavage from recombinant proteins by TEV protease using the primary and secondary antibodies listed in the Table 5.2. Protein samples were first resolved by SDS-PAGE, and then transferred onto the nitrocellulose membranes (Whatman Protran) using a tank-blotting chamber (Bio Rad) for 2 hours at a constant current of 300 mA in precooled transfer buffer in a cold room (4 ˚C). The transfer buffer used was: 0.025 M Tris, 0.192 M Glycine and 20 % Methanol (Towbin et al., 1992). The membranes with the protein of interest were first blocked by 5% nonfat milk (dissolved in PBST buffer- PBS and 1% Tween-20) for 1 hour at room temperature, followed by three rounds of washes with PBST buffer. Blocked membranes were then incubated with primary antibody (diluted in blocking solution) against the protein of interest for 2 hours at room temperature. Membranes were washed thrice with PBST for 5 minutes each and then incubated with horseradish peroxidase conjugated secondary antibody (diluted in blocking solution) for 1 hour, then washed with PBST (three times, 5 minutes). Finally, chemiluminescence substrate (from Amersham ECL Advance – Western Blotting detection Kit) was added to the blot and the signal was visualised using an Image Quant LAS 400 detector (GE Healthcare).

5.4 Protein expression

5.4.1 Protein expression in E. coli

Proteins were expressed in *Escherichia coli* BL21-RIL competent cells (Stratagene, Cat no: 230240). For expression in *E. coli,* 100 ng of plasmid DNA was added to 50 µl of cells and incubated on ice, followed by heat shocked for 45 seconds at 42˚C and transferred back on ice for 5 minute supplemented with 1 ml standard LB medium (media kitchen LRI) and incubated for 1 hour at 37˚C. The LB medium with grown transformed cell was then spread onto agar plates (media kitchen, with 30 µg/µl Chloramphenicol and Kanamycin (30 µg/µl) or Amplicilin (100 µg/µl). Agar plates were incubated over night at 37 ˚C. On the following day, a single colony was picked for an overnight culture (1 l LB medium, supplemented with antibiotics and 2% Glucose at 160 RPM and 37˚C using a 5 l Erlenmeyer flask and a shaker. On the next

day, overnight cultures were diluted 1:10 in LB medium containing antibiotics and (but without glucose) and were transferred to 37˚C while shaking at 160 RPM was maintained. The cell proliferation was monitored using the OD_{600} on a conventional spectrophotometer (Ultrospec 3100 pro, Amersham). Once an OD_{600} of 0.8 was reached, the cultures were transferred to 18˚C and expression was induced with 1 mM Isopropyl β-D-1-thiogalactopyranoside (Roche, 11411446001) overnight. The next day, cells were harvested by centrifuging (20 min, 4000g, JLA 81000 rotor (Beckman) 4 ˚C) and the pellets were recovered. The Pellets were re-suspended in ice-cold PBS (10 mM Na2HPO4, 18 mM KH2PO4, 27 mM KCl, 137 mM NaCl, pH 7.4), transferred into 50 ml Falcon tubes (Corning) and centrifuged (15 min, 4000g, centrifuge (Multifuge X1R, Thermo). The washed cell pellet was flash frozen and stored at -80ºC.

5.4.2 Insect cell culture and expression

Sf21 (*Spodoptera frugiperda* 21) insect cells (originally provided by Imre Berger, EMBL Grenoble) and Sf-900 II SFM serum-free medium (Invitrogen) was used cell culture. Cells were counted every 24 h and maintained at 0.5 x 10^6 cells/ml in Erlenmeyer flasks (Corning, Sigma Aldrich) of five times the cell culture volume. DH10MultiBac10 cells (Bieniossek et al., 2012). (Life technologies) were used for generation of the recombinant bacmids. DH10 MultiBac cells were transformed with 100 ng pFastBac vector (Fitzgerald et al., 2006) containing the gene of interest using standard electroporation (Dower et al., 1988) and were grown in SOC (Life technologies) medium for 6 hours and plated onto agar plates with Gentamycin (7 μg/ml), Teracyclin (10 μg/ml), Kanamycin (50 μg/ml), Bluo-Gal/X-Gal (0.1 mg/ml) and Isopropyl β-D-1- thiogalactopyranoside (40 μg/ml). Colonies were selected based blue white screen, (Ullmann et al., 1967) after 2 days at 37 ˚C. To confirm selection of positive clones and to check if the colonies maintained colour, the colonies were restreaked and incubated for another 2 days. Bacmids were isolated from 100 ml LB overnight cultures (160 RPM, 37 ˚C) using NucleoBond® Xtra Midi prep kits (Macherey-Nagel, 740410.10).

Freshly prepared recombinant bacmids in combination with FuGENE transfection reagent (Roche) were used to transfect *Sf21* cells in 6-well plates used for tissue culture.

Viruses were collected 48 hours after the transfection and used for virus amplification and to obtain high-titer viruses. Generally, 2 ml of initial viruses were used for infection of 25 ml of *Sf21* cell culture (at $0.6x10^6$ cells/ml) and the cells were split every 24 hours to $0.6x10^6$ until *Sf21* cells were arrested. Viruses were collected 48 hours after proliferation arrest. These second generations of high-titer viruses were used for large-scale (~600 ml) expression of the recombinant proteins in *Sf21* cells. The viruses were used in a dilution that allowed one round of doubling of the infected *Sf21* cells before cell proliferation was arrested (low multiplicity of infection) (Fitzgerald et al., 2006). The dynein complex subunits, His_6-GFP-DHC and DIC1 were expressed for 60 h after proliferation arrest. The pdyn3 construct, the three constructs of His_6-GFP-cc-Dyn380kD with different linker lengths, His_6-GFP-yeast-Dyn331kD, and Lis1-mCherry-His_6 were expressed for 72 h after the arrest. After the expression, the cells were harvested by centrifugation at 6,000 rpm at 4ºC (JLA 8.1 rotor). The pellets were washed with ice-cold PBS, flash frozen and stored at -80ºC.

5.5 Protein Purification

5.5.1 Recombinant human dynein complex

The human dynein complex used in this thesis were expressed and purified from insect cells by two methods:

1. Step-wise assembly of dynein subunits expressed sepeartely
2. Coexpression and purification of all the six dynein subunits from a single plasmid

For the step-wise assembly of the dynein subunits the method described in (Trokter et al., 2012) was followed. The full-length dynein heavy chain (DHC), with N-terminal His tag followed by an mGFP tag, was expressed in *Sf21* cells(Trokter et al., 2012). The dynein intermediate chain 1 (DIC1) was expressed in separate *Sf21* culture (Trokter et al., 2012). The other dynein subunits, dynein light intermediate chain2 (DLIC2), light chains (LCs: Roadblock, Tctex1, LC8) were expressed and purified from *E. coli*

(Trokter et al., 2012). The full-length DHC protein is insoluble and requires DIC and DLIC2 for solubility (Trokter et al., 2012). Therefore, for solubility of dynein the DHC and DIC lysates and purified DLIC2 were mixed, and this dynein subcomplex is purified by **i**mmobilized **m**etal **a**ffinity **c**hromatography (IMAC) (Trokter et al., 2012). The LCs were then added to the affinity purified dynein subcomplex. Further purification by gelfiltration allowed separation of the aggregated dynein complex and nonspecific proteins from the fully assembled dynein complex (Trokter et al., 2012).

Detailed purification protocol

At the beginning of the purification, the affinity column (HiTrap chelating HP 5ml) was washed with 3 column volumes (CVs) ultrapure water, 1 CV $CoCl_2$, 3 CVs water, 10 CVs lysis buffer (50 mM HEPES, 250 mM K-acetate, 2 mM MgSO4, 0.25 mM EDTA, 10% glycerol (vol/vol), 0.2 mM Mg-ATP, 1 mM β-mercaptoethanol, 20 mM imidazole, pH 7.4, protease inhibitors (Complete EDTA-free, Roche)). Pellet of His_6-mGFP-CDHC from ~1 L *Sf21* heavy chain and pellet of DIC1 from ~250 ml were thawed and resuspend in ~30 ml of ice-cold lysis buffer and mixed together. Resuspended pellet mixture of DIC and CDHC was then lysed using a dounce homogenizer (20 tight strokes). 2 mg of purified LIC2 was added to the lysates. The lysate was then clarified by centrifugation at 50,000 rpm for 30 minutes at 4°C (Ti70 rotor), and the supernatant was recovered and kept at 4°C. The clarified lysate was applied to a 5 ml HiTrap HP column loaded with Co^{2+} ions equilibrated in lysis buffer at 1 ml/min flow rate.

After loading the column was washed with the lysis buffer equivalent to 15 CVs. The mixture of His_6-mGFP-DHC, DIC1, and LIC2 was eluted with elution buffer (50 mM HEPES pH 7.4, 250 mM K-acetate, 2 mM MgSO4, 0.25 mM EDTA, 10% glycerol (vol/vol), 0.2 mM Mg-ATP, 1 mM β-mercaptoethanol, 350 mM imidazole, protease inhibitors (Complete EDTA-free, Roche)), and collect 0.5 ml fractions. To the affinity-purified dynein (containing three subunits), 150 μg of each light chains (LC8, RB1 and Tctex1 purified from *E. coli*) was added, followed by buffer exchange (using PD10 column) into gel filtration buffer (30 mM HEPES pH 7.2, 150 mM K-acetate, 2 mM MgSO4, 0.5 mM EGTA, 10% glycerol (vol/vol), 0.05 mM Mg-ATP, 10 mM β-mercaptoethanol). His_6 tag of DHC was cleaved with TEV protease; by adding 1 mg TEV per 30 mg protein and incubated overnight at 4°C.

The affinity purified dynein complex was further purified by gel filtration using protein using Superose 6 XK 16/70 prep grade column equilibrated in gel filtration buffer. The dynein containing fractions were pooled (fractions close to the column void volume was not collected) and concentrate using Vivaspin column with 50 kDa cut-off (up to 0.2 mg/ml). The concentrated protein was centrifuged at 100,000 g for 10 minutes at 4°C (TLA 120 rotor). The purified protein (Figure 5.2) was supplemented with 10% glycerol (vol/vol), flash frozen in 5 μl aliquots and store in liquid nitrogen. The final concentration was 0.18 mg/ml.

The human dynein complex was also purified from mGFP pdyn3 construct that expressed all the six dynein subunit from one plasmid, as described in (Schlager et al., 2014). The cell pellet (~800 ml) transfected with GFP pdyn3 expressing all the dynein subunits was resuspended in the lysis buffer (50 mM HEPES pH 7.4, 250 mM K-acetate, 2 mM MgSO4, 0.25 mM EDTA, 10% glycerol (vol/vol), 0.2 mM Mg-ATP, 1 mM β-mercaptoethanol, 20 mM imidazole, protease inhibitors (Complete EDTA-free, Roche)) and lysed by dounce homogenization, clarified by centrifugation following the same procedure as described in the above protocol. The complex was purified by IMAC (Figure 5.1A) via the His tag on the DHC subunit and further purified by gel filtration (gel filtration buffer was: 30 mM HEPES pH 7.4, 150 mM K-acetate, 2 mM MgSO4, 0.5 mM EGTA, 10% glycerol (vol/vol), 0.05 mM Mg-ATP, 10 mM β-mercaptoethanol) using Superose 6 XK 16/70 prep grade (Figure 5.1 B and C). The dynein complex was pooled supplemented with 10% glycerol and flash frozen in 5 μl aliquot size and stored in liquid nitrogen. The final concentration was 0.30 mg/ml.

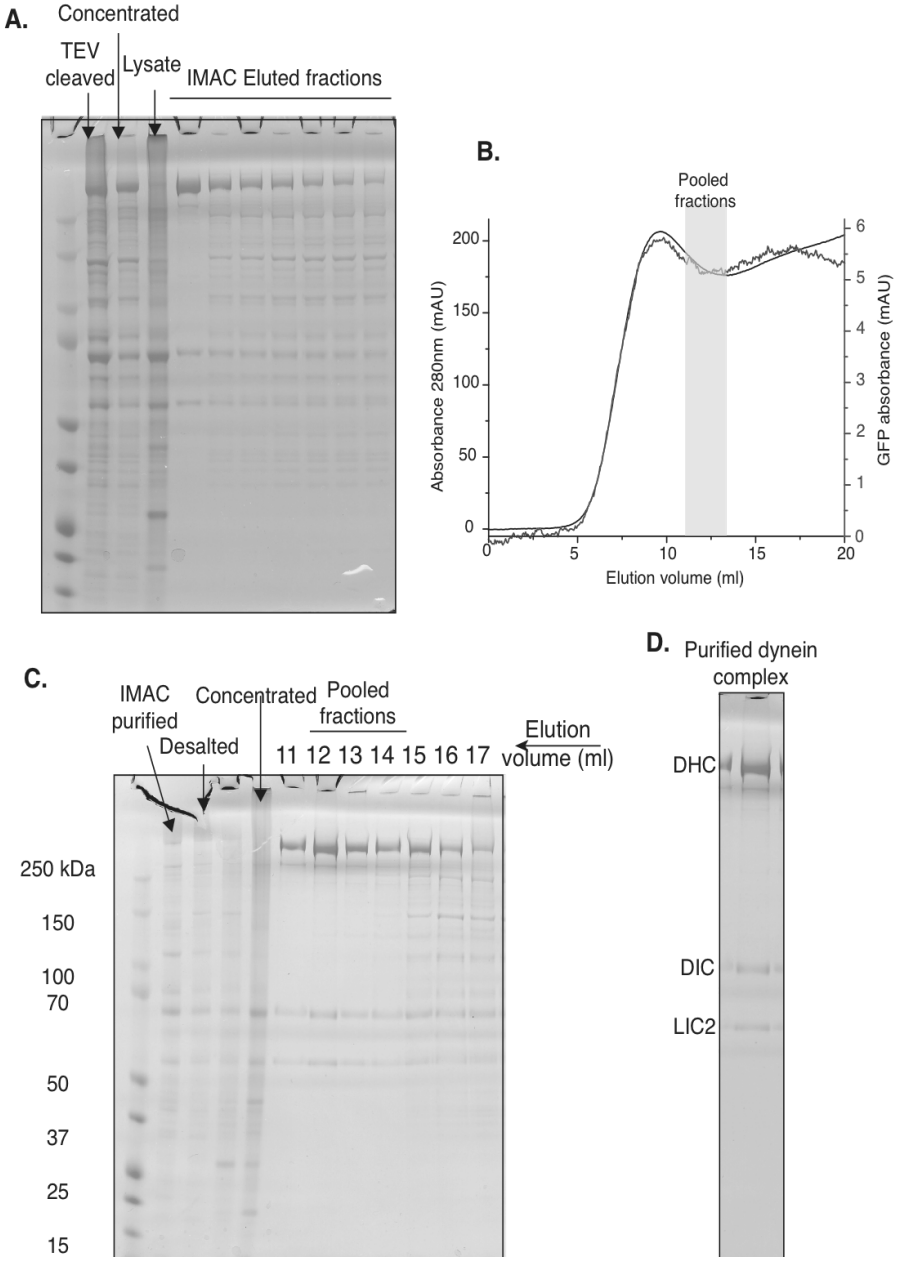

Figure 5.1 Purification of the human dynein complex from mGFP pdyn3

(A) SDS-PAGE of IMAC purification of recombinant dynein complex; Lysate: the clarified lysate that was loaded on to the column for IMAC purification. IMAC eluted fractions: the fractions eluted by imidazole and pooled. TEV cleaved: dynein complex after His tag purification. Concentrated: TEV cleaved dynein complex concentrated before gel filtration (**B)** Gel filtration elution profile. Red and black curves are GFP and 280 nm absorbance respectively. (**C)** SDS-PAGE of gel filtration of recombinant dynein showing: IMAC purified: Dynein after the first round of purification. Desalted: Dynein eluted from IMAC column was exchanged into gel filtration buffer using PD10. Concentrated: the desalted dynein complex was concentrated before loading to Superose 6 XK 16/70 prep grade column. Pooled fractions: Fractions from gel filtration containing dynein that was pooled and stored (also shown in the gel filtration profile). **D.** SDS-PAGE of dynein complex showing dynein subunits.

5.5.2 Artificially dimerised human dynein fragment

The His_6-GFP-cc-Dyn380kD of different linker lengths were expressed in Sf21 cells. Typically cell pellet from ~600 ml Sf21 cell culture was used for purification of each construct. The pellet was thawed and resuspend in ~20 ml of ice-cold lysis buffer (50 mM HEPES pH 7.4, 250 mM K-acetate, 2 mM MgSO4, 0.25 mM EDTA, 10% glycerol (vol/vol), 0.2 mM Mg-ATP, 1 mM β-mercaptoethanol, 20 mM imidazole, protease inhibitors (Complete EDTA-free, Roche)). The resuspended pellet was lysed using a glass homogenizer (20 tight strokes). The lysate was clarified by centrifugation at 50,000 rpm for 30 minutes at 4°C (Ti70 rotor). The supernatant was recovered and applied to the HiTrap HP column loaded with Co^{2+} ions equilibrated in lysis buffer at 1 ml/min flow rate. After loading the column with lysis buffer (10 CV) and eluted with elution buffer (50 mM HEPES pH 7.4, 250 mM K-acetate, 2 mM MgSO4, 0.25 mM EDTA, 10% glycerol (vol/vol), 0.2 mM Mg-ATP, 1 mM β-mercaptoethanol, 350 mM imidazole, protease inhibitors (Complete EDTA-free, Roche)) and collected in 0.5 ml fractions. The pooled protein containing fractions were desalted to the buffer into gel filtration (30 mM HEPES pH 7.4, 150 mM K-acetate, 2 mM MgSO4, 0.25 mM EDTA, 10% glycerol (vol/vol), 0.2 mM Mg-ATP, 1 mM β-mercaptoethanol, 20 mM imidazole) buffer supplemented with protease inhibitors using a PD10 desalting column.

His-tag was cleaved using TEV protease (by adding 1 mg TEV per 30 mg protein) and cleave overnight at 4°C. The proteins were gel filter the protein using Superose 6 10/300 GL column equilibrated in gel filtration buffer. The pool dynein containing fractions and concentrate using Vivaspin with 50 kDa cut-off, centrifuged at 100,000 g for 10 minutes at 4°C (TLA 120). The pooled protein was supplement with 10% glycerol (vol/vol), flash freeze in small aliquots and store in liquid nitrogen. The final yields of purified His_6-GFP-cc-Dyn380kD of the three different linker lengths were typically ~2 mg from 500 ml Sf21 cell culture, with a final concentration up to ~1 mg/ml (Figure 5.2).

5.5.3 Artificially dimerised yeast dynein fragment

His6-GFP-yeastDyn331 was expressed and purified from *Sf21* cells. Because of low expression of yeast dynein construct, cell pellet from ~1.2 l of culture was used for one round of purification. The buffers, purification steps and storage condition were the same as described for purification of human dynein fragments. The final concentration was 0.3 mg/ml.

5.5.4 Human LIS1

His_6-mCherry-Lis1 was expressed and purified from *Sf21* cells using the construct cloned by Martina Trokter. The cell pellet from ~600ml cell culture was resuspended in lysis buffer (50 mM HEPES pH 7.4, 100 mM KCl, 1 mM ßME, 0.05 mM ATP, 10% (v/v) glycerol, protease inhibitor), lysed using dounce homogenizer and clarified by centrifugation. The clarified lysate (40ml in volume) was incubated with 1g of Proteino Ni-TED beads (Macherey-Nagel) in a batch format, transferred to a column and washed with ~ 100 ml lysis buffer. After washing, the Lis1 bound to the resin via His tag was eluted by incubating with TEV protease (5 mg/ml TEV mixed in lysis buffer) for 1 hour at room temperature (resuspending the beads every 5 minutes). The cleaved protein was separated from the beads by centrifugation (at 1000 g for 2 minutes at 4ºC) and the supernatant was recovered. The cleaved Lis1-mCherry was concentrated to 0.5ml volume and loaded onto Superdex 200 10/300 GL column (GE healthcare) for gel filtration (gel filtration buffer was same as lysis buffer). Lis1 containing fractions were identified by SDS-PAGE Coomassie staining and pooled. mCherry Lis1 (Figure 5.2) was supplemented with 20% glycerol (vol/vol), flash frozen in 5 μl aliquots and stored in liquid nitrogen. The final concentration estimated by Bradford was 2mg/ml.

5.5.5 Human $BicD2_{400}$

His_6-$BicD2_{400}$ and His_6-SNAP-$BicD2_{400}$ were expressed in BL21 RIL *E. coli* strain. Typically pellets from 4 l cell culture were used for purification of both the $BicD2_{400}$ constructs. The pellets were resuspended in lysis buffer (50 mM HEPES pH 7.4, 100

mM KCl, 10 mM Imidazole, 1 mM ßME, 0.1 mM ATP, protease inhibitor). The resuspended pellet was lysed using a microfluidizer. The lysate was clarified by centrifugation (at 38000 rpm for 45 minutes, at 4ºC using Ti70 rotor). The clarified lysate was loaded onto a prepacked 5 ml HisTrap column (GE Healthcare), which was equilibrated with the lysis buffer. Afer loading the column was washed with 20 CVs of lysis buffer. The protein was eluted using imidazole contacting elution buffer (50 mM HEPES pH 7.4, 100 mM KCl, 300mM Imidazole, 1 mM ßME, 0.1 mM ATP, protease inhibitor). The BicD2 containing fractions were pooled and dialysed into gel filtration buffer (50 mM HEPES pH 7.4, 100 mM KCl, 1 mM EGTA, 1 mM ßME, 0.1 mM ATP). To build BicD2 column used for dynactin purification, the dialysed $BicD2_{400}$ was stored in 1 ml aliquots at -80ºC until further use. The final concentration was 10mg/ml. Untagged $BicD2_{400}$ used for reconstitution experiments was further purified by gel filtration using Superdex 200 10/300 GL column (GE healthcare). The fractions of $BicD2_{400,}$ were pooled, concentrated to 2 mg/ml and flash frozen in 5 μl aliquots and stored in liquid nitrogen (Figure 5.2).

For labelling SNAP-$BicD2_{400}$, the IMAC purified SNAP-$BicD2_{400}$ was mixed with same molar concentration of Alexa 647SNAP dye, and incubated overnight at 4ºC. The mixture was the passed through HiPrep 26/60 Desalting columns to remove excess Alexa 647 SNAP dye. The fraction containing SNAP-$BicD2_{400}$ was pooled and further purified by Superdex 200 column (GE healthcare). The fractions of Alexa 647 labelled SNAP-$BicD2_{400,}$ were pooled, concentrated 0.8 mg/ml and flash frozen in 5 μl aliquots and stored in liquid nitrogen. The labelling ratio with Alexa 647-SNAP dye was 1.1.

5.5.6 Human EB3

I expressed SNAP EB3 from *E. coli* (BL21 RIL strain) using a construct cloned by Julian Gannon (from Surrey Lab). The first round of purification by IMAC was done by Johanna Roostalu (from Surrey Lab) following the same procedure described for $BicD2_{400}$ purification. The SNAP EB3 was labelled with Alexa 647-SNAP dye (method as described for labelling $BicD2_{400}$). I carried out the subsequent round of purification, using HiPrep 26/60 desalting columns and gel filtration using Superdex 200 10/300

column (GE healthcare). The fractions of Alexa 647-SNAP-EB3 were pooled and stored at 0.6 mg/ml by flash freezing and storage in liquid nitrogen.

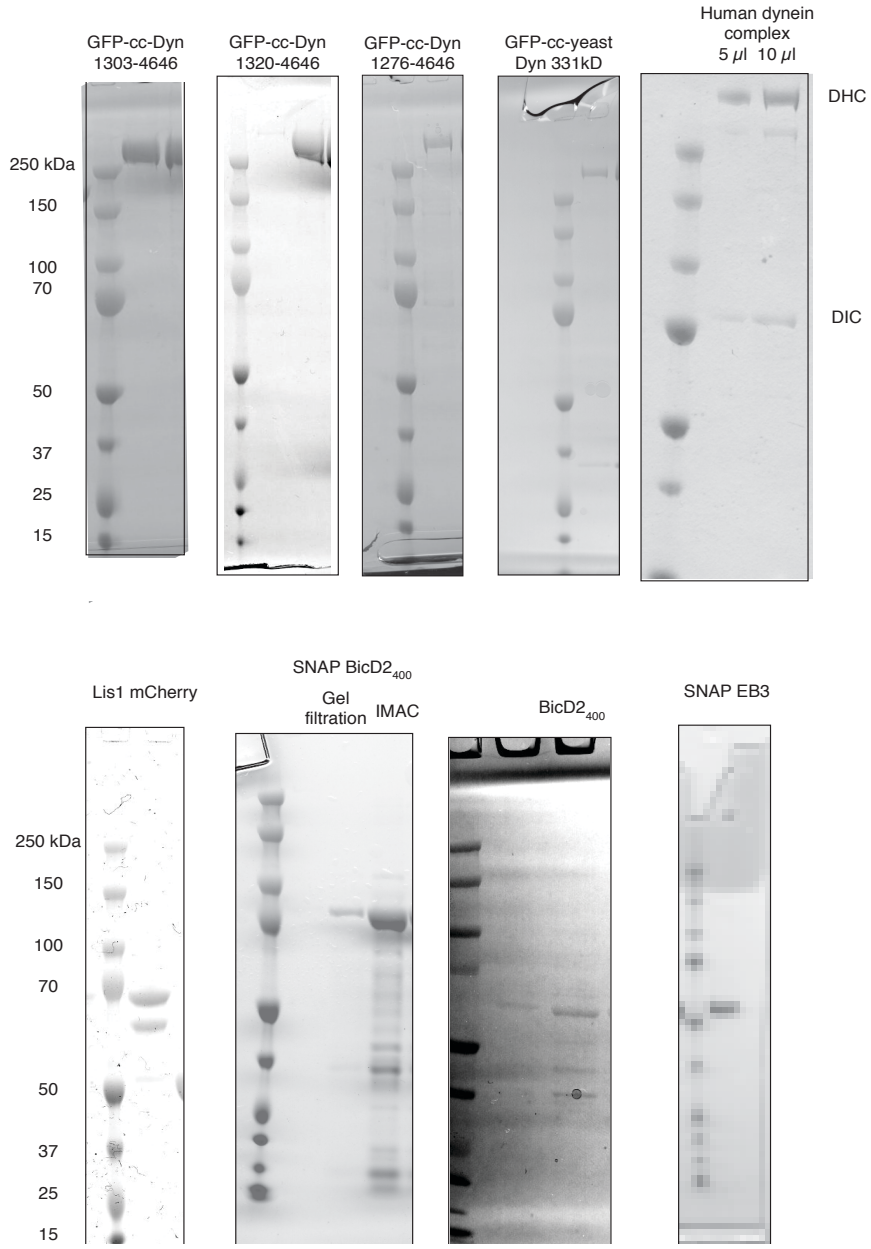

Figure 5.2 SDS PAGE gels of purification of the recombinant proteins

SDS-PAGE coomassie stained gels of purified recombinant proteins. GFP-cc-Dyn gels of three different linker lengths studied in Chapter 2. The lengths DHC sequence in the dynein constructs were: 1303-4646; 1320-4646; and 1276-4646 amino acids. cc is the kinesin-1 coiled-coil neck linker sequence used for dimerisation of truncated DHC fragments. The gels show the final purified protein after gel filtration except the SNAP-BicD2$_{400}$ where both IMAC purified (used for building BicD2 column for dynactin purification) and SNAP-BicD2$_{400}$ after gel filtration (used for reconstitution experiments) is shown in the gel.

Table 5.3 Total yield and final concentrations of recombinant proteins

Protein	Culture volume (ml)	Total yield (mg)	Concentration (mg/ml)
Dynein complex	600	0.5	0.3
Human dynein artificial dimers	600	2	1
Yeast dynein artificial dimer	1200	0.2	0.3
SNAP-BicD2$_{400}$	3000	20	10
Alexa 647-SNAP-BicD2$_{400}$	3000	20	2
mCherry Lis1	600	2	2
Alexa 647-SNAP-EB3	3000	1.2	0.6

5.6 Extended method of dynactin purification

In this section I present the detailed protocol for purification of the dynactin complex described in Chapter 3.

i) Preparation of BicD2 Column:

His$_6$-SNAP-BicD2$_{400}$ fusions to HiTrap NHS-activated HP column 5 ml.

Before coupling: Column washed with 3 CV of ice-cold 1 mM HCl 1.5 CV/min

Coupling BicD2: Continuously recirculating the BicD (1.5 CV/min, 4 CV of a 4 mg/ml preparation) for 30 min at room temperature. i.e. about 4ml of purified protein.

Blocking unreacted group: Unreacted NHS groups were blocked by washing with 6 CV of 0.5 M ethanolamine and 0.5 M NaCl at pH 8.3 and then incubated for 30 min at room temperature.

Washing the blocked column: The column was washed with 6x PBS, followed by 1x PBS with 50% glycerol (storage buffer) and stored at –20°C.

Storage and re-equilibrating: Column could be used repetitively if washed between runs with: 10 CV of 10× PBS, followed by 5 CV of 1×PBS and then 5 CV of storage buffer (1× PBS with 50% glycerol).

ii) BicD2 affinity purification:

Lysis: 4 pellets of 25 l culture (2 × 10^6 cells/ml) of Hela S3 cells were used for purification on one day, and for each pellet one BicD2 column of 5 ml CV was used.

The volume of each cell pellet was approximately 70 ml, and was resuspended in equal volume of dynein buffer supplemented with 1 mM DTT and protease inhibitors.
Cell pellets were resuspended in dynein buffer: 30 mM HEPES pH 7.2, 50 mM KAc, 1 mM EGTA, 5 mM MgAc, 0.5 mM ATP, 2 mM BME, supplemented with protease inhibitor and 10 μg/ml DNAse. The resuspended pellets were homogenised using polytron tissue dispenser (Blending cycle: $4x10^3$ rpm, 1.5 mins; 2 minutes incubation on ice; 6.6 $x10^3$ rpm, 1.5 mins; 2 minutes incubation on ice; and last 6.6 $x10^3$ rpm,1.5 mins). The homogenised extract from all the four pellets were cleared by centrifugation (at 38,000 rpm for 40 min at 4°C in a Ti45 rotor). The clarified lysate was then filtered through a 0.22 μm Steritop filter of 250 ml capacity (Millipore, Bedford, MA). The filtered extract (approx. 400 ml) was equally divided in four parts each to loaded on separate BicD2 column.

Loading the lysate onto BicD2 column: Approximately 100 ml filtered lysate was loaded at 0.5 CV/min onto a BicD2 column, which was preequilibrated with dynein buffer. Four columns were loaded in parallel. The column was washed with 5 CV of wash buffer (dynein buffer with 100 mM NaCl) at 1 CV/min flow rate.

Salt gradient elution: The elution was done on Akta FPLC system (GE healthcare). Before elution the pumps were first washed with degassed water and the dynein buffer.
Two BicD2 column were connected in series onto one AKTA system, and the dynein-dynactin was eluted by applying linear NaCl gradient. The fractions enriched in dynactin were pooled, divided in 1 ml aliquots, flash frozen and stored at -80ºC.

Storage and re-equilibriating of BicD2 column: Column can be used repetitively if washed between runs with: 10 CV of 10× PBS, followed by 5 CV of 1×PBS and then 5 CV of storage buffer (1× PBS with 50% glycerol).
BicD2 affinity purification was done for three days using a total 300 l of HelaS3 cell culture. All the BicD2 column eluate were pooled and subject to anion exchange chromatography.

iii) Anion exchange chromatography – Mono Q 5/50 HR column

BicD2 column eluate was exchanged into Mono Q equilibration buffer (35 mM Tris pH 7.2, 5 mM MgSO4, with 0.5 mM ATP and 2 mM ßME) using 6 HiPrep 26/60 Desalting columns connected in series. The desalted protein was pooled and centrifuged (at 70,000 rpm for 20 minutes using Ti70 rotor) and injected to an equilibrated Mono Q (washed with degassed water and in Mono Q equilibration buffer) column using a 150 ml Superloop. After injection, the column was washed with 5 CV of Mono Q equilibration buffer, and the dynactin complex was eluted by applying a stepwise gradient of 1 M NaCl (1 M NaCl dissolved in Mono Q equilibration buffer), using the following programme:

Table 5.4 Mono Q elution programme for purification of dynactin

NaCl concentration	Volume (ml)	Flowrate
0	14.9	1.0
0-280	25.2	1.0
280-320	Step	
320-340	46.8	0.5
340-390	Step	
390-500	28.0	0.5
500-1000	2.0	1.0
1000	12.0	1.0
1000-0	2.0	1.0

The dynactin complex eluted at 390 mM NaCl in three fractions of 0.5 ml size. The fractions were pooled and exchanged to cryostorage buffer (30 mM HEPES, 50 mM KAc, 1 mM EGTA, 2 mM MgAc, 0.5 mM ATP, 2 mM BME, 10% glycerol, pH 7.2). After buffer exchange dynactin was centrifuged (at 70,000 rpm, at 4ºC in TLA 110), flash frozen in 5 μl aliquots and stored in liquid nitrogen.

For dynactin purification from pig brains, all the steps were the same except the following:

1. Lysis: Two frozen pig brains were chopped into small pieces, the volume of lysis buffer added was two times the total volume of chopped brain pieces. The brain was thawed on ice and homogenized using a polytron dispenser following the same cycle as mentioned for HeLa S3 cell lysis.
2. Clarifying the lysate: The homogenate after lysis was centrifuged twice, first: 29000 g, 30 mins, in JLA 16.25 at 4ºC; and second: 35000 rpm Ti45, 30 mins, 4ºC. The clarified lysate was not filtered.

3. Number of BicD2 columns: The lysate from two brains were loaded onto one BicD2 column, and the first round of purification was done in one day. The BicD2 column eluate were stored at 4ºC and loaded onto MonoQ 5/50 HR the next day, following the same procedure as mentioned for purification from Hela S3 cells.

5.7 Tubulin purification and polymerisation

Tubulin was purified as described (Castoldi and Popov, 2003)and NHS- biotin (Pierce), NHS-Alexa 568 (Life technology) or NHS-Atto 647N (Sigma Aldrich) was covalently bound as decribed (Hyman, 1991).

Preparation of GMPCPP-stabilized microtubules

To prepare GMPCPP microtubule seeds, 0.8 µl labelled (Alexa 568 or Atto 647) tubulin (stock [150 μM]), 2 μl biotinylated Tubulin (150 μM), 2 μl of untagged tubulin (20 mg/ml) were mixed, 5 μl of GMPCPP was added to the tubulin mix and BRB80 was added to make the total volume to 50 μl. This mixture was incubated for 1 hour at 37ºC for polymerization of microtubules. After polymerization, 450 μl warm BRB80 was added and centrifuge for 10 minutes at 17000 rpm in a tabletop centrifuge. The pelleted microtubule was washed with 100 μl of warm BRB80 and resuspend in 50 μl of warm BRB80. This method generated short GMPCPP seeds that were used in dynamic microtubule assays.

For gliding and single molecule assays using stabilized microtubules (used in chapter 2 and 3), the polymerized GMPCPP seeds were incubated at room temperature overnight to allow fusion and formation of long GMPCPP microtubules. Next day the microtubules were centrifuged again, washed twice with 100 μl of warm BRB80 and resuspended in 50 μl of warm BRB80.

5.8 Surface chemistry

Functionalising glass with Tris-NTA and biotin-PEG

Tris-NTA-PEG and biotin-PEG functionalised glass coverslips were prepared as previously described (Bieling et al., 2010), with the following modification for the biotin-PEG glass preparation: After silanisation, a mixture of 90% hydroxy-PEG-2000-amine and 10% biotin- PEG-3000-amine (from Rapp Polymere) was coupled to the glass. Glass coverslips were stored at 4ºC.

To assemble the flow cells, first the counter glass surface was passivated by streaking and drying PLL-PEG (poly (L-lysine)-PEG) and then washed extensively with distilled water. Four flow cells of approximately 10 μl volume each were built from one-fourth part of a functionalized coverslip and one PLL-PEG passivated counter glass, separated by two stripes of double sticky tape (Tesa).

5.9 TIRF microscopy

All microscopy data for results chapter 3 and 4 were acquired on a TILL Imic 4001 TIRF microscope (http://www.till-photonics.com/Products/tirf.php) in 360 mode. Each fluorescent channel was split onto an individual cooled Evolve EMCCD camera (Photometrics), which allowed simultaneous imaging of a 488, 561 and 640 (based on excitation) channels. All microscopy data for results chapter 2 were acquired on an Olympus XI71 TIRF microscope. All TIRF imaging experiments in chapter 4 were performed at 30˚C.

5.9.1 MT gliding assay

(a) Microtubule gliding assay on Ni^{+2}-Tris-NTA surface

Tris-NTA-PEG functionalized glass coverslips were loaded with Ni^{+2} by incubating the surface with the following series of solutions: (1) 100 mM HCl for 2.5 min to clean the 120 surface, (2) wash buffer (20 mM HEPES, 150 mM NaCl, pH 7.5) for 15 min, (3) 20 mM $NiCl_2$ in wash buffer for 5 min and (4) 200 mM imidazole in wash buffer for 5 min. The Ni^{+2}-loaded slides were stored in wash buffer and used on the same day. Flow cells

were built from Ni-Tris-NTA-PEG functionalized coverslips and PLL-PEG passivated counter glass. The flow cells were first passivated by incubation with 50 µl 5% Pluronic F-127 in water for 5 minutes. The flow cells were then placed on an ice and washed with 50 µl immobilization buffer (motor storage buffer lacking glycerol). 20 µl His_6-motor diluted in immobilization buffer (the concentrations of motors are mentioned in the figures) was incubated for 30 minutes, followed by saturation of free Ni-Tris-NTA-binding sites by incubation with 50 µl 10 µM His_6-GFP (purified by Iris Lueke) diluted in immobilization buffer for 3 minutes. The non-bound proteins were washed off with 50 µl immobilization buffer and 50 µl gliding assay buffer (GB: 10 mM PIPES, 35 mM KOAc, 2 mM MgSO4, 1 mM EGTA, 2 mM Mg-ATP, 2 mM β-mercaptoethanol, 20 mM glucose, pH 7.0). The flow cells were warmed to room temperature and 50 µl of GB supplemented with oxygen scavengers (20 µg/ml catalase and 160 µg/ml glucose oxidase) and diluted Alexa 568-labeled GMPCPP microtubules (diluted in BRB80) were flown in the chamber. Microtubules were visualized at 25°C by time-lapse TIRF microscopy, using 100x objective. Microtubule transport was observed in 532 nm and time-lapsed images were acquired at 1s time intervals with 100 ms exposure times.

(b) Kymograph analysis of gliding assays

To determine the velocities of microtubule gliding from a time-lapse movie, the tracks of gliding microtubules were analyzed with the 'Multiple Kymograph' plug-in for ImageJ (J. Rietdorf and A. Seitz, EMBL Heidelberg). Velocities were determined from kymographs for gliding intervals of 2 minutes. About 100 microtubules were analyzed per condition. Microtubule gliding velocities were displayed in a histogram, and a Gaussian function was fitted to each histogram using Origin. The reported mean velocity is the center of the peak of the fitted Gaussian function and reported errors are standard error of the mean (s.e.m.).

5.9.2 Single dynein motility on static MT

For dynein motility experiments reported in Chapter 3, single GFP-labelled motors (artificially dimerised human and yeast dynein motors and human dynein complex) were imaged at low concentrations on immobilized fluorescently labelled GMPCPP

microtubules using TIRF microscopy (Bieling et al., 2010). The assay buffer was (AB): 30 mM HEPES pH 7.2, 50 mM K-acetate, 2 mM MgSO4, 1 mM EGTA, 10 mM β-mercaptoethanol, 1 mM ATP previously used to study dynein motility in (Reck-Peterson et al., 2006). Flow cells were built from biotin-PEG functionalized coverslips and PLL-PEG passivated counter glass. The flow chamber was passivated by incubation on an ice-cold metal block with 20 µl 5% Pluronic F-127 in water for 5 minutes, followed by washing with 50 µl of 50 µg/ml kappa-casein (Sigma) dissolved in assay buffer (AB). To enable microtubule immobilization, 50 µl of 50 µg/ml kappa-casein and 50 µg/ml NeutrAvidin (Invitrogen) in AB were incubated for 5 minutes and the flow chamber was washed with 50 µl of kappa-casein containing AB and 50 µl of AB. The flow chamber was then allowed to warm up to room temperature, and 50 µl of diluted Alexa 568-labelled biotinylated GMPCPP microtubules in BRB80 were flown into the chamber and incubated for 5 minutes. Non-bound microtubules were washed out with 50 µl BRB80 and finally, 50 µl of AB containing a 2 mM Mg-ATP, oxygen scavenger system (20 mM glucose, 20 µg/ml catalase and 160 µg/ml glucose oxidase) and mGFP-motor (at concentration as indicated in the legends of the figures of experiments shown in results chapters) was flown into the chamber.

Motors were immediately visualized by TIRF microscopy (100x objective and 1.6x optovar) and recorded by continuous streaming in the mGFP channel (488 nm excitation, 100 ms exposure) for 2 minutes, followed by generation of a static image of microtubules averaging a continuous stream of 10 images (532 nm excitation, 100 ms exposure time). The temperature was maintained at 25°C.

5.9.3 DDB motility on static MT

To study the processive motility of DDB (dynein-dynactin-BicD2$_{400}$) on static microtubules (Chapter 3), the final assay buffer used was: 30 mM HEPES pH 7.2, 50 mM K-acetate, 1 mM EGTA, 2 mM $MgCl_2$, 1 mM ATP, 2 mM ßME, 20 mM Glucose, 1.3 mg/ml Glucose oxidase (Serva) and 0.66 mg/ml Catalse (Sigma). All the other steps were the same as single molecule dynein motility assay except the last step where instead of GFP dynein alone, a DDB mix (1 nM GFP Dynein, 2 nM purified human dynactin and 20 nM BicD2$_{400}$ mixed and incubated at 4°C for 10 minutes) was added to

the final assay buffer. DDB motion was imaged via the GFP tagged dynein complex in 488 nm channel by continuous streaming at 100 ms exposure for 2 minutes.

5.9.4 Single molecule motility and end tracking on dynamic MT

Reconstitution of plus end tracking and motion of dynein in the presence of combinations of EB1 and other dynein regulators was done in conventional flow cells. The experiments were based on (Telley et al., 2011). The flow cells were assembled, passivated and blocked as described in the previous single molecule assay (in section 5.6.2). To the blocked flow cells, 50 μl of BRB80 with 50 μg/ml kappa-casein (BRB80k) was passed twice. Next, 50 μg/ml of NeutrAvidin (diluted in BRB80k) was flown and incubated for 5 minutes at 4°C. The unbound NeutrAvidin was washed from the flow chamber by flowing BRB80. After warming the flow cell to room temperature, Alexa 568 labelled biotinylated GMPCPP seeds diluted in BRB80 was passed through and incubated for 5 minutes in the flow cells. Depending on whether the final aim was to study DDB motility, dynein end tracking, or both in the same assay, the protein combinations and the subsequent steps were:

(a) DDB motility assay on dynamic MT

DDB mix was prepared [10 nM GFP dynein, 20 nM dynactin and 200 nM SNAP-BicD2$_{400}$ (for three colour imaging SNAP^{Alexa647}BicD2$_{400}$ was used instead of SNAP-BicD2$_{400}$)] and incubated for 10 minutes at 4°C. The flow cell was washed with BRB80 and the final assay buffer (FB): 20 mM K-PIPES (pH 6.9), 50 mM KCl, 1 mM EGTA, 2 mM MgCl2, 5 mM ßME, 1 mg/ml BSA (Sigma), 0.1 % Methylcellulose, 20 mM Glucose, 1.3 mg/ml Glucose oxidase (Serva) and 0.66 mg/ml Catalse (Sigma), 2 mM GTP and 2 mM ATP. 17.5 μM tubulin (with 10% Alexa 568 tubulin), and the DDB mix were added in the FB (the final volume was 30 μl). The FB mix with DDB and free tubulin was flown and the flow cell was sealed using vacuum grease (Beckman), and imaged by TIRF microscopy.

(b) GFP dynein plus end tracking assay

The mixture of GFP dynein, dynactin and EB1 (the concentrations of each protein are mentioned in the figure captions of Chapter 4, typically 10-20 nM) were mixed and incubated for 5 minutes at 4°C. The dynein-dynactin-EB1 mix and 17.5 μM tubulin (10% Alexa 568) were added to the FB (same as above in (a))

(c) Simultaneously GFP dynein motion and end tracking assay

The mixture of GFP dynein, dynactin, SNAP-BicD2$_{400}$ and EB1 (DDB-EB) (the concentrations of each protein are mentioned in the figure captions of Chapter 4) were mixed and preincubated for 5 minutes at 4°C before adding to the final assay buffer. To the experiments with mCherry Lis1 (1 μM and 5 μM) was added to the DDB-EB mix and all the proteins were pre-incubated for 5 minutes at 4°C before adding to the flow cells. This pre-incubated mix and 17.5 μM tubulin (10% Alexa 568) were added to the FB (same as above)

(d) TIRF Imaging

DDB motility and end tracking on dynamic microtubule was visualised by TIRF microscopy (100x objective) and recorded by timelapse in the mGFP channel at 488 nm excitation, and 100 ms exposure time. Images were recorded at 1 fps for 500 frames; simultaneously dynamic microtubule growth was recorded by timelapse in 561 channel by 532 nm excitation, 100 ms exposure time at 1 fps for 500 frames. The temperature was maintained at 30°C. Three colour imaging of the DDB motility on dynamic microtubule was visualized by simultaneous imaging of GFP dynein in 488 nm channel and Alexa 568 in 561 nm channel, and alternate imaging of SNAP^{Alexa647}BicD2$_{400}$ in 640 nm channel. The exposure in all channels was 200 ms. Images were recorded at 1 fps for 500 frames. For three colour imaging of end tracking experiment simultaneous imaging of GFP dynein in 488 nm channel and Alexa 568 in 561 nm channel, and alternate imaging of SNAP^{Alexa647}EB3 in 640 nm channel. The exposure in all channels was 200 ms at 1 fps for 500 frames.

5.10 Image analysis

Image processing was performed using ImageJ (https://imagej.nih.gov/ij/) to generate kymographs and to merge image sequence from different channels. For multi-colour imaging, a calibration grid was used to correct for camera drifts. A Matlab based script for alignment, as described in (Maurer et al., 2014) was used merge image sequences based on the alignment of the grid images of different channels/camera.

5.10.1 KymographDirect for dynein motion analysis

A single kymograph of DDB motion shows complex trajectories, with moving, diffusing and static particles, often with crisscrossing paths which makes the manual analysis difficult. To this end, an ImageJ plugin KymographClear (Schneider et al., 2012; Mangeol et al., 2016) allowed automated analysis of DDB. To analyse DDB motion on dynamic microtubules (results in Chapter 4), kymographs were generated from image sequences using KymographClear 2.0 ImageJ plugin developed by (Mangeol et al., 2016) (www.nat.vu.nl/~erwinp/downloads.html) (Figure 5.3). First, a maximum intensity projection image was generated that was used to define tracks using segmented the line tool. After drawing a single track, the plugin generated kymograph by Fourier filtering (Mangeol et al., 2016), which produced three distinct kymographs showing forward moving, backward moving and pausing or static particles, which were present within a kymograph of a single trajectory.

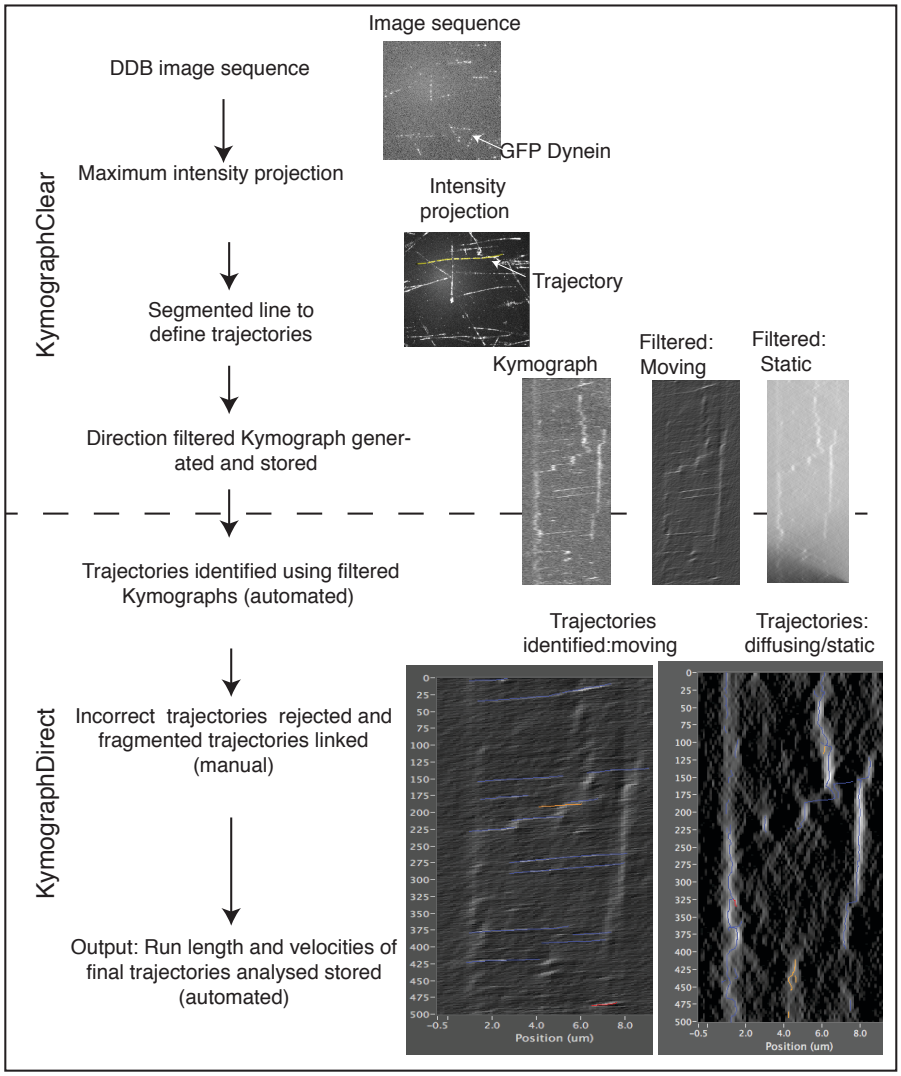

Figure 5.3 Kymograph analysis of DDB motion.

Analysis using KymographClear (to generate Fourier filtered kymographs) and KymographDirect (to trace,link and analyse trajectories in filtered kymographs)

The kymographs are further analysed with the KymographDirect software developed by the same group (Mangeol et al., 2016). It allowed automated analysis of trajectories of moving and static kymograph. It is especially useful for obtaining accurate tracks while staying resilient to high noise content in images. The spurious trajectories were rejected manually, while the fragmented trajectory from a single track were linked manually using 'link' option of KymographDirect. Statistical analysis of the velocity and intensity along these trajectories are computed automatically (Mangeol et al., 2016).

5.10.2 Fluorescent intensity measurement at microtubule ends

To quantify and compare the fluorescence intensity of dynein at plus end for various end-tracking experiments (in Chapter 4 of this thesis), GFP dynein intensities were measured from kymographs. The average intensity profiles were generated from dynamic microtubule assays data of GFP dynein at the growing microtubule end of labelled (Atto 647 and Alexa 568 labelled) dynamic microtubules (Figure 5.4): each kymograph was straightened and re-centred using the previously marked microtubule end positions. All the kymographs from one data set were aligned and averaged. The fluorescence intensities were then averaged for all time points at each position along the resulting kymographs to generate time-averaged spatial intensity profiles. For each assay conditions, the mean values of GFP dynein intensities from three experiments were plotted and the error bars show the standard deviation of each mean values.

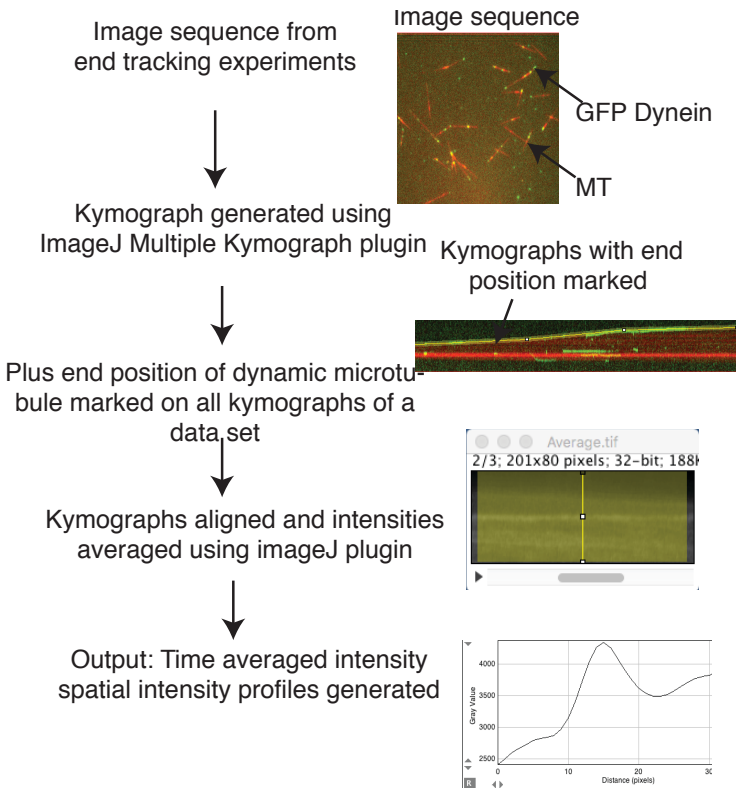

Figure 5.4 Fluorescent end intensity measurement

The kymographs from each data set were straightened, aligned and averaged according to the premarked position of the ends to generate time averaged spatial GFP dynein intensity profiles.

5.10.3 Analysis of microtubule growth

To determine the velocities of microtubule gliding from a time-lapse movie, the tracks of gliding microtubules were analyzed with the 'Multiple Kymograph' plug-in for ImageJ (J.Rietdorf and A. Seitz, EMBL Heidelberg). 50 microtubules were analyzed per condition. The mean growth velocity and standard error of the mean (s.e.m.) were plotted as column graph.

5.11 Reproducibility

All microscopy experiments were performed in triplicates (or more). For measurement of velocity and run length of processive DDB (dynein-dynactin-BicD2) over 200 complexes were analysed per condition. For the GFP dynein end intensity at least 50 MT plus ends were analysed per condition. All the test of significance reported are Student's t-test.

5.12 General computer software

Image processing was performed using ImageJ and KymographDirect. Data analysis was performed using Microsoft Excel, Origin, and Matlab. These programs were also used to prepare graphs presented in the result figures. Mass-spectrometry data were analysed using proteomic software Scaffold (http://www.proteomesoftware.com/products/scaffold/). Figures were prepared using Adobe Illustrator. The thesis was written in Microsoft word. Sequencing data were analysed using Ape. In silico PCR reaction, primer designing for infusion cloning were performed using SnapGene.

Chapter 6. Conclusion and Future Direction

Besides transporting cargos to the microtubule minus ends, dynein often localises to the microtubule plus ends, and for both these tasks regulation of dynein is important (Cianfrocco et al., 2015; Kardon and Vale, 2009; Splinter et al., 2012). This thesis highlights how metazoan dynein regulators control the switch between dynein's processive motion and its end tracking behaviour. While the non-processive dynein-dynactin complex binds to EB1 at microtubule plus ends, addition of BicD2 activates processive dynein motion, and at high concentration reduces the dynein pool at plus ends starkly. This presents an *in vitro* evidence of biasing characteristics of BicD2, where BicD2 seems to bias dynein's proceesive behaviour and a motion and reduces dynien's plus end tracking. This also explains why expression of adaptors (Num1—a cortical adaptor of yeast dynein and BicD2 fragments) depleted dynein from plus ends in yeast and mammalian cells (Lammers and Markus, 2015; Splinter et al., 2012). My findings also show that BicD2 and Lis1 compete to establish a shift between dynein motion and its microtubule localisation. When Lis1 and BicD2 are present in similar concentrations, Lis1 restores the dynein pool at plus ends, which was lost by the addition of BicD2. On the other hand, at levels lower than BicD2, Lis1 acts as an initiator of dynein motion (possibly by increasing the assembly of dynein-dynactin-BicD2 processive complex on the microtubules). These findings explain the requirement of Lis1 in both plus end tracking (Coquelle et al., 2002; Splinter et al., 2012), and processive dynein motion in cells (Splinter et al., 2012).

Taken together, these results emphasize that dynactin, Lis1, and BicD2 are instrumental in guiding the key steps of dynein motion, namely, its microtubule recruitment, transport initiation and activation.

The present work generates many avenues for further exploration of dynein regulation. First, how do Lis1 and BicD2 compete for binding to the dynein-dynactin complex? To understand this, a quantitative biochemical study of BicD2 and Lis1 interaction with the dynein-dynactin complex may be required. Second, do additional factors further regulate dynein during its plus end localisation and transport? For example, NudE could provide an additional layer of regulation by cooperating with Lis1 (Huang et al., 2012;

McKenney et al., 2010; Wang and Zheng, 2011) and competing with dynactin (McKenney et al., 2011) to bind to dynein. Further, CLIP170 could also provide additional regulation by interacting with dynactin and Lis1 at plus ends(Moughamian and Holzbaur, 2012; Moughamian et al., 2013). Finally, does the kinesin-dependent plus end transport of dynein also operate to further accumulate dynein pool at plus ends? In this regard reconstitution of plus end transport with the full-length BicD2 that can simultaneously interact with kinesin-1 and dynein (Grigoriev et al., 2007; Splinter et al., 2010) may provide important insights about the coordination of plus end and minus end dynein transport.

It is intriguing how the myriads of dynein regulators act together to balance dynein activity spatio-temporally in cells. Dynein regulation in cells is mainly studied by overexpression or down regulation of dynein regulators, which may not represent the regulation observed at the physiological concentrations of these regulators. To this end, a cellular study of dynein regulation by fluorescently tagging dynein regulators, such as dynactin, Lis1 and BicD2 at their endogenous locus by CRISPR/Cas (Feng et al., 2013) would allow the dissection of physiological regulation of dynein in different stages of cell-cycle.

Appendix

External contribution

Chapter 1

The recombinant human dynein complex and the artificially dimerised motor fragments were cloned by Martina Trokter.

The pdyn3 construct was gifted by Dr. Andrew Carter (MRC LMB, Cambridge)

Pauline Vercruysse cloned the yeast dynein motor fragment.

Chapter 3

Martina Trokter cloned mCherry Lis1 construct

Johanna Roostalu provided the EB1 protein and provided experimental suggestions.

Julian Gannon cloned the SNAP-EB3 construct.

Nic Cade provide help with TIRF microscopy

Reference List

Akhmanova, A., and Steinmetz, M.O. (2008). Tracking the ends: a dynamic protein network controls the fate of microtubule tips. Nature reviews Molecular cell biology *9*, 309-322.
Allan, V.J. (2011). Cytoplasmic dynein. Biochemical Society transactions *39*, 1169-1178.
Amos, L. (2008). Spindle assembly: kinesin-5 is in control. Current biology : CB *18*, R1146-1149.
Amos, L., and Klug, A. (1974). Arrangement of subunits in flagellar microtubules. Journal of cell science *14*, 523-549.
Amos, L.A. (2011). What tubulin drugs tell us about microtubule structure and dynamics. Seminars in cell & developmental biology *22*, 916-926.
Aniento, F., Emans, N., Griffiths, G., and Gruenberg, J. (1993). Cytoplasmic dynein-dependent vesicular transport from early to late endosomes. The Journal of cell biology *123*, 1373-1387.
Askham, J.M., Vaughan, K.T., Goodson, H.V., and Morrison, E.E. (2002). Evidence that an interaction between EB1 and p150(Glued) is required for the formation and maintenance of a radial microtubule array anchored at the centrosome. Molecular biology of the cell *13*, 3627-3645.
Belyy, V., Schlager, M.A., Foster, H., Reimer, A.E., Carter, A.P., and Yildiz, A. (2016). The mammalian dynein-dynactin complex is a strong opponent to kinesin in a tug-of-war competition. Nature cell biology *18*, 1018-1024.
Bieling, P., Telley, I.A., Hentrich, C., Piehler, J., and Surrey, T. (2010). Fluorescence microscopy assays on chemically functionalized surfaces for quantitative imaging of microtubule, motor, and +TIP dynamics. Methods in cell biology *95*, 555-580.
Bingham, J.B., King, S.J., and Schroer, T.A. (1998). Purification of dynactin and dynein from brain tissue. Methods in enzymology *298*, 171-184.
Bullock, S.L., and Ish-Horowicz, D. (2001). Conserved signals and machinery for RNA transport in Drosophila oogenesis and embryogenesis. Nature *414*, 611-616.
Carter, A.P., Cho, C., Jin, L., and Vale, R.D. (2011). Crystal structure of the dynein motor domain. Science *331*, 1159-1165.
Carter, A.P., Diamant, A.G., and Urnavicius, L. (2016). How dynein and dynactin transport cargos: a structural perspective. Current opinion in structural biology *37*, 62-70.
Carvalho, P., Gupta, M.L., Jr., Hoyt, M.A., and Pellman, D. (2004). Cell cycle control of kinesin-mediated transport of Bik1 (CLIP-170) regulates microtubule stability and dynein activation. Developmental cell *6*, 815-829.
Castoldi, M., and Popov, A.V. (2003). Purification of brain tubulin through two cycles of polymerization-depolymerization in a high-molarity buffer. Protein Expr Purif *32*, 83-88.
Cheong, F.K., Feng, L., Sarkeshik, A., Yates, J.R., 3rd, and Schroer, T.A. (2014). Dynactin integrity depends upon direct binding of dynamitin to Arp1. Molecular biology of the cell *25*, 2171-2180.
Cho, C., Reck-Peterson, S.L., and Vale, R.D. (2008). Regulatory ATPase sites of cytoplasmic dynein affect processivity and force generation. The Journal of biological chemistry *283*, 25839-25845.

Chowdhury, S., Ketcham, S.A., Schroer, T.A., and Lander, G.C. (2015). Structural organization of the dynein-dynactin complex bound to microtubules. Nature structural & molecular biology *22*, 345-347.
Cianfrocco, M.A., DeSantis, M.E., Leschziner, A.E., and Reck-Peterson, S.L. (2015). Mechanism and regulation of cytoplasmic dynein. Annual review of cell and developmental biology *31*, 83-108.
Coquelle, F.M., Caspi, M., Cordelieres, F.P., Dompierre, J.P., Dujardin, D.L., Koifman, C., Martin, P., Hoogenraad, C.C., Akhmanova, A., Galjart, N.*, et al.* (2002). LIS1, CLIP-170's key to the dynein/dynactin pathway. Molecular and cellular biology *22*, 3089-3102.
Corthesy-Theulaz, I., Pauloin, A., and Pfeffer, S.R. (1992). Cytoplasmic dynein participates in the centrosomal localization of the Golgi complex. The Journal of cell biology *118*, 1333-1345.
Culver-Hanlon, T.L., Lex, S.A., Stephens, A.D., Quintyne, N.J., and King, S.J. (2006). A microtubule-binding domain in dynactin increases dynein processivity by skating along microtubules. Nature cell biology *8*, 264-270.
Desai, A., and Mitchison, T.J. (1997). Microtubule polymerization dynamics. Annual review of cell and developmental biology *13*, 83-117.
DeWitt, M.A., Cypranowska, C.A., Cleary, F.B., Belyy, V., and Yildiz, A. (2015). The AAA3 domain of cytoplasmic dynein acts as a switch to facilitate microtubule release. Nature structural & molecular biology *22*, 73-80.
Dix, C.I., Soundararajan, H.C., Dzhindzhev, N.S., Begum, F., Suter, B., Ohkura, H., Stephens, E., and Bullock, S.L. (2013). Lissencephaly-1 promotes the recruitment of dynein and dynactin to transported mRNAs. The Journal of cell biology *202*, 479-494.
Dixit, R., Levy, J.R., Tokito, M., Ligon, L.A., and Holzbaur, E.L. (2008). Regulation of dynactin through the differential expression of p150Glued isoforms. The Journal of biological chemistry *283*, 33611-33619.
Dower, W.J., Miller, J.F., and Ragsdale, C.W. (1988). High efficiency transformation of E. coli by high voltage electroporation. Nucleic acids research *16*, 6127-6145.
Duellberg, C., Fourniol, F.J., Maurer, S.P., Roostalu, J., and Surrey, T. (2013). End-binding proteins and Ase1/PRC1 define local functionality of structurally distinct parts of the microtubule cytoskeleton. Trends in cell biology *23*, 54-63.
Duellberg, C., Trokter, M., Jha, R., Sen, I., Steinmetz, M.O., and Surrey, T. (2014). Reconstitution of a hierarchical +TIP interaction network controlling microtubule end tracking of dynein. Nature cell biology *16*, 804-811.
Dujardin, D.L., and Vallee, R.B. (2002). Dynein at the cortex. Current opinion in cell biology *14*, 44-49.
Eckley, D.M., Gill, S.R., Melkonian, K.A., Bingham, J.B., Goodson, H.V., Heuser, J.E., and Schroer, T.A. (1999). Analysis of dynactin subcomplexes reveals a novel actin-related protein associated with the arp1 minifilament pointed end. The Journal of cell biology *147*, 307-320.
Efimov, V.P. (2003). Roles of NUDE and NUDF proteins of Aspergillus nidulans: insights from intracellular localization and overexpression effects. Molecular biology of the cell *14*, 871-888.
Efimov, V.P., and Morris, N.R. (2000). The LIS1-related NUDF protein of Aspergillus nidulans interacts with the coiled-coil domain of the NUDE/RO11 protein. The Journal of cell biology *150*, 681-688.

Egan, M.J., Tan, K., and Reck-Peterson, S.L. (2012). Lis1 is an initiation factor for dynein-driven organelle transport. The Journal of cell biology *197*, 971-982.
Faulkner, N.E., Dujardin, D.L., Tai, C.Y., Vaughan, K.T., O'Connell, C.B., Wang, Y., and Vallee, R.B. (2000). A role for the lissencephaly gene LIS1 in mitosis and cytoplasmic dynein function. Nature cell biology *2*, 784-791.
Feng, Z., Zhang, B., Ding, W., Liu, X., Yang, D.L., Wei, P., Cao, F., Zhu, S., Zhang, F., Mao, Y.*, et al.* (2013). Efficient genome editing in plants using a CRISPR/Cas system. Cell research *23*, 1229-1232.
Fitzgerald, D.J., Berger, P., Schaffitzel, C., Yamada, K., Richmond, T.J., and Berger, I. (2006). Protein complex expression by using multigene baculoviral vectors. Nature methods *3*, 1021-1032.
Froger, A., and Hall, J.E. (2007). Transformation of plasmid DNA into E. coli using the heat shock method. Journal of visualized experiments : JoVE, 253.
Fujita, I., Yamashita, A., and Yamamoto, M. (2015). Dynactin and Num1 cooperate to establish the cortical anchoring of cytoplasmic dynein in S. pombe. Journal of cell science *128*, 1555-1567.
Gaglio, T., Dionne, M.A., and Compton, D.A. (1997). Mitotic spindle poles are organized by structural and motor proteins in addition to centrosomes. The Journal of cell biology *138*, 1055-1066.
Ganem, N.J., and Compton, D.A. (2004). The KinI kinesin Kif2a is required for bipolar spindle assembly through a functional relationship with MCAK. The Journal of cell biology *166*, 473-478.
Gassmann, R., Holland, A.J., Varma, D., Wan, X., Civril, F., Cleveland, D.W., Oegema, K., Salmon, E.D., and Desai, A. (2010). Removal of Spindly from microtubule-attached kinetochores controls spindle checkpoint silencing in human cells. Genes & development *24*, 957-971.
Gennerich, A., Carter, A.P., Reck-Peterson, S.L., and Vale, R.D. (2007). Force-induced bidirectional stepping of cytoplasmic dynein. Cell *131*, 952-965.
Gibbons, I.R., Garbarino, J.E., Tan, C.E., Reck-Peterson, S.L., Vale, R.D., and Carter, A.P. (2005). The affinity of the dynein microtubule-binding domain is modulated by the conformation of its coiled-coil stalk. The Journal of biological chemistry *280*, 23960-23965.
Gibbons, I.R., Lee-Eiford, A., Mocz, G., Phillipson, C.A., Tang, W.J., and Gibbons, B.H. (1987). Photosensitized cleavage of dynein heavy chains. Cleavage at the "V1 site" by irradiation at 365 nm in the presence of ATP and vanadate. The Journal of biological chemistry *262*, 2780-2786.
Gibbons, I.R., and Rowe, A.J. (1965). Dynein: A Protein with Adenosine Triphosphatase Activity from Cilia. Science *149*, 424-426.
Gill, S.R., Schroer, T.A., Szilak, I., Steuer, E.R., Sheetz, M.P., and Cleveland, D.W. (1991). Dynactin, a conserved, ubiquitously expressed component of an activator of vesicle motility mediated by cytoplasmic dynein. The Journal of cell biology *115*, 1639-1650.
Goshima, G., Nedelec, F., and Vale, R.D. (2005). Mechanisms for focusing mitotic spindle poles by minus end-directed motor proteins. The Journal of cell biology *171*, 229-240.
Griffis, E.R., Stuurman, N., and Vale, R.D. (2007). Spindly, a novel protein essential for silencing the spindle assembly checkpoint, recruits dynein to the kinetochore. The Journal of cell biology *177*, 1005-1015.

Grigoriev, I., Splinter, D., Keijzer, N., Wulf, P.S., Demmers, J., Ohtsuka, T., Modesti, M., Maly, I.V., Grosveld, F., Hoogenraad, C.C.*, et al.* (2007). Rab6 regulates transport and targeting of exocytotic carriers. Developmental cell *13*, 305-314.
Han, G., Liu, B., Zhang, J., Zuo, W., Morris, N.R., and Xiang, X. (2001). The Aspergillus cytoplasmic dynein heavy chain and NUDF localize to microtubule ends and affect microtubule dynamics. Current biology : CB *11*, 719-724.
Harrison, R.E., Bucci, C., Vieira, O.V., Schroer, T.A., and Grinstein, S. (2003). Phagosomes fuse with late endosomes and/or lysosomes by extension of membrane protrusions along microtubules: role of Rab7 and RILP. Molecular and cellular biology *23*, 6494-6506.
Hendricks, A.G., Lazarus, J.E., Perlson, E., Gardner, M.K., Odde, D.J., Goldman, Y.E., and Holzbaur, E.L. (2012). Dynein tethers and stabilizes dynamic microtubule plus ends. Current biology : CB *22*, 632-637.
Henry, T., Gorvel, J.P., and Meresse, S. (2006). Molecular motors hijacking by intracellular pathogens. Cellular microbiology *8*, 23-32.
Holleran, E.A., Ligon, L.A., Tokito, M., Stankewich, M.C., Morrow, J.S., and Holzbaur, E.L. (2001). beta III spectrin binds to the Arp1 subunit of dynactin. The Journal of biological chemistry *276*, 36598-36605.
Holleran, E.A., Tokito, M.K., Karki, S., and Holzbaur, E.L. (1996). Centractin (ARP1) associates with spectrin revealing a potential mechanism to link dynactin to intracellular organelles. The Journal of cell biology *135*, 1815-1829.
Honnappa, S., Gouveia, S.M., Weisbrich, A., Damberger, F.F., Bhavesh, N.S., Jawhari, H., Grigoriev, I., van Rijssel, F.J., Buey, R.M., Lawera, A.*, et al.* (2009). An EB1-binding motif acts as a microtubule tip localization signal. Cell *138*, 366-376.
Honnappa, S., John, C.M., Kostrewa, D., Winkler, F.K., and Steinmetz, M.O. (2005). Structural insights into the EB1-APC interaction. The EMBO journal *24*, 261-269.
Hoogenraad, C.C., Akhmanova, A., Howell, S.A., Dortland, B.R., De Zeeuw, C.I., Willemsen, R., Visser, P., Grosveld, F., and Galjart, N. (2001). Mammalian Golgi-associated Bicaudal-D2 functions in the dynein-dynactin pathway by interacting with these complexes. The EMBO journal *20*, 4041-4054.
Hook, P. (2010). The mechanical components of the dynein motor. TheScientificWorldJournal *10*, 857-864.
Horgan, C.P., Hanscom, S.R., Jolly, R.S., Futter, C.E., and McCaffrey, M.W. (2010). Rab11-FIP3 links the Rab11 GTPase and cytoplasmic dynein to mediate transport to the endosomal-recycling compartment. Journal of cell science *123*, 181-191.
Huang, J., Roberts, A.J., Leschziner, A.E., and Reck-Peterson, S.L. (2012). Lis1 acts as a "clutch" between the ATPase and microtubule-binding domains of the dynein motor. Cell *150*, 975-986.
Hyman, A.A. (1991). Preparation of marked microtubules for the assay of the polarity of microtubule-based motors by fluorescence. Journal of cell science Supplement *14*, 125-127.
Imai, H., Narita, A., Schroer, T.A., and Maeda, Y. (2006). Two-dimensional averaged images of the dynactin complex revealed by single particle analysis. Journal of molecular biology *359*, 833-839.
Janke, C. (2014). The tubulin code: molecular components, readout mechanisms, and functions. The Journal of cell biology *206*, 461-472.
Jha, R., and Surrey, T. (2015). Regulation of processive motion and microtubule localization of cytoplasmic dynein. Biochemical Society transactions *43*, 48-57.

Johansson, M., Rocha, N., Zwart, W., Jordens, I., Janssen, L., Kuijl, C., Olkkonen, V.M., and Neefjes, J. (2007). Activation of endosomal dynein motors by stepwise assembly of Rab7-RILP-p150Glued, ORP1L, and the receptor betalll spectrin. The Journal of cell biology *176*, 459-471.
Jordan, M.A., Thrower, D., and Wilson, L. (1992). Effects of vinblastine, podophyllotoxin and nocodazole on mitotic spindles. Implications for the role of microtubule dynamics in mitosis. Journal of cell science *102 (Pt 3)*, 401-416.
Kardon, J.R., Reck-Peterson, S.L., and Vale, R.D. (2009). Regulation of the processivity and intracellular localization of Saccharomyces cerevisiae dynein by dynactin. Proceedings of the National Academy of Sciences of the United States of America *106*, 5669-5674.
Kardon, J.R., and Vale, R.D. (2009). Regulators of the cytoplasmic dynein motor. Nature reviews Molecular cell biology *10*, 854-865.
Karki, S., and Holzbaur, E.L. (1995). Affinity chromatography demonstrates a direct binding between cytoplasmic dynein and the dynactin complex. The Journal of biological chemistry *270*, 28806-28811.
Kim, H., Ling, S.C., Rogers, G.C., Kural, C., Selvin, P.R., Rogers, S.L., and Gelfand, V.I. (2007). Microtubule binding by dynactin is required for microtubule organization but not cargo transport. The Journal of cell biology *176*, 641-651.
Kim, M.H., Cooper, D.R., Oleksy, A., Devedjiev, Y., Derewenda, U., Reiner, O., Otlewski, J., and Derewenda, Z.S. (2004). The structure of the N-terminal domain of the product of the lissencephaly gene Lis1 and its functional implications. Structure *12*, 987-998.
King, S.J., Brown, C.L., Maier, K.C., Quintyne, N.J., and Schroer, T.A. (2003). Analysis of the dynein-dynactin interaction in vitro and in vivo. Molecular biology of the cell *14*, 5089-5097.
King, S.J., and Schroer, T.A. (2000). Dynactin increases the processivity of the cytoplasmic dynein motor. Nature cell biology *2*, 20-24.
Kiyomitsu, T., and Cheeseman, I.M. (2012). Chromosome- and spindle-pole-derived signals generate an intrinsic code for spindle position and orientation. Nature cell biology *14*, 311-317.
Kobayashi, T., and Murayama, T. (2009). Cell cycle-dependent microtubule-based dynamic transport of cytoplasmic dynein in mammalian cells. PloS one *4*, e7827.
Kon, T., Mogami, T., Ohkura, R., Nishiura, M., and Sutoh, K. (2005). ATP hydrolysis cycle-dependent tail motions in cytoplasmic dynein. Nature structural & molecular biology *12*, 513-519.
Kon, T., Nishiura, M., Ohkura, R., Toyoshima, Y.Y., and Sutoh, K. (2004). Distinct functions of nucleotide-binding/hydrolysis sites in the four AAA modules of cytoplasmic dynein. Biochemistry *43*, 11266-11274.
Kon, T., Oyama, T., Shimo-Kon, R., Imamula, K., Shima, T., Sutoh, K., and Kurisu, G. (2012). The 2.8 A crystal structure of the dynein motor domain. Nature *484*, 345-350.
Kotak, S., Busso, C., and Gonczy, P. (2012). Cortical dynein is critical for proper spindle positioning in human cells. The Journal of cell biology *199*, 97-110.
Laan, L., Pavin, N., Husson, J., Romet-Lemonne, G., van Duijn, M., Lopez, M.P., Vale, R.D., Julicher, F., Reck-Peterson, S.L., and Dogterom, M. (2012). Cortical dynein controls microtubule dynamics to generate pulling forces that position microtubule asters. Cell *148*, 502-514.

Laemmli, U.K. (1970). Cleavage of structural proteins during the assembly of the head of bacteriophage T4. Nature *227*, 680-685.
Lam, C., Vergnolle, M.A., Thorpe, L., Woodman, P.G., and Allan, V.J. (2010). Functional interplay between LIS1, NDE1 and NDEL1 in dynein-dependent organelle positioning. Journal of cell science *123*, 202-212.
Lammers, L.G., and Markus, S.M. (2015). The dynein cortical anchor Num1 activates dynein motility by relieving Pac1/LIS1-mediated inhibition. The Journal of cell biology *211*, 309-322.
Lawrence, C.J., Dawe, R.K., Christie, K.R., Cleveland, D.W., Dawson, S.C., Endow, S.A., Goldstein, L.S., Goodson, H.V., Hirokawa, N., Howard, J.*, et al.* (2004). A standardized kinesin nomenclature. The Journal of cell biology *167*, 19-22.
Lazarus, J.E., Moughamian, A.J., Tokito, M.K., and Holzbaur, E.L. (2013). Dynactin subunit p150(Glued) is a neuron-specific anti-catastrophe factor. PLoS biology *11*, e1001611.
Lee, W.L., Oberle, J.R., and Cooper, J.A. (2003). The role of the lissencephaly protein Pac1 during nuclear migration in budding yeast. The Journal of cell biology *160*, 355-364.
Lehmann, M., Milev, M.P., Abrahamyan, L., Yao, X.J., Pante, N., and Mouland, A.J. (2009). Intracellular transport of human immunodeficiency virus type 1 genomic RNA and viral production are dependent on dynein motor function and late endosome positioning. The Journal of biological chemistry *284*, 14572-14585.
Lenz, J.H., Schuchardt, I., Straube, A., and Steinberg, G. (2006). A dynein loading zone for retrograde endosome motility at microtubule plus-ends. The EMBO journal *25*, 2275-2286.
Li, S., Oakley, C.E., Chen, G., Han, X., Oakley, B.R., and Xiang, X. (2005). Cytoplasmic dynein's mitotic spindle pole localization requires a functional anaphase-promoting complex, gamma-tubulin, and NUDF/LIS1 in Aspergillus nidulans. Molecular biology of the cell *16*, 3591-3605.
Liang, Y., Yu, W., Li, Y., Yang, Z., Yan, X., Huang, Q., and Zhu, X. (2004). Nudel functions in membrane traffic mainly through association with Lis1 and cytoplasmic dynein. The Journal of cell biology *164*, 557-566.
Ligon, L.A., Shelly, S.S., Tokito, M., and Holzbaur, E.L. (2003). The microtubule plus-end proteins EB1 and dynactin have differential effects on microtubule polymerization. Molecular biology of the cell *14*, 1405-1417.
Ligon, L.A., Shelly, S.S., Tokito, M.K., and Holzbaur, E.L. (2006). Microtubule binding proteins CLIP-170, EB1, and p150Glued form distinct plus-end complexes. FEBS letters *580*, 1327-1332.
Lloyd, T.E., Machamer, J., O'Hara, K., Kim, J.H., Collins, S.E., Wong, M.Y., Sahin, B., Imlach, W., Yang, Y., Levitan, E.S.*, et al.* (2012). The p150(Glued) CAP-Gly domain regulates initiation of retrograde transport at synaptic termini. Neuron *74*, 344-360.
Lomakin, A.J., Semenova, I., Zaliapin, I., Kraikivski, P., Nadezhdina, E., Slepchenko, B.M., Akhmanova, A., and Rodionov, V. (2009). CLIP-170-dependent capture of membrane organelles by microtubules initiates minus-end directed transport. Developmental cell *17*, 323-333.
Ma, S., and Chisholm, R.L. (2002). Cytoplasmic dynein-associated structures move bidirectionally in vivo. Journal of cell science *115*, 1453-1460.
Mallik, R., Carter, B.C., Lex, S.A., King, S.J., and Gross, S.P. (2004). Cytoplasmic dynein functions as a gear in response to load. Nature *427*, 649-652.

Mallik, R., Petrov, D., Lex, S.A., King, S.J., and Gross, S.P. (2005). Building complexity: an in vitro study of cytoplasmic dynein with in vivo implications. Current biology : CB *15*, 2075-2085.
Mangeol, P., Prevo, B., and Peterman, E.J. (2016). KymographClear and KymographDirect: two tools for the automated quantitative analysis of molecular and cellular dynamics using kymographs. Molecular biology of the cell *27*, 1948-1957.
Mao, Y., Varma, D., and Vallee, R. (2010). Emerging functions of force-producing kinetochore motors. Cell cycle *9*, 715-719.
Mateja, A., Cierpicki, T., Paduch, M., Derewenda, Z.S., and Otlewski, J. (2006). The dimerization mechanism of LIS1 and its implication for proteins containing the LisH motif. Journal of molecular biology *357*, 621-631.
Maurer, S.P., Cade, N.I., Bohner, G., Gustafsson, N., Boutant, E., and Surrey, T. (2014). EB1 accelerates two conformational transitions important for microtubule maturation and dynamics. Current biology : CB *24*, 372-384.
Maurer, S.P., Fourniol, F.J., Bohner, G., Moores, C.A., and Surrey, T. (2012). EBs recognize a nucleotide-dependent structural cap at growing microtubule ends. Cell *149*, 371-382.
Mazumdar, M., Mikami, A., Gee, M.A., and Vallee, R.B. (1996). In vitro motility from recombinant dynein heavy chain. Proceedings of the National Academy of Sciences of the United States of America *93*, 6552-6556.
McGrail, M., and Hays, T.S. (1997). The microtubule motor cytoplasmic dynein is required for spindle orientation during germline cell divisions and oocyte differentiation in Drosophila. Development *124*, 2409-2419.
McKenney, R.J., Huynh, W., Tanenbaum, M.E., Bhabha, G., and Vale, R.D. (2014). Science *345*, 337-341.
McKenney, R.J., Huynh, W., Vale, R.D., and Sirajuddin, M. (2016). Tyrosination of alpha-tubulin controls the initiation of processive dynein-dynactin motility. The EMBO journal *35*, 1175-1185.
McKenney, R.J., Vershinin, M., Kunwar, A., Vallee, R.B., and Gross, S.P. (2010). LIS1 and NudE induce a persistent dynein force-producing state. Cell *141*, 304-314.
McKenney, R.J., Weil, S.J., Scherer, J., and Vallee, R.B. (2011). Mutually exclusive cytoplasmic dynein regulation by NudE-Lis1 and dynactin. The Journal of biological chemistry *286*, 39615-39622.
Merdes, A., Heald, R., Samejima, K., Earnshaw, W.C., and Cleveland, D.W. (2000). Formation of spindle poles by dynein/dynactin-dependent transport of NuMA. The Journal of cell biology *149*, 851-862.
Merdes, A., Ramyar, K., Vechio, J.D., and Cleveland, D.W. (1996). A complex of NuMA and cytoplasmic dynein is essential for mitotic spindle assembly. Cell *87*, 447-458.
Meyer, T.S., and Lamberts, B.L. (1965). Use of coomassie brilliant blue R250 for the electrophoresis of microgram quantities of parotid saliva proteins on acrylamide-gel strips. Biochimica et biophysica acta *107*, 144-145.
Minke, P.F., Lee, I.H., Tinsley, J.H., Bruno, K.S., and Plamann, M. (1999). Neurospora crassa ro-10 and ro-11 genes encode novel proteins required for nuclear distribution. Molecular microbiology *32*, 1065-1076.
Mitchison, T., and Kirschner, M. (1984). Dynamic instability of microtubule growth. Nature *312*, 237-242.

Moore, J.K., Stuchell-Brereton, M.D., and Cooper, J.A. (2009). Function of dynein in budding yeast: mitotic spindle positioning in a polarized cell. Cell motility and the cytoskeleton *66*, 546-555.
Morris, R.L., and Hollenbeck, P.J. (1995). Axonal transport of mitochondria along microtubules and F-actin in living vertebrate neurons. The Journal of cell biology *131*, 1315-1326.
Moughamian, A.J., and Holzbaur, E.L. (2012). Dynactin is required for transport initiation from the distal axon. Neuron *74*, 331-343.
Moughamian, A.J., Osborn, G.E., Lazarus, J.E., Maday, S., and Holzbaur, E.L. (2013). Ordered recruitment of dynactin to the microtubule plus-end is required for efficient initiation of retrograde axonal transport. The Journal of neuroscience : the official journal of the Society for Neuroscience *33*, 13190-13203.
Muresan, V., Stankewich, M.C., Steffen, W., Morrow, J.S., Holzbaur, E.L., and Schnapp, B.J. (2001). Dynactin-dependent, dynein-driven vesicle transport in the absence of membrane proteins: a role for spectrin and acidic phospholipids. Molecular cell *7*, 173-183.
Neveling, K., Martinez-Carrera, L.A., Holker, I., Heister, A., Verrips, A., Hosseini-Barkooie, S.M., Gilissen, C., Vermeer, S., Pennings, M., Meijer, R.*, et al.* (2013). Mutations in BICD2, which encodes a golgin and important motor adaptor, cause congenital autosomal-dominant spinal muscular atrophy. American journal of human genetics *92*, 946-954.
Nicholas, M.P., Hook, P., Brenner, S., Wynne, C.L., Vallee, R.B., and Gennerich, A. (2015). Control of cytoplasmic dynein force production and processivity by its C-terminal domain. Nature communications *6*, 6206.
Nirschl, J.J., Magiera, M.M., Lazarus, J.E., Janke, C., and Holzbaur, E.L. (2016). alpha-Tubulin Tyrosination and CLIP-170 Phosphorylation Regulate the Initiation of Dynein-Driven Transport in Neurons. Cell reports *14*, 2637-2652.
Nogales, E., Whittaker, M., Milligan, R.A., and Downing, K.H. (1999). High-resolution model of the microtubule. Cell *96*, 79-88.
Numata, N., Shima, T., Ohkura, R., Kon, T., and Sutoh, K. (2011). C-sequence of the Dictyostelium cytoplasmic dynein participates in processivity modulation. FEBS letters *585*, 1185-1190.
O'Brien, E.T., Voter, W.A., and Erickson, H.P. (1987). GTP hydrolysis during microtubule assembly. Biochemistry *26*, 4148-4156.
Oates, E.C., Rossor, A.M., Hafezparast, M., Gonzalez, M., Speziani, F., MacArthur, D.G., Lek, M., Cottenie, E., Scoto, M., Foley, A.R.*, et al.* (2013). Mutations in BICD2 cause dominant congenital spinal muscular atrophy and hereditary spastic paraplegia. American journal of human genetics *92*, 965-973.
Pandey, J.P., and Smith, D.S. (2011). A Cdk5-dependent switch regulates Lis1/Ndel1/dynein-driven organelle transport in adult axons. The Journal of neuroscience : the official journal of the Society for Neuroscience *31*, 17207-17219.
Paschal, B.M., Holzbaur, E.L., Pfister, K.K., Clark, S., Meyer, D.I., and Vallee, R.B. (1993). Characterization of a 50-kDa polypeptide in cytoplasmic dynein preparations reveals a complex with p150GLUED and a novel actin. The Journal of biological chemistry *268*, 15318-15323.
Paschal, B.M., Shpetner, H.S., and Vallee, R.B. (1987). MAP 1C is a microtubule-activated ATPase which translocates microtubules in vitro and has dynein-like properties. The Journal of cell biology *105*, 1273-1282.

Paschal, B.M., and Vallee, R.B. (1987). Retrograde transport by the microtubule-associated protein MAP 1C. Nature *330*, 181-183.
Pazour, G.J., Dickert, B.L., and Witman, G.B. (1999). The DHC1b (DHC2) isoform of cytoplasmic dynein is required for flagellar assembly. The Journal of cell biology *144*, 473-481.
Pfister, K.K., Shah, P.R., Hummerich, H., Russ, A., Cotton, J., Annuar, A.A., King, S.M., and Fisher, E.M. (2006). Genetic analysis of the cytoplasmic dynein subunit families. PLoS genetics *2*, e1.
Pierre, P., Scheel, J., Rickard, J.E., and Kreis, T.E. (1992). CLIP-170 links endocytic vesicles to microtubules. Cell *70*, 887-900.
Porter, M.E., Bower, R., Knott, J.A., Byrd, P., and Dentler, W. (1999). Cytoplasmic dynein heavy chain 1b is required for flagellar assembly in Chlamydomonas. Molecular biology of the cell *10*, 693-712.
Raaijmakers, J.A., Tanenbaum, M.E., and Medema, R.H. (2013). Systematic dissection of dynein regulators in mitosis. The Journal of cell biology *201*, 201-215.
Rai, A.K., Rai, A., Ramaiya, A.J., Jha, R., and Mallik, R. (2013). Molecular adaptations allow dynein to generate large collective forces inside cells. Cell *152*, 172-182.
Reck-Peterson, S.L., Yildiz, A., Carter, A.P., Gennerich, A., Zhang, N., and Vale, R.D. (2006). Single-molecule analysis of dynein processivity and stepping behavior. Cell *126*, 335-348.
Reddy, B.J., Mattson, M., Wynne, C.L., Vadpey, O., Durra, A., Chapman, D., Vallee, R.B., and Gross, S.P. (2016). Load-induced enhancement of Dynein force production by LIS1-NudE in vivo and in vitro. Nature communications *7*, 12259.
Roberts, A.J., Goodman, B.S., and Reck-Peterson, S.L. (2014). Reconstitution of dynein transport to the microtubule plus end by kinesin. eLife *3*, e02641.
Roberts, A.J., Kon, T., Knight, P.J., Sutoh, K., and Burgess, S.A. (2013). Functions and mechanics of dynein motor proteins. Nature reviews Molecular cell biology *14*, 713-726.
Roberts, A.J., Malkova, B., Walker, M.L., Sakakibara, H., Numata, N., Kon, T., Ohkura, R., Edwards, T.A., Knight, P.J., Sutoh, K.*, et al.* (2012). ATP-driven remodeling of the linker domain in the dynein motor. Structure *20*, 1670-1680.
Roberts, A.J., Numata, N., Walker, M.L., Kato, Y.S., Malkova, B., Kon, T., Ohkura, R., Arisaka, F., Knight, P.J., Sutoh, K.*, et al.* (2009). AAA+ Ring and linker swing mechanism in the dynein motor. Cell *136*, 485-495.
Ross, J.L., Wallace, K., Shuman, H., Goldman, Y.E., and Holzbaur, E.L. (2006). Processive bidirectional motion of dynein-dynactin complexes in vitro. Nature cell biology *8*, 562-570.
Salina, D., Bodoor, K., Eckley, D.M., Schroer, T.A., Rattner, J.B., and Burke, B. (2002). Cytoplasmic dynein as a facilitator of nuclear envelope breakdown. Cell *108*, 97-107.
Sasaki, S., Shionoya, A., Ishida, M., Gambello, M.J., Yingling, J., Wynshaw-Boris, A., and Hirotsune, S. (2000). A LIS1/NUDEL/cytoplasmic dynein heavy chain complex in the developing and adult nervous system. Neuron *28*, 681-696.
Savoian, M.S., Goldberg, M.L., and Rieder, C.L. (2000). The rate of poleward chromosome motion is attenuated in Drosophila zw10 and rod mutants. Nat Cell Biol *2*, 948-952.
Schafer, D.A., Gill, S.R., Cooper, J.A., Heuser, J.E., and Schroer, T.A. (1994). Ultrastructural analysis of the dynactin complex: an actin-related protein is a component of a filament that resembles F-actin. The Journal of cell biology *126*, 403-412.

Schlager, M.A., Hoang, H.T., Urnavicius, L., Bullock, S.L., and Carter, A.P. (2014a). In vitro reconstitution of a highly processive recombinant human dynein complex. The EMBO journal *33*, 1855-1868.
Schlager, M.A., Serra-Marques, A., Grigoriev, I., Gumy, L.F., Esteves da Silva, M., Wulf, P.S., Akhmanova, A., and Hoogenraad, C.C. (2014b). Bicaudal D Family Adaptor Proteins Control the Velocity of Dynein-Based Movements. Cell reports.
Schmidt, H. (2015). Dynein motors: How AAA+ ring opening and closing coordinates microtubule binding and linker movement. BioEssays : news and reviews in molecular, cellular and developmental biology *37*, 532-543.
Schnorrer, F., Bohmann, K., and Nusslein-Volhard, C. (2000). The molecular motor dynein is involved in targeting swallow and bicoid RNA to the anterior pole of Drosophila oocytes. Nature cell biology *2*, 185-190.
Schroeder, H.W., 3rd, Mitchell, C., Shuman, H., Holzbaur, E.L., and Goldman, Y.E. (2010). Motor number controls cargo switching at actin-microtubule intersections in vitro. Current biology : CB *20*, 687-696.
Schroer, T.A. (2004). Dynactin. Annual review of cell and developmental biology *20*, 759-779.
Schroer, T.A., and Sheetz, M.P. (1991b). Two activators of microtubule-based vesicle transport. The Journal of cell biology *115*, 1309-1318.
Schuster, M., Lipowsky, R., Assmann, M.A., Lenz, P., and Steinberg, G. (2011). Transient binding of dynein controls bidirectional long-range motility of early endosomes. Proceedings of the National Academy of Sciences of the United States of America *108*, 3618-3623.
Sharp, D.J., Rogers, G.C., and Scholey, J.M. (2000). Cytoplasmic dynein is required for poleward chromosome movement during mitosis in Drosophila embryos. Nat Cell Biol *2*, 922-930.
Sheeman, B., Carvalho, P., Sagot, I., Geiser, J., Kho, D., Hoyt, M.A., and Pellman, D. (2003). Determinants of S. cerevisiae dynein localization and activation: implications for the mechanism of spindle positioning. Current biology : CB *13*, 364-372.
Shu, T., Ayala, R., Nguyen, M.D., Xie, Z., Gleeson, J.G., and Tsai, L.H. (2004). Ndel1 operates in a common pathway with LIS1 and cytoplasmic dynein to regulate cortical neuronal positioning. Neuron *44*, 263-277.
Siglin, A.E., Sun, S., Moore, J.K., Tan, S., Poenie, M., Lear, J.D., Polenova, T., Cooper, J.A., and Williams, J.C. (2013). Dynein and dynactin leverage their bivalent character to form a high-affinity interaction. PloS one *8*, e59453.
Smith, D.S., Niethammer, M., Ayala, R., Zhou, Y., Gambello, M.J., Wynshaw-Boris, A., and Tsai, L.H. (2000). Regulation of cytoplasmic dynein behaviour and microtubule organization by mammalian Lis1. Nature cell biology *2*, 767-775.
Splinter, D., Razafsky, D.S., Schlager, M.A., Serra-Marques, A., Grigoriev, I., Demmers, J., Keijzer, N., Jiang, K., Poser, I., Hyman, A.A.*, et al.* (2012). BICD2, dynactin, and LIS1 cooperate in regulating dynein recruitment to cellular structures. Molecular biology of the cell *23*, 4226-4241.
Splinter, D., Tanenbaum, M.E., Lindqvist, A., Jaarsma, D., Flotho, A., Yu, K.L., Grigoriev, I., Engelsma, D., Haasdijk, E.D., Keijzer, N.*, et al.* (2010). Bicaudal D2, dynein, and kinesin-1 associate with nuclear pore complexes and regulate centrosome and nuclear positioning during mitotic entry. PLoS biology *8*, e1000350.

Stehman, S.A., Chen, Y., McKenney, R.J., and Vallee, R.B. (2007). NudE and NudEL are required for mitotic progression and are involved in dynein recruitment to kinetochores. The Journal of cell biology *178*, 583-594.
Stewart, R.J., Farrell, K.W., and Wilson, L. (1990). Role of GTP hydrolysis in microtubule polymerization: evidence for a coupled hydrolysis mechanism. Biochemistry *29*, 6489-6498.
Stuurman, N., Haner, M., Sasse, B., Hubner, W., Suter, B., and Aebi, U. (1999). Interactions between coiled-coil proteins: Drosophila lamin Dm0 binds to the bicaudal-D protein. European journal of cell biology *78*, 278-287.
Tai, C.Y., Dujardin, D.L., Faulkner, N.E., and Vallee, R.B. (2002). Role of dynein, dynactin, and CLIP-170 interactions in LIS1 kinetochore function. The Journal of cell biology *156*, 959-968.
Tarricone, C., Perrina, F., Monzani, S., Massimiliano, L., Kim, M.H., Derewenda, Z.S., Knapp, S., Tsai, L.H., and Musacchio, A. (2004). Coupling PAF signaling to dynein regulation: structure of LIS1 in complex with PAF-acetylhydrolase. Neuron *44*, 809-821.
Telley, I.A., Bieling, P., and Surrey, T. (2011). Reconstitution and quantification of dynamic microtubule end tracking in vitro using TIRF microscopy. Methods in molecular biology *777*, 127-145.
Terasaki, M., Chen, L.B., and Fujiwara, K. (1986). Microtubules and the endoplasmic reticulum are highly interdependent structures. The Journal of cell biology *103*, 1557-1568.
Terenzio, M., and Schiavo, G. (2010). The more, the better: the BICD family gets bigger. The EMBO journal *29*, 1625-1626.
Tirnauer, J.S., Canman, J.C., Salmon, E.D., and Mitchison, T.J. (2002). EB1 targets to kinetochores with attached, polymerizing microtubules. Molecular biology of the cell *13*, 4308-4316.
Toba, S., Watanabe, T.M., Yamaguchi-Okimoto, L., Toyoshima, Y.Y., and Higuchi, H. (2006). Overlapping hand-over-hand mechanism of single molecular motility of cytoplasmic dynein. Proceedings of the National Academy of Sciences of the United States of America *103*, 5741-5745.
Torisawa, T., Ichikawa, M., Furuta, A., Saito, K., Oiwa, K., Kojima, H., Toyoshima, Y.Y., and Furuta, K. (2014). Autoinhibition and cooperative activation mechanisms of cytoplasmic dynein. Nature cell biology *16*, 1118-1124.
Torisawa, T., Nakayama, A., Furuta, K., Yamada, M., Hirotsune, S., and Toyoshima, Y.Y. (2011). Functional dissection of LIS1 and NDEL1 towards understanding the molecular mechanisms of cytoplasmic dynein regulation. The Journal of biological chemistry *286*, 1959-1965.
Toropova, K., Zou, S., Roberts, A.J., Redwine, W.B., Goodman, B.S., Reck-Peterson, S.L., and Leschziner, A.E. (2014). Lis1 regulates dynein by sterically blocking its mechanochemical cycle. eLife *3*.
Towbin, H., Staehelin, T., and Gordon, J. (1992). Electrophoretic transfer of proteins from polyacrylamide gels to nitrocellulose sheets: procedure and some applications. 1979. Biotechnology *24*, 145-149.
Trokter, M., Mucke, N., and Surrey, T. (2012). Reconstitution of the human cytoplasmic dynein complex. Proceedings of the National Academy of Sciences of the United States of America *109*, 20895-20900.

Ullmann, A., Jacob, F., and Monod, J. (1967). Characterization by in vitro complementation of a peptide corresponding to an operator-proximal segment of the beta-galactosidase structural gene of Escherichia coli. Journal of molecular biology *24*, 339-343.
Urnavicius, L., Zhang, K., Diamant, A.G., Motz, C., Schlager, M.A., Yu, M., Patel, N.A., Robinson, C.V., and Carter, A.P. (2015). The structure of the dynactin complex and its interaction with dynein. Science *347*, 1441-1446.
Vale, R.D. (2003). The molecular motor toolbox for intracellular transport. Cell *112*, 467-480.
Valetti, C., Wetzel, D.M., Schrader, M., Hasbani, M.J., Gill, S.R., Kreis, T.E., and Schroer, T.A. (1999). Role of dynactin in endocytic traffic: effects of dynamitin overexpression and colocalization with CLIP-170. Molecular biology of the cell *10*, 4107-4120.
Vallee, R.B., Wall, J.S., Paschal, B.M., and Shpetner, H.S. (1988). Microtubule-associated protein 1C from brain is a two-headed cytosolic dynein. Nature *332*, 561-563.
van der Kant, R., Fish, A., Janssen, L., Janssen, H., Krom, S., Ho, N., Brummelkamp, T., Carette, J., Rocha, N., and Neefjes, J. (2013). Late endosomal transport and tethering are coupled processes controlled by RILP and the cholesterol sensor ORP1L. Journal of cell science *126*, 3462-3474.
Varma, D., Monzo, P., Stehman, S.A., and Vallee, R.B. (2008). Direct role of dynein motor in stable kinetochore-microtubule attachment, orientation, and alignment. The Journal of cell biology *182*, 1045-1054.
Vasquez, R.J., Howell, B., Yvon, A.M., Wadsworth, P., and Cassimeris, L. (1997). Nanomolar concentrations of nocodazole alter microtubule dynamic instability in vivo and in vitro. Molecular biology of the cell *8*, 973-985.
Vaughan, K.T., Tynan, S.H., Faulkner, N.E., Echeverri, C.J., and Vallee, R.B. (1999). Colocalization of cytoplasmic dynein with dynactin and CLIP-170 at microtubule distal ends. Journal of cell science *112 (Pt 10)*, 1437-1447.
Vaughan, K.T., and Vallee, R.B. (1995). Cytoplasmic dynein binds dynactin through a direct interaction between the intermediate chains and p150Glued. The Journal of cell biology *131*, 1507-1516.
Vaughan, P.S., Miura, P., Henderson, M., Byrne, B., and Vaughan, K.T. (2002). A role for regulated binding of p150(Glued) to microtubule plus ends in organelle transport. The Journal of cell biology *158*, 305-319.
Vergnolle, M.A., and Taylor, S.S. (2007). Cenp-F links kinetochores to Ndel1/Nde1/Lis1/dynein microtubule motor complexes. Current biology : CB *17*, 1173-1179.
Vershinin, M., Xu, J., Razafsky, D.S., King, S.J., and Gross, S.P. (2008). Tuning microtubule-based transport through filamentous MAPs: the problem of dynein. Traffic *9*, 882-892.
Vijayachandran, L.S., Thimiri Govinda Raj, D.B., Edelweiss, E., Gupta, K., Maier, J., Gordeliy, V., Fitzgerald, D.J., and Berger, I. (2013). Gene gymnastics: Synthetic biology for baculovirus expression vector system engineering. Bioengineered *4*, 279-287.
Volkov, V.A., Zaytsev, A.V., Gudimchuk, N., Grissom, P.M., Gintsburg, A.L., Ataullakhanov, F.I., McIntosh, J.R., and Grishchuk, E.L. (2013). Long tethers provide high-force coupling of the Dam1 ring to shortening microtubules. Proceedings of the National Academy of Sciences of the United States of America *110*, 7708-7713.

Wade, R.H. (2009). On and around microtubules: an overview. Mol Biotechnol *43*, 177-191.
Wang, L., Li, J., Jia, M., Yue, W., Ruan, Y., Lu, T., Zhang, J., Liu, J., and Zhang, D. (2011). No association of polymorphisms in the CDK5, NDEL1, and LIS1 with autism in Chinese Han population. Psychiatry research *190*, 369-371.
Wang, S., Ketcham, S.A., Schon, A., Goodman, B., Wang, Y., Yates, J., 3rd, Freire, E., Schroer, T.A., and Zheng, Y. (2013). Nudel/NudE and Lis1 promote dynein and dynactin interaction in the context of spindle morphogenesis. Molecular biology of the cell *24*, 3522-3533.
Wang, S., and Zheng, Y. (2011). Identification of a novel dynein binding domain in nudel essential for spindle pole organization in Xenopus egg extract. The Journal of biological chemistry *286*, 587-593.
Wang, Z., Khan, S., and Sheetz, M.P. (1995). Single cytoplasmic dynein molecule movements: characterization and comparison with kinesin. Biophysical journal *69*, 2011-2023.
Watson, P., Forster, R., Palmer, K.J., Pepperkok, R., and Stephens, D.J. (2005). Coupling of ER exit to microtubules through direct interaction of COPII with dynactin. Nature cell biology *7*, 48-55.
Watson, P., and Stephens, D.J. (2006). Microtubule plus-end loading of p150(Glued) is mediated by EB1 and CLIP-170 but is not required for intracellular membrane traffic in mammalian cells. Journal of cell science *119*, 2758-2767.
Widlund, P.O., Podolski, M., Reber, S., Alper, J., Storch, M., Hyman, A.A., Howard, J., and Drechsel, D.N. (2012). One-step purification of assembly-competent tubulin from diverse eukaryotic sources. Molecular biology of the cell *23*, 4393-4401.
Xiang, X., Osmani, A.H., Osmani, S.A., Xin, M., and Morris, N.R. (1995). NudF, a nuclear migration gene in Aspergillus nidulans, is similar to the human LIS-1 gene required for neuronal migration. Molecular biology of the cell *6*, 297-310.
Yamada, M., Toba, S., Yoshida, Y., Haratani, K., Mori, D., Yano, Y., Mimori-Kiyosue, Y., Nakamura, T., Itoh, K., Fushiki, S.*, et al.* (2008). LIS1 and NDEL1 coordinate the plus-end-directed transport of cytoplasmic dynein. The EMBO journal *27*, 2471-2483.
Yi, J.Y., Ori-McKenney, K.M., McKenney, R.J., Vershinin, M., Gross, S.P., and Vallee, R.B. (2011). High-resolution imaging reveals indirect coordination of opposite motors and a role for LIS1 in high-load axonal transport. The Journal of cell biology *195*, 193-201.
Zhang, J., Li, S., Fischer, R., and Xiang, X. (2003). Accumulation of cytoplasmic dynein and dynactin at microtubule plus ends in Aspergillus nidulans is kinesin dependent. Molecular biology of the cell *14*, 1479-1488.
Zhang, J., Qiu, R., Arst, H.N., Jr., Penalva, M.A., and Xiang, X. (2014). HookA is a novel dynein-early endosome linker critical for cargo movement in vivo. The Journal of cell biology *204*, 1009-1026.
Zhapparova, O.N., Bryantseva, S.A., Dergunova, L.V., Raevskaya, N.M., Burakov, A.V., Bantysh, O.B., Shanina, N.A., and Nadezhdina, E.S. (2009). Dynactin subunit p150Glued isoforms notable for differential interaction with microtubules. Traffic *10*, 1635-1646.
Zylkiewicz, E., Kijanska, M., Choi, W.C., Derewenda, U., Derewenda, Z.S., and Stukenberg, P.T. (2011). The N-terminal coiled-coil of Ndel1 is a regulated scaffold that recruits LIS1 to dynein. The Journal of cell biology *192*, 433-445.